# HIGH-EFFICIENCY BIOFABRICATION OF CELL-LADEN GELATIN METHACRYLOYL HYDROGELS

by

Mohamed Gamaleldin Abdelkhalek Mohamed

M.Sc. in Stem Cells and Regeneration, University of Bristol, 2012

B. Pharm., Ain Shams University, 2005

A THESIS SUBMITTED IN PARTIAL FULFILLMENT OF

THE REQUIREMENTS FOR THE DEGREE OF

DOCTOR OF PHILOSOPHY

in

THE COLLEGE OF GRADUATE STUDIES

(Mechanical Engineering)

THE UNIVERSITY OF BRITISH COLUMBIA

(Okanagan)

March 2020

The following individuals certify that they have read, and recommend to the College of Graduate Studies for acceptance, a thesis/dissertation entitled:

High-Efficiency Biofabrication of Cell-Laden Gelatin Methacryloyl Hydrogels

submitted by Mohamed Gamaleldin Abdelkhalek Mohamed in partial fulfillment of the requirements of the degree of Doctor of Philosophy in Mechanical Engineering.

Dr. Keekyoung Kim, School of Engineering, The University of British Columbia

**Supervisor**

Dr. Mina Hoorfar, School of Engineering, The University of British Columbia

**Supervisory Committee Member**

Dr. Ian Foulds, School of Engineering, The University of British Columbia

**Supervisory Committee Member**

Dr. Zheng Liu, School of Engineering, The University of British Columbia

**University Examiner**

Dr. Xinyu Liu, University of Toronto

**External Examiner**

## Abstract

Biofabrication is the automated manufacturing technology of biologically functional, organized cell-material constructs through bioassembly or 3D bioprinting. Microfluidic and bioprinting principles have served as powerful tools for fabricating cell-laden 3D gels for various biological applications, the most important of which is bottom-up tissue engineering. However, the inherently limited throughput of micro-scale devices coupled with the low cost-effectiveness of producing biomaterials has rendered these methodologies unsuitable for practical application. It is also necessary that the biomaterial used for these applications be biocompatible, display adequate mechanical properties, and be manufactured through a reliable manufacturing technology. Due to its printability and biocompatibility, GelMA hydrogel has attracted considerable interest as a scaffolding material for tissue engineering. Nevertheless, the detoxification, purification, dehydration, and sterilization steps for synthesizing GelMA hydrogels are expensive, time-consuming, and serve as a significant reason for its low and irreproducible yields. This research aims to tackle these hurdles in efficiency. First, this work integrated all the required steps of fabricating monodisperse cell-laden microgels onto one chip. The elimination of the off-chip droplet handling requirement enables a high-throughput process. The stability of the operation resulted in a reasonable cell distribution among the microgels over various cell seeding concentrations. Furthermore, cells showed a high viability of around 85% over 5 days in culture. Second, we devised a rapid approach for GelMA detoxification in an aprotic solvent medium with moderate polarity by employing the ion-pairing and desolvation concepts. The GelMA produced through this method displayed a significantly higher yield in comparison to conventionally synthesized batches while also demonstrating a comparable degree of methacrylation. Moreover, this

GelMA displayed high biocompatibility and bioprintability. Third, the dehydration step of GelMA was eliminated by using a toluene-based precipitation approach. The extreme hydrophobicity of toluene protects the protein from hydrolysis and leads to the production of a reproducible yield. Toluene also has the advantages of being volatile and lighter than water, which allows for the direct reconstitution of the extracted known yield of GelMA in the aqueous phase.

## Lay Summary

Combining cells and gels into a single construct can be used to treat or replace an affected human tissue, this is termed “Biofabrication”. Several biofabrication methods are proved for the concept; however, they are not scalable or cost-effective. In this research, we tackle three of these inefficiency hurdles. First, we sought to simplify the incorporation of cells into microgels by having a device that can integrate all the required complex steps. This device displayed higher and faster throughput while minimizing gradual product loss that usually occurs in every step. Second, the slow detoxification step that is characteristic of contemporary synthesis methods was replaced by a new approach that simultaneously undertakes the purification step with the sterilization step. Finally, the need for lengthy dehydration of the produced biomaterial is eliminated, thus producing a ready-to-use biomaterial quickly and efficiently.

## Preface

The research presented in this thesis is conducted in the UBC Advanced Biofabrication Laboratory (ABL) under the supervision of Dr. Keekyoung Kim. Parts of this thesis have been published in peer-reviewed journals and conference proceedings. This work has been made possible through the financial support of the Natural Sciences and Engineering Research Council of Canada (NSERC) and the Canadian Foundation for Innovation John R. Evans Leaders Opportunity Fund. Details of publications with the author's contributions are explained below:

**Patents:**

1. US62/884,408 **"**A Rapid, High Yield, and Sterilized Method to Synthesize Gelatin Methacryloyl (GelMA) Hydrogels," **M.G.A. Mohamed**, and K. Kim. US provisional patent filed, August 2019.

   Role in this invention: I developed a method to synthesize gelatin methacryloyl in a much efficient manner than conventional methods. I conducted experiments, analyzed data, and prepared the invention disclosure documents under the supervision of Dr. Kim.

**Journal Articles:**

1. **M.G.A. Mohamed**, S. Kheiri, S. Islam, H. Kumar, A. Yang, and K. Kim, "An Integrated Microfluidic Flow-Focusing Platform for On-Chip Fabrication and Filtration of Cell-Laden Microgels," *Lab Chip*. 2019. doi:10.1039/C9LC00073A.

Role in this manuscript: I developed a novel microfluidic platform for fabricating cell-laden microgels. I conducted all experiments, analyzed data, and wrote and revised the manuscript under the supervision of Dr. Kim.

2. **M.G.A. Mohamed**, H. Kumar, Z. Wang, N. Martin, B. Mills, and K. Kim, "Rapid and Inexpensive Fabrication of Multi-Depth Microfluidic Device using High-Resolution LCD Stereolithographic 3D Printing," *J Manuf Mater Process*. 2019;3(1):26. doi:10.3390/jmmp3010026.

   Role in this paper: I developed a new rapid and inexpensive way to fabricate microfluidic devices with multi-depth channels using 3D printing technology.

3. **M.G.A. Mohamed,** P. Ambhorkar, R. Samanipour, A. Yang, A. Ghaffour, and K. Kim, "Microfluidics-based Biofabrication of Cell-laden Microgels," submitted to *Biomicrofluidics*, 2019.

   Role in this manuscript: This is a review paper. I collected and sorted articles and wrote and revised the manuscript under the supervision of Dr. Kim.

4. **M.G.A. Mohamed**, H. Kumar, K.Sakthivel, P. Ambhorkar, S. Mahdavi, A. Ghaffour, and K. Kim, "Rapid and High Yield Synthesizing of Sterile Gelatin Methacryloyl (GelMA) Bioinks," submitted to *Biofabrication*, under review, 2019.

   Role in this manuscript: I developed a novel process to synthesize gelatin methacryloyl in a much faster way than the conventional method. I conducted all experiments, analyzed data, and am preparing the manuscript under the supervision of Dr. Kim.

5. H. Montazerian, **M.G.A. Mohamed**, M. M. Montazeri, S. Kheiri, A. S. Milani, K. Kim, and M. Hoorfar, “Permeability and mechanical properties of gradient porous PDMS scaffolds fabricated by 3D-printed sacrificial templates designed with minimal surfaces,” *Acta Biomaterialia*, https://doi.org/10.1016/j.actbio.2019.06.040

   Role in this manuscript: I helped in fabricating the scaffolds, conducting the biocompatibility assessment of the method and the scaffolds, and in writing the manuscript.

6. Z. Wang, R. Samanipour, **M.G.A. Mohamed**, K. Sakthivel, and K. Kim, "An automated system for high- throughput generation and optimization of microdroplets," *Biomicrofluidics*, 2016;10(5). doi:10.1063/1.4963666.

   Role in this paper: I helped Mr. Wang to investigate problems and visualize data. In addition, I wrote a portion of the materials and methods section and edited the manuscript.

7. S. Kheiri, **M.G.A. Mohamed**, M. Amereh, D. Roberts, and K. Kim, "Antibacterial efficiency assessment of polymer-nanoparticle composites using a high-throughput microfluidic platform," submitted to *Materials Science & Engineering C*, 2019.

   Role in this manuscript: I helped Mr. Kheiri to conduct experiments and analyze data. In addition, I reviewed and edited the manuscript.

8. H. Kumar, K.Sakthivel, **M.G.A. Mohamed**, E. Boras, and K. Kim, "Low Gelation Point Gelatin Methacryloyl Hydrogels for Stereolithography 3D Bioprinting," submitted to *Biomaterials*, 2019.

   Role in this paper: I helped Mr. Kumar to conceptualize the paper and visualize data. In addition, I wrote the introduction, a portion of the materials and methods section, and edited the manuscript.

**Conference Proceedings:**

1. **M.G.A. Mohamed**, and K. Kim, "A flow focusing-based special microfluidic configuration for cell-laden microgels production – experiments and simulation," *5th Annual Engineering Graduate Symposium*, Kelowna, Canada, February 2019.

   Role in this proceeding: I conducted all simulations and experiments, analyzed data, and wrote and revised abstract under the supervision of Dr. Kim. In addition, I gave an oral presentation.

2. **M.G.A. Mohamed**, S. Kheiri, S. Islam, and K. Kim, "An integrated high-throughput microfluidic platform to fabricate well distributed cell-laden gelatin methacryloyl microgels for injectable tissue engineering," *International Conference on Miniaturized Systems for Chemistry and Life Sciences (MicroTAS)*, Kaohsiung, Taiwan, November 2018.

   Role in this proceeding: I developed a novel microfluidic platform for fabricating cell-laden microgels. I conducted all experiments, analyzed data, and wrote and revised 4 pages abstract under the supervision of Dr. Kim.

3. **M.G.A. Mohamed**, S. Kheiri, S. Islam, Hitendra Kumar, Annie Yang, and K. Kim, "On-chip generation, photocrosslinking, and filtration of uniform microscale cell-laden hydrogel spheroids," *BC Regenerative Medicine Virtual Symposium,* Vancouver and California, October 2018.

   Role in this proceeding: I conducted all experiments, analyzed data, and wrote and revised abstract under the supervision of Dr. Kim. In addition, I gave a poster presentation.

4. **M.G.A. Mohamed**, S. Kheiri, S. Islam, and K. Kim, "An integrated high-throughput microfluidic platform to fabricate microgels with controlled cell distribution," *BC Regenerative Medicine Annual Symposium*, Vancouver, Canada, May 2018.

   Role in this proceeding: I conducted all experiments, analyzed data, and wrote and revised abstract under the supervision of Dr. Kim. In addition, I gave a poster presentation.

5. **M.G.A. Mohamed** and K. Kim, "High-throughput fabrication of cell-laden gelatin methacrylate microgels for tissue engineering," *Annual Meeting of Canadian Biomaterials Society*, Winnipeg, Canada, May 2017.

   Role in this proceeding: I conducted all experiments, analyzed data, and wrote and revised abstract under the supervision of Dr. Kim. In addition, I gave an oral presentation.

6. H. Kumar, **M.G.A. Mohamed**, E. Boras, and K. Kim, "Thermally Insensitive Gelatin-based Bioinks for Visible Light Stereolithography 3D Bioprinting," *International Conference on Biofabrication*, USA, October 2019.

Role in this proceeding: I helped Mr. Kumar to conceptualize the experiments and visualize data. In addition, I wrote the introduction, a portion of the materials and methods section, and edited the proceeding.

7. M. Sakr, **M.G.A. Mohamed**, S. Siddiqua, and K. Kim, "Bentonite Clay Nanocomposite Hydrogels for Tissue Engineering," *Western Canada Biophysics Conference*, Kelowna, Canada, September 2019.

   Role in this proceeding: I helped in conducting the experiments and the visualization of the data.

8. Z. Wang, R. Samanipour, **M.G.A. Mohamed**, K. Sakthivel, and K. Kim, "High-throughput semi-automatic microdroplet generation and characterization system," *Canadian Society for Mechanical Engineering International Congress*, Kelowna, Canada, June 2016.

   Role in this proceeding: I helped Mr. Wang to investigate problems and visualize data. In addition, I wrote a portion of the materials and methods section and edited the proceeding.

## Table of Contents

## List of Tables

## List of Figures

## Acknowledgments

First and foremost, I would like to express my enduring gratitude to my supervisor, Dr. Keekyoung Kim, for his continuous guidance and support. He has been an invaluable source of inspiration and encouragement. He patiently provided me with invaluable advice and ideas in research and in life.

In addition, I would like to extend my enduring gratitude to Dr. Mina Hoorfar and Dr. Ian Foulds for providing guidance and many great ideas throughout this research period.

I would like to sincerely thank my great friends at the "Advanced Biofabrication Laboratory." I wish all of them the best in his life and career.

I cannot acknowledge my wife enough for her continuous kindness and support.

## Dedication

To my mother, who is not able to see this thesis completed, and to my beloved family; my father, sisters, wife, and kids for their ongoing love and support.

# Chapter 1： Introduction and Literature Review

Tissue engineering entails the combination of materials, mechanical, chemical, and biological engineering and sciences to recreate tissue structures that could repair or even replace lost biological function.[1,2] Within tissue scaffolding structures, cells can grow under biologically favorable conditions.[3] Ideally, upon being transplanted *in vivo*, the scaffolds gradually degrade and are replaced by the new desired tissue.[1] The artificial tissues were first transplanted in 1964 and carried cells to minimize complications resulting from immune rejection that might occur post-transplantation.[4] The encapsulated cells were also able to effectively implement their intended therapeutic works to the surrounding environment, which include tissue regeneration and *in situ* production of proteins.[5] Biofabrication is defined as "the automated fabrication and subsequent tissue maturation processes of biologically functional products from living cells, bioactive molecules, biomaterials, cell aggregates such as micro-tissues, or hybrid cell-material constructs, through bioprinting or bioassembly techniques".[6] Biofabrication relies on technologies that can accurately control the position of cells and materials because the end product is usually complex and has multiple elements including cellular and structural components. These biofabricated constructs can be used in a wide variety of applications from testing platforms for high-throughput drug screening to studying cell biology.[7] Moreover, the biofabrication is considered as a major methodology for the future of tissue engineering and regenerative medicine to treat or replace diseased or damaged tissues and organs.[8]

## 1.1 Bottom-up Biofabrication

In conventional macroscale "top-down" tissue engineering, cells are cultured within a biodegradable polymeric scaffolding material (Figure 1-1).[9] As the scaffold degrades over time, cells grow and produce their own extracellular matrix (ECM) in the process to create the engineered tissue. However, macroscopic approaches often fall short of adequately

creating the intricate microstructure of native tissues, which is an essential requirement for the realization of the successful functionality of engineered tissues.[10,11] Moreover, culturing cells within such macroscale scaffolds often results in limited cell-cell communication and inefficient exchange of oxygen, nutrients, and metabolites. In comparison, the "bottom-up" biofabrication approach aims to create biomimetic engineered microtissues by manipulating the microstructural features (Figure 1-1).[9] This strategy mainly has benefits of the high surface-area-to-volume ratio that is a characteristic in a microscale domain. This allows for the efficient exchange of oxygen and nutrients and enhances cell-matrix interactions.[11] For these reasons, such biomimetic constructs are more suitable for realizing properties of the native extracellular matrices of cells.

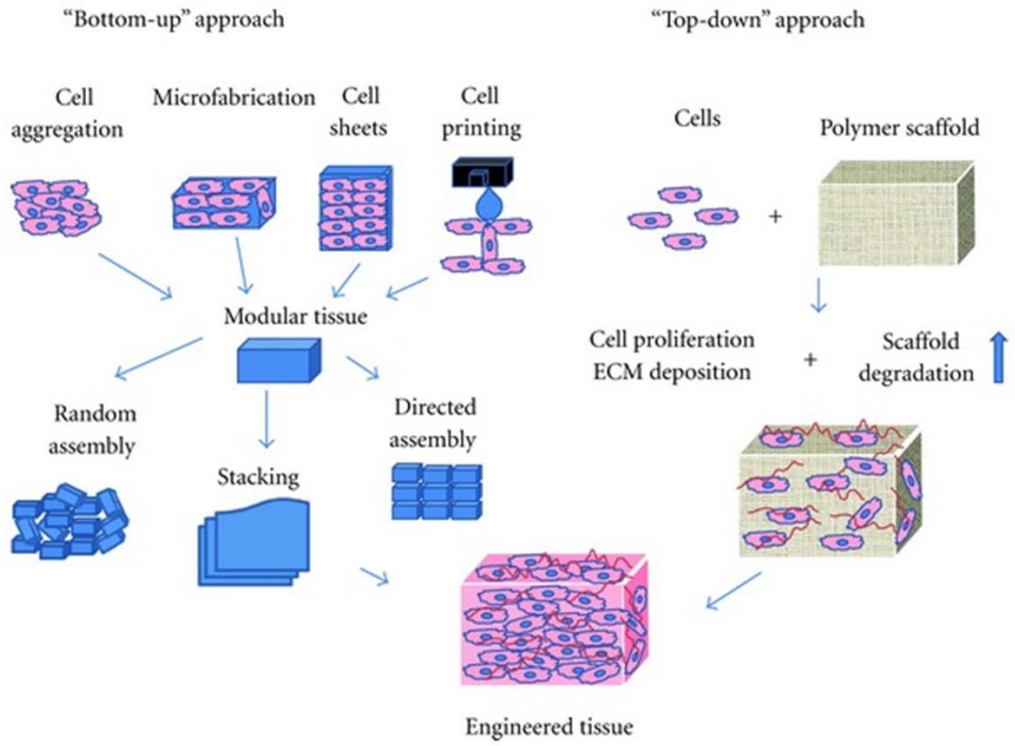


**Figure 1-1. "Top-down" tissue engineering approach and "Bottom-up" biofabrication approach. In the top-down approach (right), cells are cultured within scaffolds until the cells fill the structure, creating an engineered tissue. While, in the bottom-up one (left), multiple microscale processes are used for modular tissue creation, which is to be assembled into macroscale engineered tissues with precise microarchitectures. Images are adapted from ref. 9.**

Conventional methods for encapsulating cells in microgels, such as emulsification, extrusion, or co-extrusion methods, are limited with regards to fabricating small-sized microgels (≤ 100 μm) with high monodispersity.[5,10] In order to address these problems, microfabrication techniques including microfluidics, micro-molding, and soft lithography have been developed to fabricate microscale hydrogels that are ready for encapsulating cells. These microscale cell-laden hydrogels have become quite valuable for a wide range of studies probing cell differentiation, cell-cell interaction, cell-environment interaction, shear forces imposed on cells,[12] and 3D tissue structures.[9] For the successful bottom-up biofabrication of tissues, the investigation of microscale environmental parameters for cells is crucial. For example, the porosity and stiffness of extracellular matrix (ECM) have been observed to affect cancer cell migration, and thus constructs mimicking such a tissue must take these parameters into consideration.[13] Cell fate is also influenced by various microenvironmental cues, such as cell-cell interaction, accessibility to growth factors, mechanical stimuli, and shear forces.[14] Therefore, in the following sections, we review the various facets of platforms and biomaterial synthesis methods for improving the efficiency of bottom-up biofabrication. We discuss the most widely used microfluidic device configurations for generating cell-laden microgels and the challenges that these devices are currently faced. In addition to the tissue regeneration-related applications, the various other applications of microgels are discussed. Then, hydrogel biomaterials involved in biofabrication process are discussed with an emphasized analysis of the photocrosslinkable gelatin synthesis process.

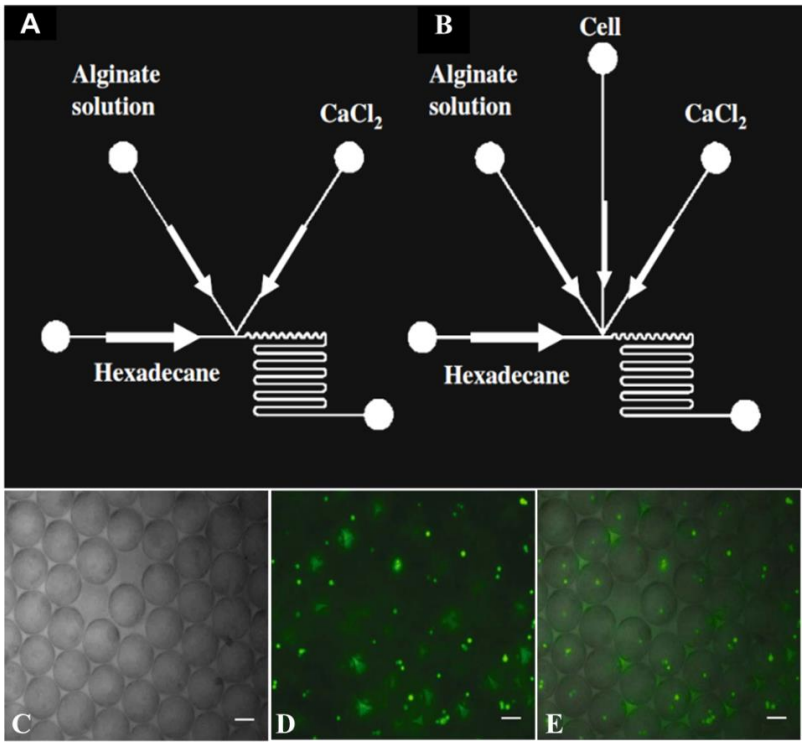


**Figure 1-2. T-junction devices for cell-laden microgel generation. (A) A diagram of a T-junction microfluidic device with two injection lines for microdroplets generation. (B) A diagram of the same device with an extra line for cell encapsulation. (C-E) Microscopic images of microbeads encapsulated with fluorescent-labeled yeasts (green); (C) an optical image, (D) a fluorescence image, and (E) a combined image. Images are adapted with permission from ref. 15.**

## 1.2 Platforms for Cell-laden Microgel Fabrication

### 1.2.1 T-junction Microfluidic Platforms

T-junction microfluidic devices are widely used for droplet generation due to the advantages of easy fabrication and operation.[16–19] In the T-junction configuration, the dispersed phase enters through the side channel, while the continuous phase enters through the main channel. The continuous phase, which intersects with the dispersed phase at the junction, leads the tip of the dispersed phase flow to the main channel. The shear stress of the continuous phase and the pressure gradient make a thin neck of the dispersed phase at the junction and finally break

a droplet.[20] The size of droplets can be controlled by the flow rates and viscosities of the dispersed and continuous phases, as well as the geometry of the channel.[20,21]

As one of pioneering studies that applied T-junction microfluidic devices for cell-laden droplet generation, Choi *et al.* demonstrated a method to fabricate alginate microgels using a T-junction device.[15] After alginate and calcium came into contact to form droplets, they were polymerized via chaotic mixing in the microfluidic device (Figure 1-2). Furthermore, the effects of the continuous phase flow rate and non-dimensional capillary number on droplet size and droplet distribution were discussed in this study. In a similar study, Tan *et al.* fabricated alginate droplets with a narrow size distribution using a new method that combined internal gelation with the T-junction microfluidic device.[22] Calcium carbonate ($CaCO_3$) nanoparticles were mixed in the Na-alginate solution to induce the internal crosslinking process. Droplets were formed at the T-junction and sheared off to the channel by a corn oil with lecithin. At the downstream of the T-junction, an acidic corn oil mixed with lecithin and acetic acid merged with the mainstream that carried the Na-alginate droplets with $CaCO_3$. The pH reduction due to the acidic corn oil released $Ca^{2+}$ from $CaCO_3$, which reacted with Na-alginate to form Ca-alginate gel downstream. Um *et al.* reported the formation of cell-laden hydrogel droplets by applying a double T-junction device.[23] This device consisted of three inlets, the pre-gel solution was entered into the first inlet, and the oil phase (mineral oil) into the second one in order to cut off the pre-gel solution and generate droplets. Downstream in the channel, a cell containing medium was introduced into the third inlet and then mixed with the droplets. Then, the hydrogel beads with cells were polymerized by ions in the cell medium.

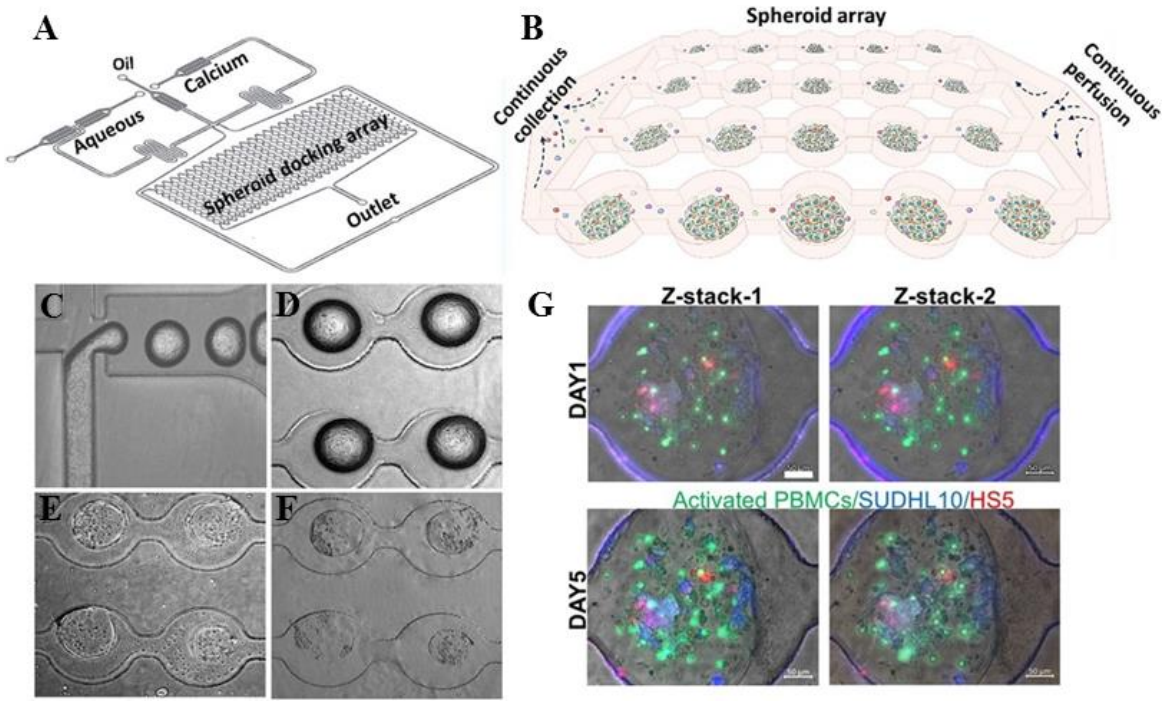


**Figure 1-3. T-junction-based microfluidic platform for anti-cancer screening. (A) A diagram of the device for generation and analysis of 3D lymphoma spheroids. (B) Illustration of a cell spheroid docking microarray device. (C) Representative micrographic pictures of the T- junction for generating cell-laden hydrogel microdroplets. (D) Docking droplets in the microarray device. (E-F) The crosslinked and cultured microgel spheroids at day 1 and day 5, respectively. (G) Representative images of fluorescently labeled spheroids to show cell proliferation for 5 days. Scale bars =50 µm. Images are adapted from ref. 24.**

Several studies have investigated cell behavior using the cell-encapsulated microgels generated by the T-junction microfluidic devices. Kumachev *et al.* used a T-junction microfluidic device to fabricate 3D microgels with varying stiffness in a high throughput way and investigated the influence of the cellular microenvironmental stiffness on cell fate.[25] Recently, Pooja *et al.* reported the development of a T-junction-based integrated microfluidic platform for the high-throughput generation of cell-laden microgels for anti-cancer therapeutic screening of the diffuse large B cell lymphoma (DLBCL) spheroids (Figure 1-3).[24] These spheroids consisted of cancer cells, fibroblasts, and lymphocytes in a hydrogel combination of alginate and PuraMatrix™ (Corning Inc., Tewksbury, MA, USA). The pre-

gel microdroplets encapsulating the cells were generated at the T-junction and were then driven into an integrated docking microarray that could house 250 cell-laden micro-spheroids. Calcium chloride in a complete growth media was perfused to crosslink the pre-gel droplets, which allowed for *in situ* microgels polymerization while maintaining their spherical structure.

### 1.2.2 Flow-focusing Microfluidic Platforms

Flow-focusing devices are another class of microfluidic devices that are used for droplet generation.[26–29] Although the fabrication of flow-focusing devices is slightly complex in comparison to those of T-junction devices, with the flow-focusing devices, it is possible to obtain better monodispersity in higher frequencies.[30] The flow-focusing devices often offer droplet generation frequencies up to approximately one thousand hertz (Hz). Also, by varying the fluid flow rates, it is possible to yield a wider range of droplet sizes.[31–33] The flow-focusing device can also produce a jetting regime wherein the size of these jets can be regulated by modifying the flow rates.[34] This jetting regime can be used to fabricate fibrous structures.

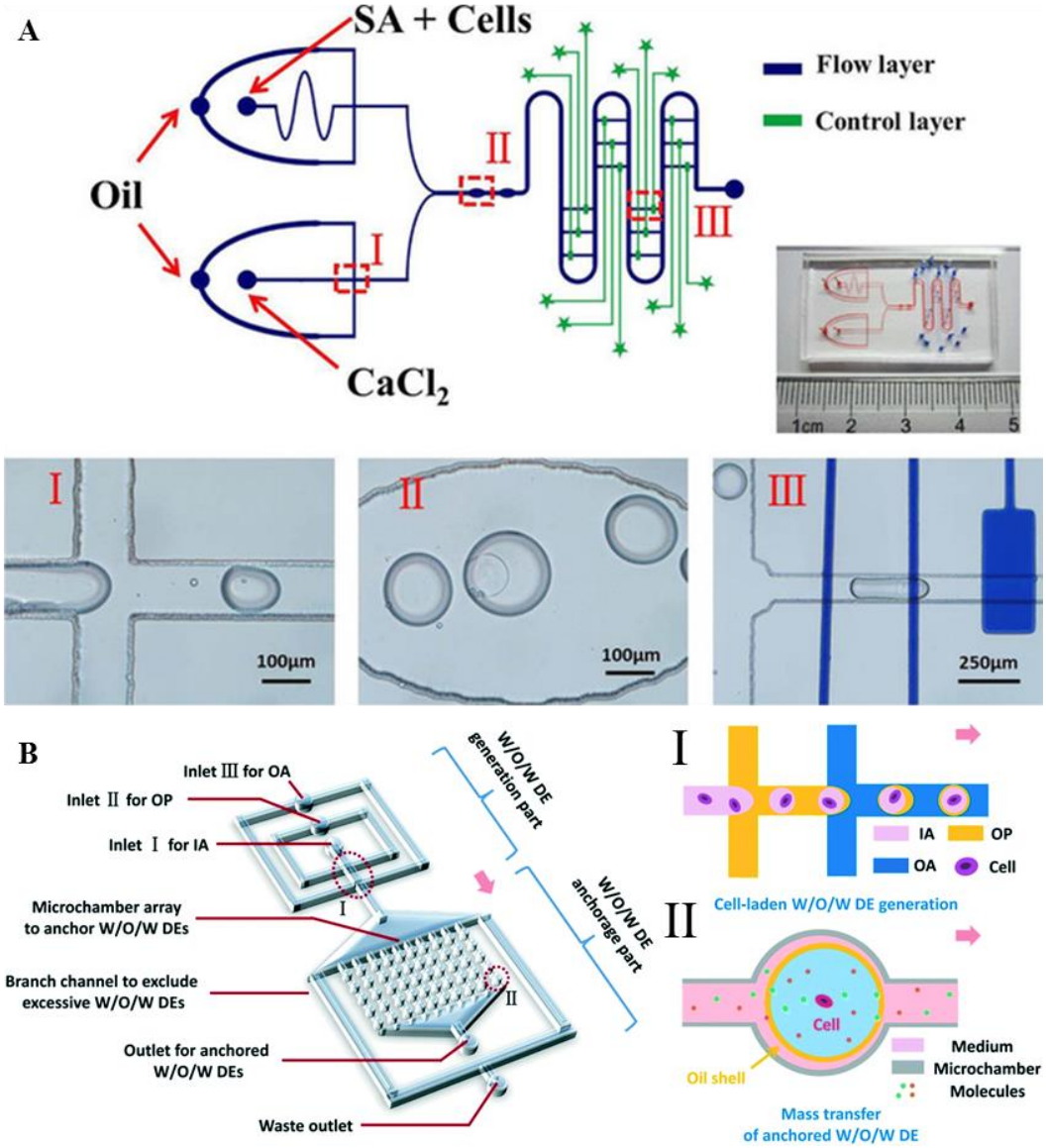


**Figure 1-4. A flow-focusing microfluidic device for cell-laden microdroplets generation and manipulation. (A) Schematic of the two-layer valve-based microfluidic platform. This device comprises of three functional parts: (I) 2 flow-focusing junctions for microdroplets generation, (II) on-chip hydrogel crosslinking chambers, and (III) the control part made of independently regulated valve-based trap-release units along the serpentine main channel. Images are adapted from ref. 35. (B) Schematics of the microfluidic platform for the generation, treatment, and monitoring of water in oil in water (W/O/W) cell-laden double emulsions (DEs). The platform consists of 2 adjacent flow-focusing junctions for (I) DE generation and (II) a DEs anchorage microarray. Images are adapted with permission from ref. 36.**

Many studies have been conducted on creating cell-encapsulated microgels using a flow-focusing microfluidic geometry. As shown in Figure 1-4A, a valve-regulated device

with double flow-focusing junctions was fabricated to integrate on-chip cell immobilization and treatment with the generated, gelled single cell-laden alginate microdroplets.[35] In another study, water-in-oil-in-water double emulsions with encapsulating single cells were generated in two sequential flow-focusing junctions (Figure 1-4B).[36] These microdroplets were subsequently anchored in an array of microchambers located downstream for at least one week. This microfluidic setup allowed for the long-term treatment and *in situ* real-time monitoring of the non-adherent cell behaviors and responses. Edd *et al.* proposed the method to encapsulate a single cell into a monodisperse picolitre droplet using the microfluidic flow-focusing devices.[37] Kim *et al.* introduced a new type of the flow-focusing device that can enhance the cell viability via the rapid exchange of the oil phase.[38] When cell-laden alginate was crosslinked with calcified oleic acid, this toxic oleic acid was transformed into harmless mineral oil, and then flushed out. They later introduced a three-dimensional flow-focusing device to generate a core-shell microcapsule for an efficient cell spheroid formation, which was achieved by adding a hillock to the device.[39] Wu *et al.* presented an integrated device with fluorescently activated sorting to increase the rate of single-cell encapsulation.[40] This device consisted of two segments: a flow-focusing component for generating droplets and a cross-shaped hydrodynamic gating for sorting droplets. Hydrogel droplets were created in the flow-focusing part, after which droplets carrying a single cell were detected at the hydrodynamic gating part and isolated in the reservoir.[40] Capretto *et al.* reported the formation and characterization of alginate/agarose microdroplets for the encapsulation of Sertoli cells using a flow-focusing device.[41] The cell viability and functional capability of Sertoli cells encapsulated in microgels were high, demonstrating the effectiveness of such a flow-focusing device for cell encapsulation. Allazetta *et al.* used a microfluidic flow-

focusing device to synthesize PEG microgels. Different chemicals were added to the reactive PEG to modify it with tethered biomolecules in order to adjust their bioactive properties and employment with different stem cell types.[42] Köster *et al.* fabricated a new microfluidic flow-focusing device that consolidates all functions into a chip including encapsulation, incubation and manipulation of cells in a picodroplet. The development of integrated microfluidic cell cytometers and sorters on the chip can further increase its functionality.[43]

## 1.3 Applications for Cell-laden Microgels

### 1.3.1 3D Microscale Cell Culture

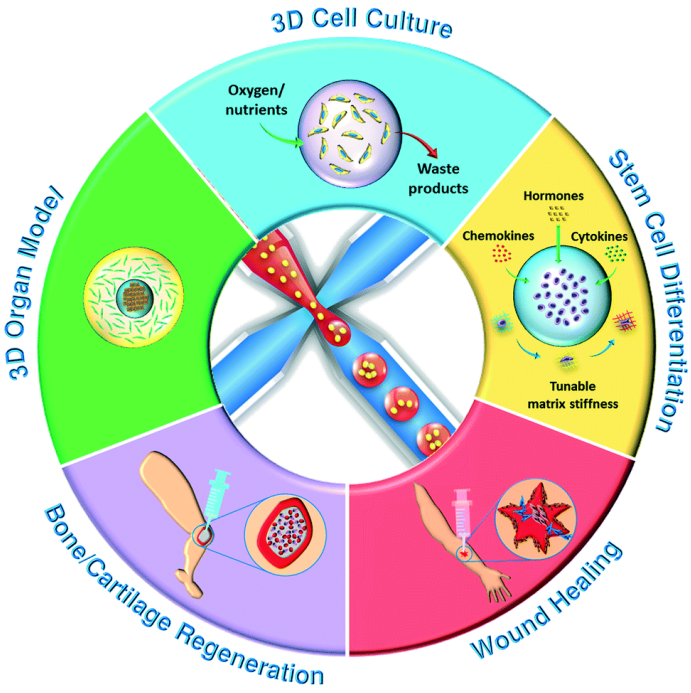


**Figure 1-5. Overview of cell-laden microgels in various biomedical applications. Adapted with permission from ref. 44.**

3D cell culturing is one of the main applications of cell-laden microgels (Figure 1-5). As reported by many previous studies[45,46] and review articles,[47–49] the 3D cell culture can

mimic *in vivo* native tissues more accurately and is more suitable for enhancing cell functionality. There have been many examples in previous literatures dedicated to use hydrogel droplets as platforms for carrying out 3D cell culturing, including 3T3 fibroblasts culturing in gelatin methacrylate hydrogel[50] and in collagen-gelatin with controllable mechanical properties,[51] murine embryonic stem cells within alginate,[25] and mesenchymal stem cells within PEG.[52] The droplet-based method has become well-accepted 3D cell culturing platforms.[53, 54] Due to the ease of droplet generation, cell-laden hydrogel droplets have become one of the most popular building blocks for the rapid construction of desired tissues.[55]

Utah *et al.* presented a method to crosslink the alginate-based droplet homogeneously for 3D cell culturing.[56] This provided a more uniform and highly controllable way to polymerize droplets without any unintended gelation. Experimental results have shown the cell viability of mesenchymal stem cells to be around 83% right after encapsulation. Recently, microfluidics-assisted annealable 20 wt% GelMA beads (B-GelMA) were fabricated to develop a microporous environment with decoupled porosity and stiffness for promoting 3D cell adhesion, spreading and proliferation (Figure 1-6A-D).[57] In this study, microfluidically generated GelMA microgels were physically crosslinked at 4°C in cold water, after which they were streamed to shape a scaffold structure and chemically annealed later. This innovative approach reaps the advantage of the orthogonal thermos-chemical responsivity of GelMA to decouple the effects of porosity and stiffness in 3D tissue engineering applications. B-GelMA, as opposed to bulk GelMA of the same concentration, exhibited remarkably high cell viability and fast 3D seeding. In a similar study, jammed microgels were used as an ink for extrusion printing, with the aim of demonstrating an

alternate approach for regular hydrogel-based 3D bioprinting (Figure 1-6E-G).[26] This approach could design tissues that can exhibit a range of properties through the individual microgels (e.g., composition, size) and the mixing them together.

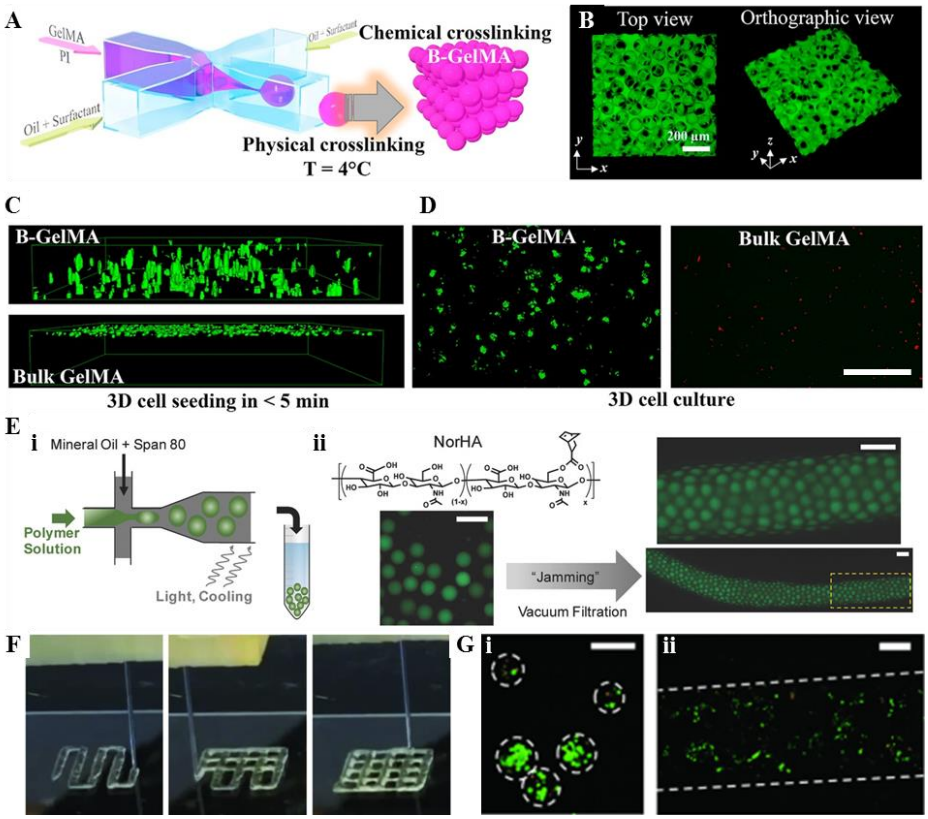


**Figure 1-6. Cell-laden hydrogel droplets for 3D cell culture. (A) Schematic of GelMA microbead generation in a flow-focusing microfluidic junction. (B) GelMA beads (B-GelMA) scaffolds pore characterization. (C) Side view fluorescence images showing on top three-dimensionally seeded HUVECs. Image dimensions ~1550 μm×1550 μm×254 μm. (D) Representative fluorescent images of live/dead cell viability assay of 3D encapsulated NIH/3T3 cells in 20% w/v B-GelMA scaffolds (live cells: green and dead cells: red). Scale bar = 500 μm. Images (A - D) are adapted with permission from ref. 57. (E) Jammed microgel ink fabrication. (i) Microdroplets were generated on a flow-focusing microfluidic device. (ii) Suspended microgels (left) that were then jammed through vacuum filtration into an extrudable solid ink (right). Scale bars = 200 μm. (F) Extrusion-based printing of lattice structures with the jammed microgel ink. (G) Representative fluorescence viability images of the 3D cell-laden microgels (i) before and (ii) after jamming and extrusion. Scale bars = 200 μm. Images (E - G) are adapted with permission from ref. 26.**

Microgels could be composed of different materials including thermos-sensitive agarose, photo-crosslinked PEG, and thiol-ene crosslinked hyaluronic acid. More importantly, the jamming and printing processes have not affected the viability of encapsulated cells. Crosslinking (wherein an additional crosslinker and photoinitiator were added) was done by exposing to a UV light when further stabilization for inter particulate crosslinking was needed.

Matsunaga *et al.* developed a rapid way to build millimeter-scale tissues via molding cell-laden microgels.[58] The cell-laden microgels were placed into a PDMS mold wherein cells were either mono-cultured or co-cultured within the microgels for several days. After 17 hours, the cells were spread out, filled the space between the microgels, and formed a 3D tissue structure. However, this method is not suitable for long-term culturing since the cells fully fill the space between microgels, which results in a lack of room for nutrients and oxygen supply. Due to the consequent insufficiency of oxygen and nutrients, cells positioned within the inner parts of the tissue begin to die.[59] A potential solution to resolve this problem is to integrate a microvascular network with the droplets during the molding process.[60,61] This can be achieved by building microchannels for nutrition supply after the formation of the microscale tissues.

In addition to tissue generation, the cell-laden hydrogel droplets can be utilized for repairing damaged tissues.[62–64] After generating and culturing cell-laden hydrogel droplets, they were injected to fill the space of damaged tissues. The droplets ultimately fused with nearby tissues and repaired the damaged area. Injectable cell-based therapy offers the advantages of a patient-friendly procedure[64] and high viability for the formation of large-scale tissues.[63] Chung *et al.* reported that mouse pre-adipocytes encapsulated in porous

microgels were injected and the injected microgles exhibited histological features to native adipose tissues within four-weeks.[63] Studies also reported the ability of hydrogel microgels to maintain and accommodate the differentiation of stem cell types.[65] Neuronal differentiation from cancer stem cells in alginate beads[66] and neural stem cells in matrigel core-alginate shells[67] have been successfully demonstrated.

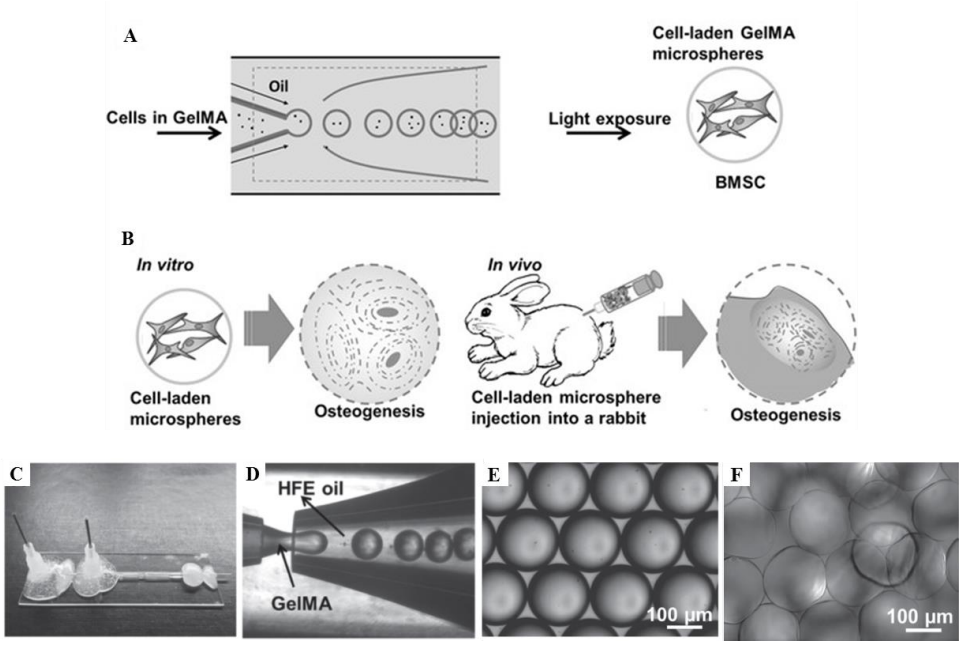


**Figure 1-7. Stem cell-laden microspheres for osteogenic tissue engineering. (A) Schematic diagrams of GelMA microgel fabrication and (B) osteogenesis of bone marrow stem cell in GelMA microgels. (C) Pictures of co-axial flow microfluidic device, (D) droplet generation process, (E) generated microdroplets in oil, and (F) crosslinked microgels. Adapted with permission from ref. 68.**

Mesenchymal stem cells (MSCs) are the most widely used stem cells to study differentiation within microgels.[69,70] Their differentiation potential into osteogenic, adipogenic, myogenic, and chondrogenic pathways has been well documented, while being encapsulated within various kinds of hydrogels, including a collagen–alginate composite, hyaluronic acid, and alginate. Moreover, MSCs have also been used to promote osteogenic differentiation by the inclusion and release of BMP-2 osteogenic growth factor (Figure

1-7).[68] Similarly, embryonic stem cells encapsulated in the microgels have also been employed for a wider range of differentiation studies due to their inherent pluripotency.[71–74] ESCs have been studied in the differentiation into hepatocytes, pancreatic cells, and cardiomyocytes while being encapsulated within various hydrogel materials such as liquid core–alginate shell, alginate, and PEG microgels.

### 1.3.2 Platforms for Studying Cellular Interactions

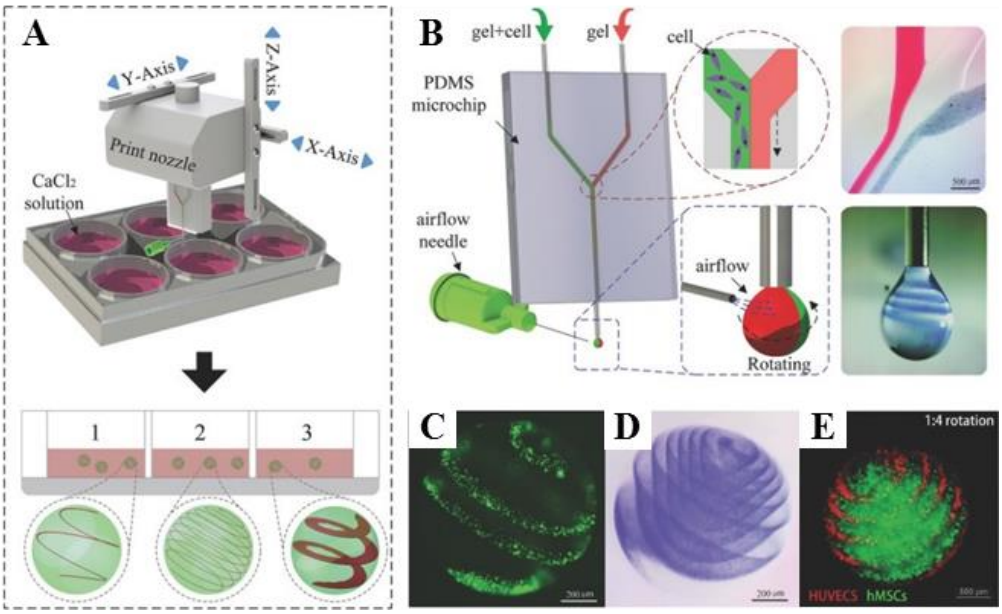


**Figure 1-8. A platform for studying micro-environmental control. (A) A schematic of the setup for the 3D fabrication of versatile spiral microarchitectures within microgels with an airflow-assisted microfluidic nozzle. (B) A schematic illustrating the proportional laminar extrusion of alginate solutions out from a microfluidic nozzle and the applied tunable airflow for microdroplets designed rotation. (C) Pictures of a spherical microgel and (D) rose-like microgel. (E) A fluorescence image of co-cultured HUVECS and HMSCs in a spatially controlled spiral-based microspheroid microenvironment. Images are adapted with permission from ref. 75.**

One of the most important advantages of microfluidic droplet generation is the ease of microenvironmental control.[55] For this reason, hydrogel microgels are also widely used in cell co-culturing systems to study cell-cell intraction.[76] As shown in Figure 1-8, 3D

fabrication of versatile spiral microarchitectures within microgels with an airflow-assisted microfluidic nozzle has been reported.[75] This method enabled to produce heterogeneous microgels that carried different cell types in asymmetrically separated compartments of controlled micro-tissues. Due to the laminar flow in microfluidics, adjacent different solutions with distinct boundaries can flow in the microfluidic channel.[77] Taking advantage of this property, alginate pre-gel mixtures with or without cells were extruded to form an droplet, while an accurately set airflow rotated the droplet and tuned originally parallel jets inside the droplet to different arrangements as it grew. These microdroplets were then immediately gelled in a $CaCl_2$ solution. By controlling the fluidic parameters, the microarchitecture inside and outside the microgels could be arranged on demand. In this study, mesenchymal stem cells and human umbilical vein endothelial cells were co-cultured in a complicated microenvironment of the microgels and subsequently the spatially controlled osteogenesis and angiogenesis were realized.

Matsunaga *et al.* co-cultured different types of cells in collagen-based droplets and screened their attachments and interactions.[58] The various cell types were co-cultured, including NIH 3T3 fibroblasts, primary neurons, human umbilical vein endothelial cells (HUVECs), primary rat hepatocytes, as well as MIN6 pancreatic cells. One cell type was encapsulated in collagen droplets, followed by the seeding of another type of cells on the surface of the droplets. Towards the same objective, Tumarkin *et al.* presented a comprehensive study of cell-cell and cell-biochemical interactions.[78] In this study, factor-dependent cells (MBA2) and reactive blood progenitor cell lines (M07e) were encapsulated together at different ratios. The viability of the M07e cells was regulated by the presence of paracrine signals proportional to the MBA2 cell population since M07e cell viability was

dependent on interleukin-3 (IL-3) which was generated by MBA-2 cells. Experimental results showed that as the ratio M07e and MBA2 cells decreased, the cell viability increased significantly. Shepherd *et al.* demonstrated a simple method to fabricate droplets containing various chemicals.[79] The focused laminar flow of different chemical compositions formed droplets without mixing the co-flowing chemicals. This was achieved using low flow rates and small channel dimensions.

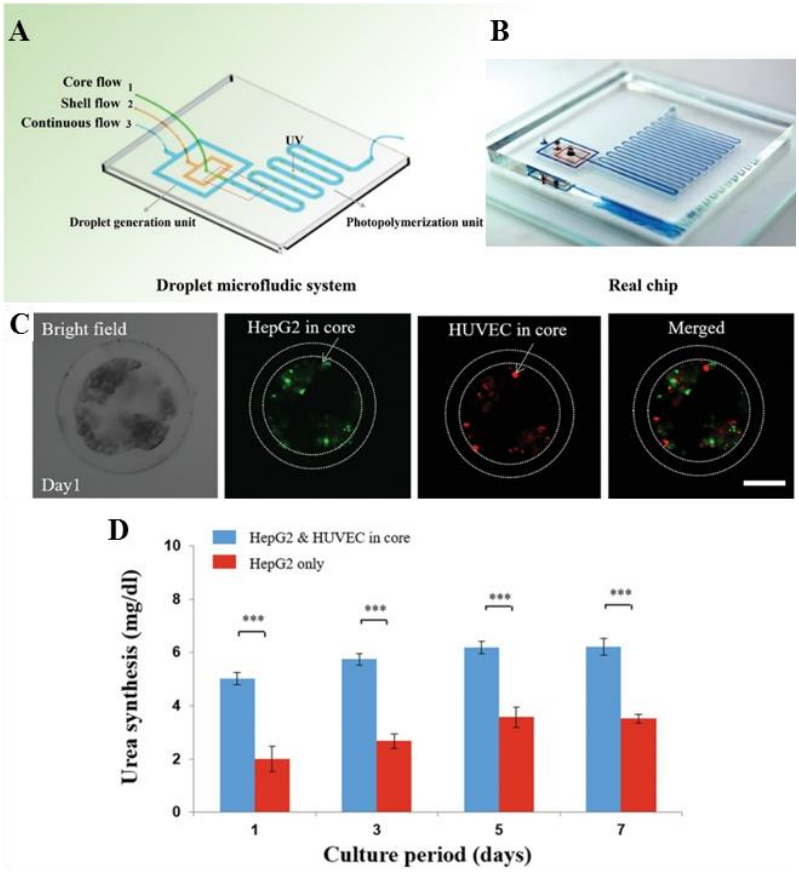


**Figure 1-9. A platform for studying cell-cell interactions. (A) Schematic of the microfluidic-based one-step fabrication of methylcellulose core–GelMA shell microgels. (B) A photograph of the fabricated chip. (C) Bright-field and fluorescence microscopic images of the co-cultured HUVECs and HepG2 cells at day 1. Scale bar = 100 µm. (D) Comparative evaluation of the effect of co-culturing and mono-culturing conditions on the urea synthesis of HepG2 cells at days 1, 3, 5, and 7. Images are adapted with permission from ref. 27.**

The laminar stream flow was interrupted by the oil flow to form Janus-like droplets (hemispherically distinct) with multiple-chemicals. These Janus droplets can be used to study cell response to certain chemicals since such droplets simulate *in vivo* chemical and mechanical anisotropies more accurately.[55,79,80] More recently, Wang *et al.* demonstrated the use of a flow-focusing microfluidic device for the one-step generation of methylcellulose core–GelMA shell microgels (Figure 1-9).[27] The encapsulated liver cells exhibited high viability for 15 days, thus demonstrating the good biocompatibility of the system. The microgels were then used to evaluate the co-culturing of HepG2 liver cells and HUVECs vascular endothelial cells within the cores of the microgels. As shown in Figure 1-9D, the level of urea production from hepatic cells in the co-culture system was found to be significantly higher than from the same number of the hepatic cells in monoculture, which expounds the role of cell-cell interactions.

## 1.4 Challenges in Microfluidic-based Microgel Fabrication

Microfluidic-based cell-laden microgels have become a high-throughput, highly tunable, and cost-effective method for bottom-up biofabrication. Despite many exciting results being realized, current microgels still have many limitations. A reasonable distribution of cells among the generated microgels was not achieved, while it is important to have uniformity and reproducibility in any subsequent applications.[81–83] The cellular encapsulation process causes high disturbance in the droplet generation process, affecting the monodispersity of the microgels in a significant extent.[81,84] Moreover, controlling cell encapsulation density is very important to address the principal concerns for assembling macroscale tissues for the bottom-up biofabrication approach. Since the cell-laden microgels are used as building blocks, the number of cells per building blocks governs the total cell density in the resultant constructs.[9]

Cell-to-cell distance and cell density are crucial factors, which determine the structural and functional characteristics of the engineered tissues.[44] Therefore, those factors are necessary to be controlled by the number of encapsulated cells per microdroplet in a consistent and reproducible manner. For example, about 220 billion cells are needed to construct a complete human liver.[44] Encapsulating more cells while maintaining both the size of cell-laden microgels and their monodispersity is essential since that can dramatically increase the biofabrication efficiency. However, most of the conventional microfluidic methods for fabricating microgels require the non-efficient off-chip processes of either crosslinking microgels or oil removal.

After the pre-gel droplets are generated in the microfluidic device, they are subjected to crosslinking. Traditionally crosslinking of the droplets is done through one of two ways, on-chip crosslinking and off-chip crosslinking. Off-chip gelation often involves a prolonged exposure to UV that is harmful to the encapsulated cells and reduces cell viability.[85] It is known that the UV light radiation can induce DNA damage or carcinogenesis.[86] In the contrary, the on-chip approach is better in terms of productivity, ease of handling, and cell viability.[87] The most common on-chip crosslinking method is chemical crosslinking of alginate hydrogels by adding ionic crosslinker through an additional inlet.[44,88] Both hydrogels and gelation methods are the major factor for determining further applications.[44] Cells do not adhere to alginate and the chemical gelation reaction may distort the droplets, negatively affecting the uniformity of microgel shape.[89] On-chip photocrosslinking with the UV light was employed by applying high-intensity UV for a short time (tens of seconds).[87] However, this process is affected by surrounding oxygen, which interacts with the free radicals of photoinitiators to prolong the gelation time.

**Table 1-1. Summary and comparison of the on-chip microgels filtration strategies.**

| Filtration Method | Technique | Challenges | Refs. |
|---|---|---|---|
| Fluid exchange with the use of filter blocks | Exchanging the oil phase by infusing the aqueous phase through multiple side channels while the microgels are retained by the filter blocks. | • Complex multiple inlets and outlets channel configuration<br>• High possibility to have clogging problems due to 90˚ angle of the washing phase inlet to the oil inlet and the filter blocks<br>• Unstable oil–aqueous interface | 90 |
| Extraction chamber with the use of filter blocks | The retained microgels by the filter blocks being collected by sinking into an aqueous chamber | • Additional fabrication of the aqueous chamber (requiring two-step lithography processes), increasing fabrication difficulties<br>• Possible clogging problems | 91 |
| Oil sacrificial layer employment | Applied a thin oil layer around microgels, which dewet from the microgel surface when in contact with an aqueous solution | • The manual fabrication of the glass capillary device limiting fabrication throughput, parallelization, and reproducibility of droplets<br>• The oil layer preventing microdroplets from gelation by the chemical agents<br>• Require washing step in a separate off-chip unit | 92 |
| The interfacial tension between oil and microparticles | Microgels being dragged into the aqueous phase when contacting a stable oil-aqueous interface by the interfacial tension | • The required conditions being impractical as it demands the microgels having a certain size and mechanical stiffness under a stable oil-aqueous interface with the limitation of surfactant use | 93 |

Another challenge in the microfluidic-based microgels fabrication is the oil filtration. The traditional method to separate microgels from the oil phase is based on the several cycles of centrifugation and washing with aqueous buffers.[65,90,91,94] The high speed and long duration of centrifugation required as compared to normal cell culturing. This process significantly reduces the viability of the encapsulated cells and the yield of the produced

droplets. In addition, the prolonged contact with the oil phase results in the reduction of cell viability. To avoid theses problems, on-chip approaches, as summarized in Table 1-1, have been recently developed to translocate the hydrogel microdroplets from the oil into an aqueous phase. Among them, a filtration method uses an oil sacrificial layer that immediately dewets from the microgel surface when it is in contact with an aqueous solution.[65,92] However, the presence of oil layer prevented microdroplets from gelation by the chemical crosslinking agents. Deng *et al.* developed a filtration method using the fluid exchange of the oil phase with the aqueous phase by infusing through multiple side channels.[90] The presence of filter gates helped to filter and to transfer the hydrogel microdroplets into the aqueous phase separated from the oil phase. With another design by applying the same concept of fluid exchange and filter gates, the droplets could also be collected in an aqueous solution chamber.[91] However, these methods could be applied either to only alginate hydrogel that can be chemically crosslinked in the chip or to a separate filtration device. The addition of another device can result in additional fabrication processes that increase fabrication difficulties. With a simple channel device under specific conditions, the microgels could be dragged into the aqueous phase when they were contacted to a stable oil-aqueous interface by the interfacial tension force.[93] However, the specific conditions are impractical in most cases since the microgels have to be certain sizes with specific mechanical stiffness and under a stable oil-aqueous interface with the limited use of the surfactant. All these approaches are impractical, adversely affect cell viability, or increase the fabrication difficulties, requiring new methods to be developed.

## 1.5 Materials for Bottom-up Biofabrication

### 1.5.1 Hydrogels for Biofabrication

Advances in biofabrication technologies for tissue regeneration require the development of highly reproducible biomaterials that can be used to regenerate or replace injured tissues.[95,96] Hydrogels have been used extensively for a wide range of tissue engineering and biofabrication applications in recent decades.[97] Bioinks for 3D bioprinting are usually hydrogel-based solutions that can encapsulate various cell-types and bioactive molecules.[95,96] Hydrogels are hydrophilic polymeric networks that can absorb high volumes of water without dissolving.[98] Their porous nature, immense water-absorbing power (90% of their weight), and tissue-like elastic property make it possible for cells to easily attach to them, receive oxygen and nutrients, and grow.[99,100] In addition, they are useful for the efficient encapsulation of cells and growth factors applicable for the minimally invasive transplantation.[28,101,102] For these reasons, hydrogels have received considerable attention in recent years for applications in tissue engineering as well as biofabrication.[100,103]

Hydrogels can broadly be classified as belonging to two categories; synthetic (initially synthesized in the laboratory) and natural (obtained from natural resources). Both synthetic and natural hydrogels are widely used because of their porous structure and good biocompatibility.[104] Natural hydrogels, can either be proteins (gelatin, collagen, and fibrin) or polysaccharides (alginate, hyaluronic acid, Chilton and agarose) and form networks via physical or ionic interactions. Whereas synthetic hydrogels consist mostly of polyethylene glycol (PEG), polyacrylic acid (PAA), and polyvinyl alcohol (PVA), and are synthesized by a radical chain or step-growth polymerization and therefore have covalent bonds as their networking force.[105,106] Hydrogels also display varying characteristics that depend on their

polymerization method and the resulting structure. These, in turn also influence cellular functions of encapsulated cells, such as growth, migration, and differentiation. Each hydrogel-type possesses its own set of advantages and drawbacks. Natural hydrogels are inherently biocompatible and promote many cellular functions. However, extra equipment is often needed to extract them from biological tissues, which only yields limited volumes. They also tend to lack in variety, while their usage remains limited to specific cells. Synthetic hydrogels, in comparison, are highly reproducible and readily available. Moreover, their composition can be tuned as needed for diverse cell lines,[107] and their protein absorption tendency, limited.[108] The most important advantage of synthetic hydrogels, however, is the controllability of their mechanical properties and biochemical cues.[98,109]

Crosslinking methods are essential for the gelation of both synthetic and natural hydrogels and are dependent on hydrogel-type. For instance, photosensitive materials such as methacrylated silk fibroin (Sil-MA), polyethylene glycol diacrylate (PEGDA), and gelatin methacrylate (GelMA) are crosslinked via exposure to light (e.g., UV),[110–112] while thermally sensitive materials (e.g., gelatin and agarose) solidify upon varying the temperature,[113] and ion-based materials (e.g. alginate) are crosslinked via divalent ions (e.g., Ca2+).[114–116] Recently, high-throughput production of monodisperse bioactive polyethylene glycol microgels applying a parallelized step emulsification technique was reported.[117] In this study, the crosslinking of the microdroplets was initiated via the dissolved proton acceptors in the oil phase, which ensured the uniform physicochemical properties of the generated microgels. However, such a crosslinking reaction is lengthy and requires to be incubated overnight. Moreover, in the study, cells were not encapsulated in 3D but seeded in a 2D orientation on the surface of the already crosslinked microgels. The cell-bearing microgels were then

covalently interconnected by an enzymatic reaction to construct a microporous scaffold wherein the cells were observed to occupy the interstitial spaces in 3D.

Ideally, in tissue-engineered graft transplantations, hydrogels degrade over time as cells replace the pre-existing structure with their own extracellular matrix. Natural hydrogels such as collagen, gelatin, fibrin, and chitosan are biodegradable. However, it is possible to modify non-degradable hydrogels such as PVA and PEG and render them degradable by adding hydrolysable esters[118] or peptide functionalities[119] in the crosslinking agents. During the degradation process, a hydrophilic backbone of the polymer chains is broken down by enzymatic activity.[120,121] As the gel breaks down, then again, the crosslinker protein is digested.[122] Through the course of the process, the hydrogel mass reduces and its mechanical stability decreases. Consequently, the newly desired tissue then replaces the transplanted cell-encapsulating hydrogel. Degradability is, therefore, a particularly important characteristic of hydrogels that must be studied before applying them for tissue engineering.

### 1.5.2 GelMA Hydrogel for Biofabrication

The selection of appropriate biomaterials is crucial for the realization of a realistic microenvironment for cells where they can migrate, proliferate, and differentiate normally, and subsequently form healthy tissues.[123] The ideal biomaterial is biocompatible, displays appropriate mechanical properties, and is manufactured through an efficient production technique.[124] GelMA is a photopolymerizable biomaterial that can be used along with biocompatible photoinitiators at different wavelengths of light, including those comprising visible light.[125–129] This property has enabled the creation of photo-patterns with high

fidelities, the fabrication of 3D microtissues, and the creation of 2D structures for in-vitro cell studies.[80,125,126,129,130]

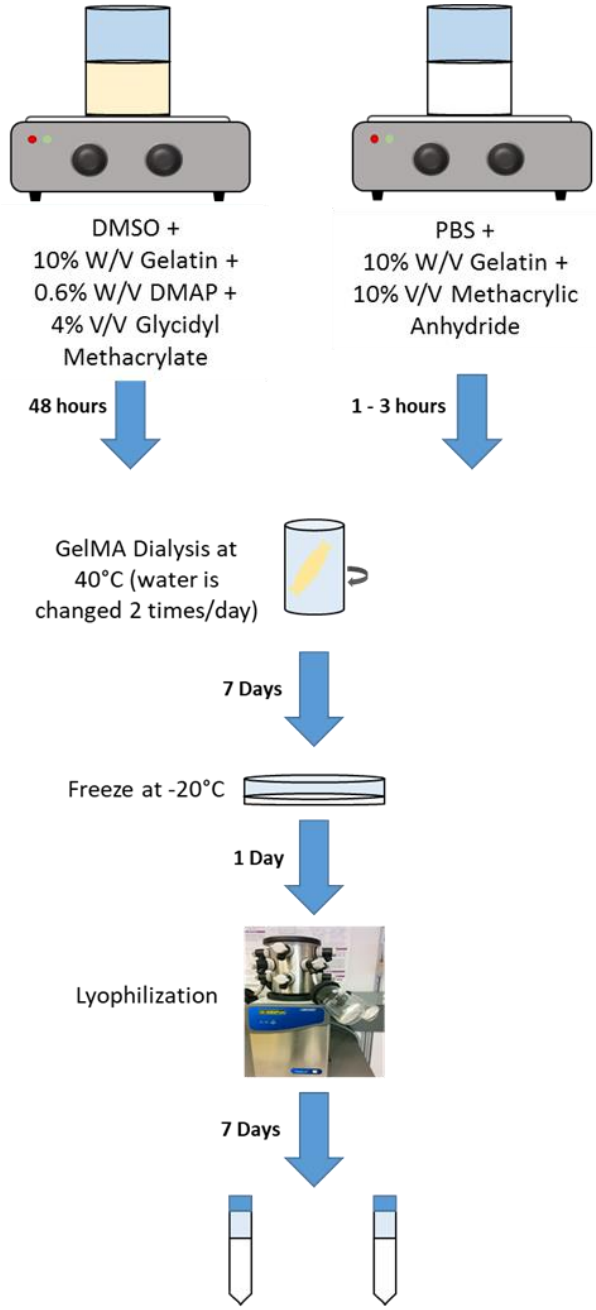


**Figure 1-10. Conventional GelMA Production Methods**

GelMA has been employed towards tissue engineering applications such as bone tissue engineering,[131] breast cancer treatment,[132] 3D biofabrication,[133] corneal stromal tissue

engineering,[134] 3D microtissue fabrication,[135] and cartilage tissue repair.[136] However, the synthesis process for GelMA is not fully characterized and is hardly reproducible, leading to high batch to batch variation. Furthermore, the process is time-consuming and highly laborious.[137,138] Contemporary synthesis processes last around 2 weeks, which is also a significant reason as to why GelMA is quite expensive to obtain commercially at about CAD 270/g.[137,139] In the commonly practiced GelMA synthesis methods (Figure 1-10), a gelatin solution is prepared in either dimethyl sulfoxide (DMSO) or phosphate-buffered saline (PBS).[137,140] This is followed by the addition of either a 4 %V/V of glycidyl methacrylate to a DMSO based mixture or 10% V/V of methacrylic anhydride to a PBS based one. It should be noted that different combinations of reagents are used according to specific chemical and physical compatibilities. For example, methacrylic anhydride is incompatible with DMSO in the presence of dissolved gelatin whereas glycidyl methacrylate is only moderately soluble in water.[141]

It takes longer for the reaction between glycidyl methacrylate and Gelatin in DMSO to take place (2 days) as compared to the reaction between methacrylic anhydride and gelatin in PBS (1-3 hours). This is mainly a result of the lower volume% of glycidyl methacrylate that is used relative to the volume% used of methacrylic anhydride. After the reaction, the reacted mixture is dialyzed against reverse osmosis (RO) water. The dialysis is conducted for about a week at 40°C. Subsequently, the dried GelMA is obtained after freeze-drying the mixture for several days. The dehydration step is also time-consuming and ensues high capital equipment costs, which is a primary motivation in minimizing process times.[142]

During GelMA synthesis, the gelatin backbone accepts the substituting methacryloyl groups from the methacrylating agent on its amino acid residues' primary amines and active

hydroxyl groups, as shown in Figure 1-11. Increasing the reaction volume of the glycidyl methacrylate to the same level as methacrylic anhydride, while anticipating a comparable reaction time to the PBS reaction mixture, is a challenge. To be stoichiometrically equivalent to the volume% of methacrylic anhydride, it is required that the volume% of glycidyl methacrylate be increased to 18% V/V (considering the densities, the molecular weights and the fact that each mole of methacrylic anhydride gives 2 units of methacrylate while each mole of glycidyl methacrylate gives only 1 unit). This very high-volume increase would make the elimination of the glycidyl methacrylate more difficult by dialysis.

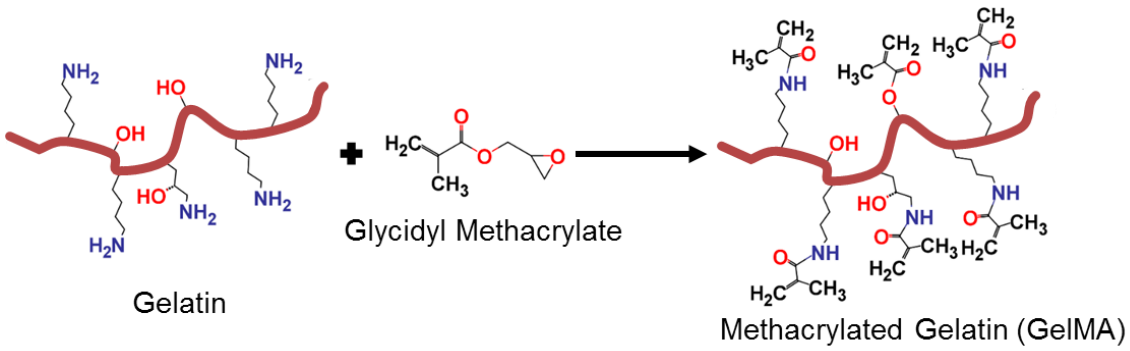


**Figure 1-11. Schematic of the chemical reaction of gelatin and glycidyl methacrylate for conjugating methacryloyl groups during GelMA synthesis.**

Additionally, it would also mandate prolonged dialysis for purification, especially when considering the moderate solubility of glycidyl methacrylate in water. This is particularly important since the concentration of glycidyl methacrylate needed for the methacrylation of one gram of gelatin is only around 1% V/V. Furthermore, the excess amount of glycidyl methacrylate (3 - 17% V/V) that is used to speed the reaction will remain in the solution mixture.[143] On the other hand, methacrylic anhydride is more soluble in water as compared to glycidyl methacrylate. Although using higher volumes of methacrylic

anhydride makes it possible to perform the dialysis purification of the PBS solution mixture within a week, it is known to be considerably toxic. It should be noted that performing the dialysis at relatively warm temperatures (≃ 40°C) exposes the protein to degradation risk.[137] Carrying out the dialysis at 35 to 40°C has been previously observed to result in a large reduction of the reaction yield.[144] This yield ranges widely from 18% to 72%, demonstrating a large inconsistency. This is one of the major reasons for the poor reproducibility and the high batch to batch variation that is observed in synthesized GelMA. As an alternative, the dialysis process could be performed at 4°C to minimize degradation[137], though; this may entail operational difficulties and result in an extended dialysis time as diffusivity reduces at lower temperatures. It can be inferred from above that the main hurdles preventing the GelMA synthesis process from being time-efficient, economical and reproducible are, therefore, the detoxification and dehydration steps.

Solvent precipitation is usually used to extract protein samples from aqueous solutions. However, protein loss and hydrolysis are known to be inevitable consequences.[145] For example, the extraction efficiency for 6 out of 10 standard proteins has been observed to be ≤15%.[146] In addition, because of the high polarity of water, high volumes of the organic solvents are required to precipitate the hydrophilic proteins. Thus, this was found to be less efficient on the basis of resulting in a high, and more importantly, reproducible yield, while also requiring much higher volumes of the precipitating organic solvents.[144] More considerably, the samples still required dialysis to get rid of the toxic by-products of the reaction, which reduced the cost effectiveness of the process further. Moreover, if that aqueous-based reaction solvent is a buffer solution (like PBS or bicarbonate buffer)

purification is not entirely possible, as most of these buffer salts have very poor solubility in organic solvents, which in turn mandates further dialysis after precipitation.

Freeze-drying (FD) and spray-drying (SD) are the most widely used drying methods for protein solutions. Freeze-drying, also known as lyophilization, is the process of drying a frozen solution by sublimating the solvent medium under appropriate temperatures and pressures.[147,148] The lyophilization is the method of choice for drying GelMA, as well as for other materials, which are susceptible to inactivation or chemical degradation at temperatures higher than ambient. Freeze drying is carried out at low temperatures, which minimizes thermal decomposition in proteins. It is also possible to control the sterility and the concentration of particulate contents levels by sterile filtering the solution directly, before dispensing it into containers for storage. Although the process can be carried out without the need for solid handling in subsequent steps, the freeze-drying process is relatively expensive due to the long processing times (typically several days), high energy consumption, and the high cost of equipment.[142] The process also results in inadequate batch sizes limiting its large-scale application. Freeze-drying is also well documented to cause batch-to-batch variation and heterogeneity within batches, which is attributed to fluid-dynamics and radiation.[149–151] The optimization of a given freeze-drying process necessitates the development of a suitable formulation, as well as the characterization of the heat and mass transfer setup of the dryer and the container system.

Spray-drying is the process wherein a dry powder can be produced from a liquid material solution through its atomization into a hot gas medium. The particle sizes of the formed powder are distributed narrowly within the micron to submicron levels. Considering the high production costs and long drying times of FD, SD could be considered a favorable

alternative.[152,153] It is remarkable that the efficiency per kilogram of material when freeze-dried is about 10 times lower than when spray dried.[154] Therefore, in contrast to FD, SD offers a higher throughput as a continuous process that is reproducible, scalable, and which can produce powders suitable for direct processing without the need for milling or further secondary processing.[152,155] Despite the high temperatures that are applied, this dehydration process does not cause any extensive thermal degradation, even for heat-sensitive materials, due to the considerably short exposure times (seconds to milliseconds). However, for protein solutions that are sensitive to heat, research in the food and pharmaceutical sciences have demonstrated that thermal, and air interface-related stresses cause inactivation or denaturation to a fraction of the spray-dried proteins.[156–158] Usually, the yield of conventional spray-dryers is low and irreproducible, ranging from 20 to 70%.[159–161] This is mainly because of powder loss witnessed in the drying chamber and the inability of the cyclone to collect the very fine particles.[162–164] Since a smaller amount of powder is lost in proportion to the total volume produced under a large scale production, the scale of work is another factor that determines yield.[165,166] To surpass a yield of 70%, a thorough optimization of the formulation and process parameters is mandated.[167] There is also an emergent need for biomaterials that are easy-to-handle and ready-to-use in a modified production system that does not involve drying.

### 1.6 Motivation and Objectives

This thesis work is directed towards tackling the inefficiencies facing bottom-up tissue engineering. The main modules of such a system that challenge its general productivity include (i) the low-throughput generation of microgels in a microfluidic device, (ii) the detoxification of the polymeric hydrogel material, and (iii) the necessary purification,

sterilization, and dehydration steps. To efficiently produce microgels in a high-throughput way, this thesis presents an integrated microfluidic device that combines the steps of fabricating a microgel tissue construct on a chip. These production steps include the generation of cell-laden hydrogel precursor droplets, microdroplet crosslinking, and the separation of these microgels from oil. The integration of these three stages enables a high-throughput process that eliminates the need for handling the droplets off-chip. However, an efficient production of a cost-effective and highly functional hydrogel is a remaining challenge.

This moved us into a broader aspect that is common between nearly all biofabrication techniques; the efficient development of applicable biomaterials. The base hydrogel material for in this research is GelMA, which is sourced from gelatin obtained via hydrolysis from collagen. Upon the addition of methacrylate groups, the gelatin become photocrosslinkable to form a stable hydrogel. While collagen can be immunogenic, GelMA being a natural hydrogel and a product of protein hydrolysis does not elicit an immune response and is non-toxic.[168,169] Additionally, GelMA, unlike synthetic hydrogels and several natural ones, offers binding sites for cellular attachment and proliferation.[168,170] Nonetheless, the typical GelMA synthesis process is quite long and takes around 10 - 14 days to complete. The main hurdles preventing the GelMA synthesis process from being time-efficient, economical, and reproducible are the detoxification, sterilization, and dehydration steps. In addition, conventional GelMA production methods display variable batch to batch yields.

Therefore, the objectives of this thesis to develop highly efficient biofabrication methods for cell-laden gelatin methacryloyl hydrogels are:

■ **Objective 1.** To develop a stable continuous and integrated microfluidic platform for the high-throughput fabrication of cell-laden microgels with a high and consistent cell viability. This research aims to have a reasonable distribution of cells among monodisperse microdroplets and to reduce the loss of generated droplets throughout the subsequent fabrication steps. This is achieved by combining all production steps onto one chip that integrates all required processes, from droplet generation in a flow-focusing microfluidic junction, through on-chip photocrosslinking, to the separation of the droplets from the continuous oil phase.

■ **Objective 2.** To develop a new GelMA detoxification and collection method using the integrated, rapid, high yield, and sterile GelMA synthesis. This new method eliminates the dialysis-related variability in the properties of the hydrogel component and integrates the sterilization step with the purification process. In this work, the method is also compared to other well-established GelMA production techniques. The newly produced GelMA is characterized by yield rate, chemical (degree of methacrylation), physical (microstructure, mechanical properties, mass swelling ratio, and degradation), and biological (cell viability and morphology analysis) properties. Nonetheless, the efficiency of the production process is still affected by the mandatory drying step.

■ **Objective 3.** To develop a dehydration-free efficient production process of biocompatible, easy-to-handle, and ready-to-use GelMA prepolymer. This method leads to reduce the production time more than 95% from 2 weeks in the conventional methods to 4 - 8 hours as well as reduce the material costs around 90%. A rigorous investigation of various organic

solvents is conducted for the selection of the most suitable agent for the dehydration-free GelMA production process. We employed a tailored production method using toluene to eliminate the labor-intensive and time-consuming drying step as well as the dialysis and sterilization steps. The produced hydrogel exhibits high yield, adequate physical properties, and high cell viability.

## 1.7 Thesis Structure

Chapter 1 briefly introduce the bottom-up biofabrication technologies as compared to top-down tissue engineering. Then, microfluidics-based techniques for fabrication of cell-laden microgels as a major bottom-up biofabrication are reviewed. The various applications of cell-laden microgels and the major challenges are also elaborated. In addition, this chapter introduces biomaterials widely used in the biofabrication and especially focuses on GelMA hydrogels and its synthesis process which requires to be improved for highly efficient biofabrication process.

Chapter 2 describes the high-throughput generation of cell-laden GelMA microgels. The design, simulation, and fabrication of the integrated microfluidic flow-focusing platform for the on-chip fabrication and filtration of cell-laden microgels are elaborated. Approaches for having a practical cellular distribution among the microdroplets without affecting its monodispersity at various cellular seeding densities are discussed.

Chapter 3 presents the principals of the efficient detoxification process for GelMA production. This chapter explains the process design concept of the combined ion pairing and protein desolvation in a solvent medium of low polarity, and the necessitated backward changes to the methacrylation reaction conditions.

Chapter 4 illustrates the tailored dehydration-free GelMA hydrogel production method using toluene. Factors considered for selecting the appropriate organic solvent are discussed. The new GelMA synthesis strategy, the process, and the product characterization are elaborated.

Finally, Chapter 5 concludes the thesis with the summary of the entire works, describes the significance of contributions of this research, and suggests directions of future works.

## Chapter 2 : Integrated Microfluidic Fabrication Platform for Cell-laden Mirogels

This chapter presents the development of a stable continuous and integrated microfluidic platform for the high-throughput fabrication of monodisperse cell-laden microgel droplets with high and maintained cellular viability. This is through combining onto one chip all the required processes from the droplet generation in a flow-focusing microfluidic junction passing through on-chip photocrosslinking to the separation of the droplets from the continuous oil phase. These approaches resulted in having a reasonable distribution of cells among monodisperse microdroplets. Using this method of controlling cell encapsulation with on-chip crosslinking and oil filtration, highly efficient cell-laden microgel production is achieved. The presented integrated microfluidic platform can be a candidate for standard cell-encapsulation experiments and other tissue engineering applications.

### 2.1 Hydrogel Synthesis

GelMA is synthesized following the protocol reported previously.[171] Briefly, 5 g of gelatin from the porcine skin was added to 50 ml of dimethyl sulfoxide (DMSO), and the solution was stirred continuously at 50°C until the gelatin completely dissolved. Subsequently, 0.3 g of 4-dimethyl aminopyridine (DMAP) was slowly supplemented to the mixture to avoid aggregation. Glycidyl methacrylate (2 ml) was then added dropwise to acquire proper dispersion and prevent aggregation. The solution was stirred consistently at 500 rpm at 50°C for 48 hours. The mixture was later dialyzed against reverse osmosis (RO) water using a dialysis membrane (MWCO: 12-14 kDa, Spectrum Labs, Rancho Dominguez, CA, USA). The dialysis was conducted for 5 days at 40°C with a stirring speed of around 400 rpm, the water was changed twice a day. The synthesized GelMA solution was frozen, and the freeze-

dried product was then obtained via lyophilization for 3 days. The Dried GelMA is then stored at -20oC until further use. All materials were purchased from Sigma-Aldrich (St. Louis, MO, USA) unless otherwise specified.

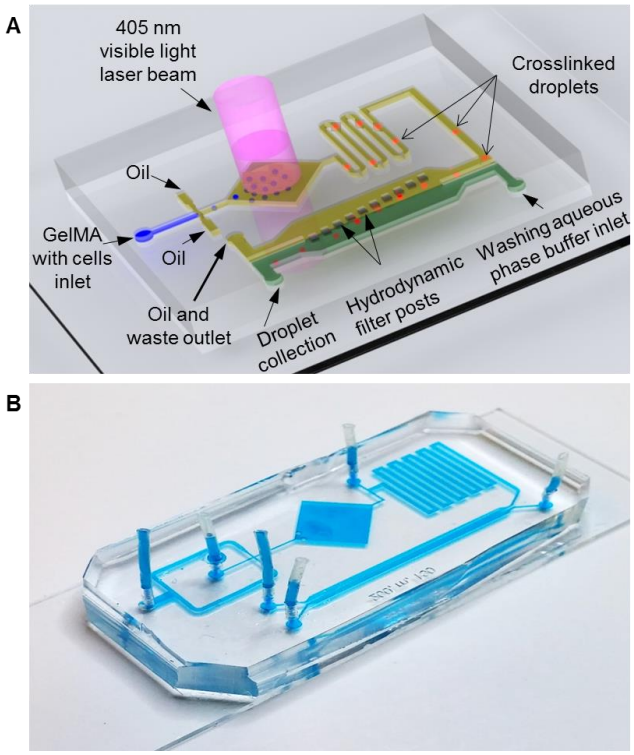


**Figure 2-1. Integrated high-throughput microfluidic platform. (A) Schematic of the integrated microfluidics platforms for the generation, crosslinking, and filtration of cell-laden GelMA microgels. The platform consists of three main functional parts—a flow-focusing junction for droplet generation, an on-chip photocrosslinking chamber, and a hydrodynamic filter for filtering oil. (B) Photograph of the microfabricated device.**

## 2.2 Design Optimization of the Microfluidic Device

Figure 2-1 shows an overview of the integrated microgel fabrication device and platform. The detailed layout and dimension of the device are also shown in Figure 2-2. The device consists of three main functional parts—a flow-focusing junction for droplet generation, an on-chip photocrosslinking chamber, and a hydrodynamic filter unit for filtering oil. A flow-

focusing nozzle is used for droplet generation and cell encapsulation. The 300 μm channel height of the device is designed for the stable generation of highly monodisperse hydrogel microdroplets with 250 μm in diameter. With this design, the stability of the droplet generation is maintained with the completely spherical shape of the droplets rather than the squeezed shape possibly in the short channel. The tall channel height coupled with a minimum channel width of 250 μm (at the flow-focusing nozzle), which is required for the designed microdroplet size, enabled the generated microdroplets not to contact with the channel walls. It also prevents the microdroplets from the friction to the walls that often causes merging droplets to form bigger droplets than the channel height.

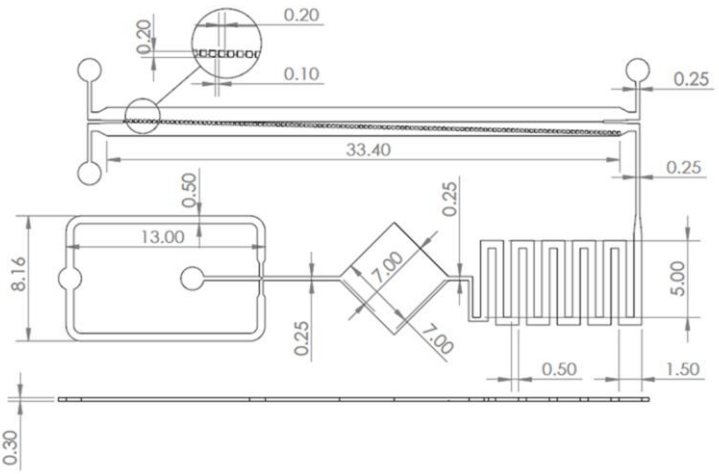


**Figure 2-2. Detailed dimensional layout of the integrated microfluidic platform (unit: mm).**

The microdroplets then pass through the crosslinking chamber where they are irradiated with a 405 nm wavelength laser beam (100 mW) for around 30 to 50 seconds. The laser diode was placed 7 cm above the microfluidic device to form a spot size of 5 mm in diameter. To provide enough crosslinking time of the microdroplets within the laser spot, we adopted a diamond-shaped crosslinking chamber design.[172] Design parameters of the

chamber, such as lengths of diagonal and each side, were optimized by COMSOL Multiphysics® software (COMSOL Inc., Burlington, MA, USA) to obtain sufficient travel time of the GelMA microdroplets from entering to exiting the crosslinking chamber (Figure 2-3). The device design configurations with different dimensions were designed in Solidworks. The 3D parts were created based on the height of the channels. The extension of the parts should be "x.t" or Parasolid to be importable to COMSOL software. The design was imported into COMSOL using import function in the GUI. For performing the simulation Creeping Flow was used. The inlet's and outlet's faces were selected and the condition for walls was selected as no slip. The mesh was generated automatically using COMOSL physics control mesh generator. The quality of mesh was then checked to be in the software. Average mesh quality was around 0.06 which is in the acceptable range based on COMSOL Manual. The creeping flow simulation was simulated in stationary to mimic the real case of the device. To study the droplets movement, "Particle tracing for fluid flow" package was used. The same inlet and outlet were selected. To simulate the droplets more like the real case "Drag force" was added to the domain. The computational simulations were done in time-dependent to check the droplet movement in different time sequences.

The obtained travel times with the 7 mm × 7 mm crosslinking chamber were 67 - 105 seconds based on the different flow rates. After laser illumination at the crosslinking chamber, the droplets pass through the serpentine channels to allow for sufficient time for complete gelation via the crosslinking chain reaction. The serpentine channels are designed to have enough length that gives the droplets around 90 seconds after exposure to the laser and before entering the filtration unit.

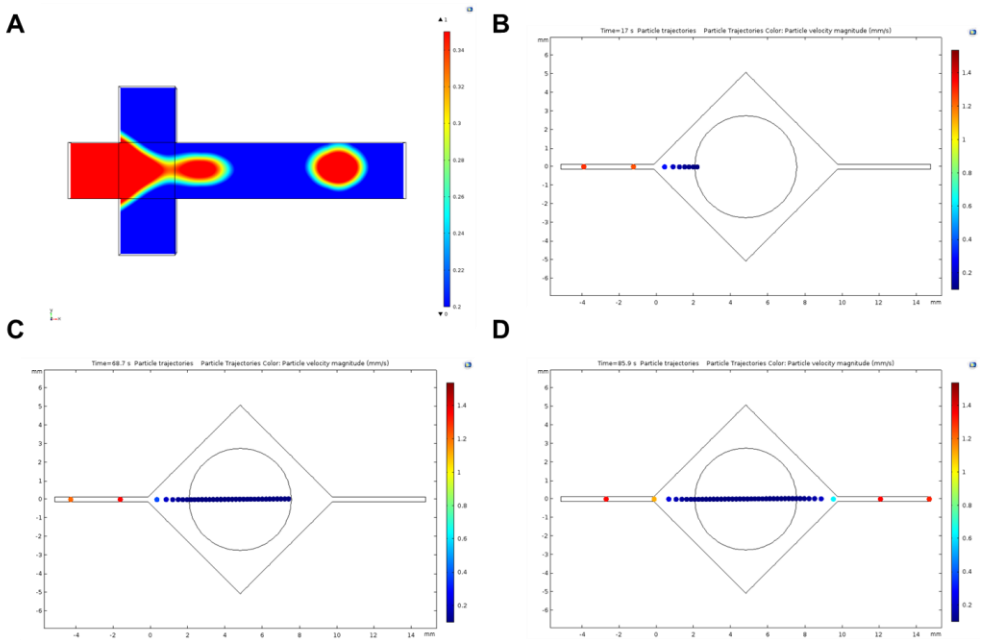


**Figure 2-3. Computational simulation results of hydrogel droplets generation and crosslinking. (A) GelMA prepolymer droplet generation at the flow-focusing cross junction (the color bar specifies the volume fraction of the dispersed phase). (B-D) Travel time estimation in the on-chip photocrosslinking chamber (diamond shape) with a laser beam spot (circular area). Droplets enter the crosslinking chamber (B), travel through the area of laser spot (C), and leave the crosslinking chamber (D).**

The droplets are then separated from the oil and suspended in an aqueous washing buffer solution (1.25% v/v of a water-based surfactant (Tween® 80, Sigma-Aldrich, St. Louis, MO, USA) in PBS) in the filtration unit of the device. The filter micropost design is adopted from the previous study.[173] The microposts are 200X200 μm squares with a 100 μm gap between each post that prevents microgels from passing through. The microposts are arrayed at an angle of 1˚ to the flow direction. This low angle helps the microgels move parallel to the flow direction of the oil and washing buffer smoothly, minimizing turbulence possibly caused by the hindrance of the microposts. Design parameters of the filter unit were optimized by COMSOL (Figure 2-4). Both the microposts and the addition of a water-based surfactant in the washing buffer enable smooth separation of the microdroplets from the oil. The filter unit channel is designed to be three times wider (1.5 mm) than the input channels

(0.5 mm) to reduce the oil flow rate and be able to gently separate the soft microgels without affecting their integrity.

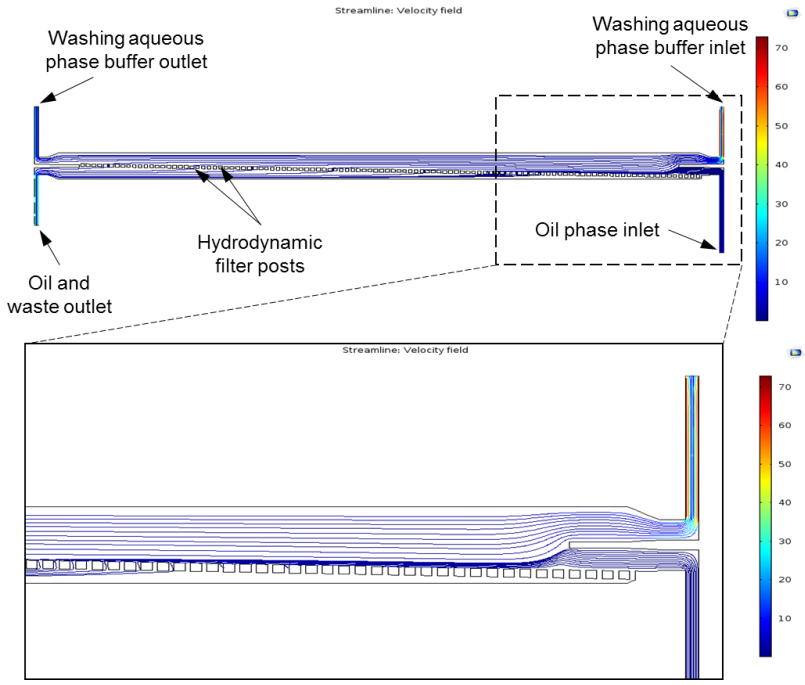


**Figure 2-4. Computational simulation results of the flow within the filter unit.**

## 2.3 Device Fabrication and Experimental Setup

Molds to form microfluidic channels were fabricated using a photolithographic technique in a class 100 cleanroom facility. A SU-8 2025 negative photoresist layer was spin-coated on a washed silicon wafer at 1000 rpm/sec for 30 seconds. The wafer was baked at 65°C for 5 min and then at 95°C for 10 min to remove the solvent. Spin coating and the two-step baking procedure was repeated twice to get microfluidic channels, 300 µm in height. A photomask with the desired patterns was then aligned on top of the wafer. Expose the wafer to UV light at 365 nm and intensity of 11 mW/cm2 for 40 seconds. Bake directly after exposure for 10 min at 95 °C. Immerse in a SU-8 developer for 12 minutes to remove unreacted photoresist. Soft lithography replica molding techniques were used to produce the microchannels. After

mixing thoroughly 10:1 polydimethylsiloxane (PDMS, SYLGARD® 184, Ellsworth Adhesives Canada, Stoney Creek, ON, Canada) to curing agent mixture was poured over the mold in a petri dish. It was then placed in a vacuum desiccator to remove bubbles. The mold was put in an oven at 70°C for three hours to cure the PDMS. The PDMS was then peeled from the mold. Tubing holes for the inlets and outlets of the device were punched. The PDMS substrate and a glass slide were exposed to oxygen plasma for 1 minute using an oxygen plasma treatment machine and then attached together. The microfluidic device was then placed in an oven at 70$^{o}$C for 5 hours.

The experimental set-up was placed on the stage of an inverted optical microscope to monitor the microdroplet generation (Figure 2-5). The aqueous dispersed phase consisted of PBS mixed with 7.5 % w/v GelMA prepolymer and 2% w/v photoinitiator (VA-086, Wako Chemicals USA, Inc., Richmond, VA, USA). The oil phase consisted of light mineral oil enriched with 20% v/v oil-based surfactant (Span® 80, Sigma-Aldrich, St. Louis, MO, USA) to prevent droplets from merging in the crosslinking chamber. The flow rate of GelMA polymer solution was kept constant at 1.12 μL/min while the flow rate of the oil phase was varied from 9 to 12 μL/min, resulting in GelMA microsphere droplets with diameters around 250 μm. The flow rate of the aqueous washing buffer solution was maintained at 150 μL/min in parallel to the oil flow.

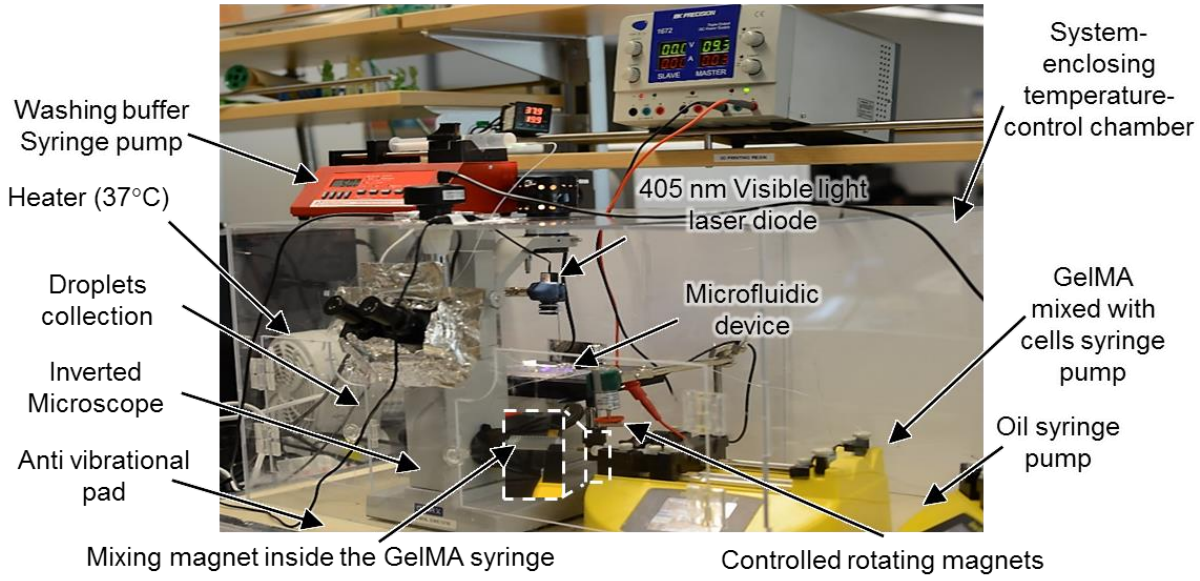


**Figure 2-5. The entire experimental system setup built around a microscope.**

## 2.4 Fabrication of Cell-laden Microdroplets

For cell encapsulation, NIH 3T3 fibroblasts were trypsinized from the cell culture flasks. Before mixing with the GelMA prepolymer solution, cells were treated with 1% bovine serum albumin (BSA) solution in PBS for 45 minutes with continuous swirling to avoid cellular aggregation. Four cell encapsulation densities ($2.5\times10^6$, $5\times10^6$, $10\times10^6$, and $20\times10^6$ cells/ml) were used. Microdroplets were generated at the flow-focusing junction of the microfluidic device. The aqueous phase (PBS solution of 7.5 % GelMA prepolymer supplemented with 2% w/v VA-086 photoinitiator) and the oil phase (20% w/v Span 80 surfactant in mineral oil) were injected into the inlets of the microfluidic device via plastic tubing connected to the syringe pumps that are controlling the flow rates and the droplets size. A magnetic mixer was applied to the aqueous phase syringe. As a control group experiment, we collected cell-laden microgels in oil without filtration and then removed the oil by using the centrifugation method (4500 rpm for 5 min). We did the centrifugation multiple times until the oil was completely removed from the microgels.

## 2.5 Biocompatibility Assessment

After incubation for 1, 3, and 5 days, the viability of the cells inside the microdroplets was examined using the live/dead cell viability assay (Biotium, Fremont, CA, USA) containing the fluorescent dyes, calcein-AM (green) and ethidium homodimer-1 (red). As per the manufacturer's instructions, encapsulated cells were washed twice with PBS. Cells were then stained by the dye solution after incubation in the dark for 20 minutes at 37 °C. Green-fluorescent live cells and red-fluorescent dead cells were imaged by using an inverted fluorescent microscope (Axio Observer 7, Carl Zeiss Canada Ltd., Toronto, ON, Canada). The obtained images of live and dead cells were quantified by using ImageJ software (NIH, Bethesda, MD, USA). Cell viability was measured as the ratio of live cells to the total number of cells.

Staining of the cell nucleus and the F-actin was done on day 5 using DAPI and phalloidin, respectively. After one wash with PBS, cells were fixed using 3.7% paraformaldehyde for 20 minutes, washed with PBS again, and then permeabilized by submersion in 0.1% Triton X-100 solution (VWR, Radnor, PA, USA) for 5 minutes. 1 ml of 100 nM solution of Phalloidin 488 (Cytoskeleton, Denver, CO, USA) was added, and the samples were incubated at room temperature, in the dark, for 45 minutes. The samples were then washed with PBS. A few drops of the DAPI (Fluoroshield with DAPI) mounting media were added. The fluorescent images were immediately taken with a fluorescence microscope.

One-way analysis of variance (ANOVA analysis) function in Microsoft Excel was used to analyze the data. The results were expressed as average + standard deviation, and statistical significance was accepted at $p < 0.05$.

## 2.6 Microgel Fabrication and Filtration

The dispersed phase of GelMA prepolymer microdroplets were generated in the continuous oil phase on the flow-focusing microfluidic junction part of the platform (Figure 2-6A). The 250 μm droplets were stably generated with a completely spherical shape rather than the squeezed shape. The shape of droplets becomes spherical due to the surface tension as long as the size of droplets is maintained smaller than the width and height of channels and thus the droplets are not squeezed. In addition, the generated droplets were not contacted with the channel wall and prevented from merging. This also allowed the droplets to be completely surrounded by mineral oil and away from the oxygen permeable PDMS channel wall during crosslinking. Thus, the generated free radicals for the photoinitiation process were only used for fast crosslinking reactions rather than reacting with the oxygen which delays the duration of crosslinking process. Also, the tall channel height slowed down droplet moving speed to have enough exposure time of the droplets under the laser beam for secure crosslinking. The GelMA concentrations are usually between the minimum concentration of 4% w/v for hydrogel formation and the maximum concentration of 10% w/v for promoting cell spreading and proliferation within the microgels. We chose the GelMA concentration of 7.5% w/v by considering reliable manufacturability and biofunctionality to enhance the integrity of microgels with cell growth and proliferation.

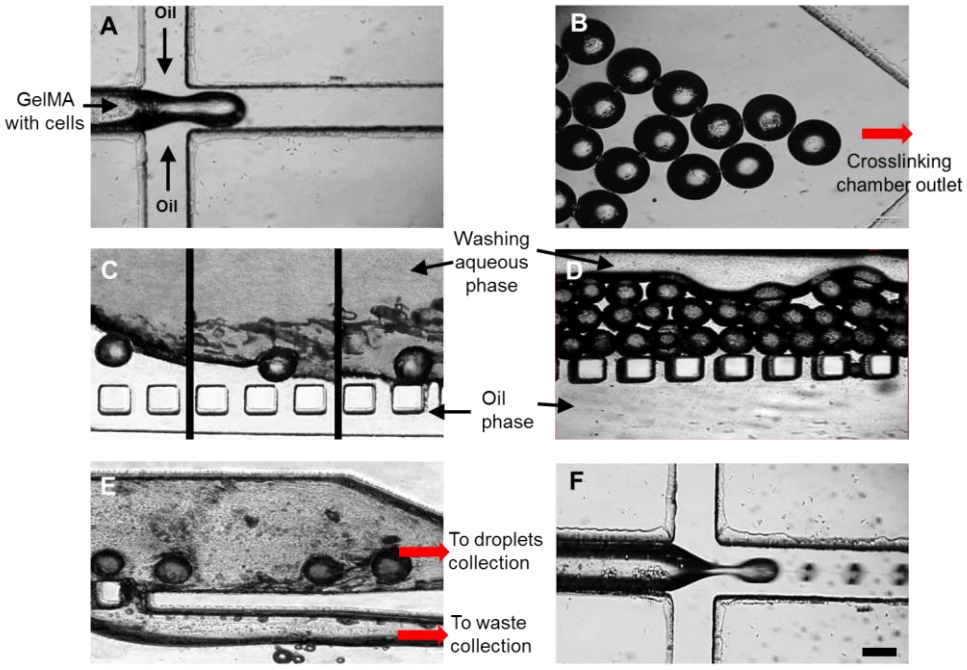


**Figure 2-6. Representative micrograph pictures for generating GelMA microdroplets. (A) Flow focusing junction for generating cell-laden microdroplets. (B) Photocrosslinking chamber with the crosslinked microgels moving toward the outlet after exposure to a laser beam. (C) Images show the railing microposts help microgels to pass the interface between the oil and aqueous buffer in the presence of surfactant. (D) An image shows that microgels are accumulated due to the inability to cross the interface between the oil and aqueous buffer in the absence of surfactant. (E) An image shows the end of the angled filter microposts array with the outlet fork to separate the microgel collection outlet from the oil waste outlet. (F) An image shows the instability of droplet generation due to cell aggregation in the absence of BSA and a cell mixer in the syringe. Scale bars = 200 µm.**

Flow rates of the aqueous prepolymer phase and the continuous oil phase were both important in regulating the microdroplet generation process. Thus, the flow rate of 1.12 µL/min for GelMA prepolymer and flow rate of 9 to 12 µL/min for mineral oil were maintained throughout the entire experiment to stably generate the droplet size of 250 µm in diameter throughout the different cell encapsulation concentrations as shown in Figure 2-6B. The droplet generation without fluctuation helped to keep the cell distribution across the GelMA microgels stable and constant. The crosslinking chamber as shown in Figure 2-6B, also plays an important role in fabricating monodisperse and reliable microgels. To provide

enough crosslinking time of the microdroplets within the laser spot, we adopted a diamond-shaped crosslinking chamber design.[172] In addition, one of the factors possibly affecting the crosslinking time is the PDMS thickness of the device as the laser intensity passing through the PDMS is decreased, and hence the crosslinking time is increased as shown in Figure 2-7. Incomplete crosslinking makes microgels much softer and squeezed into the gaps between the filter posts or damaged while passing the interface between the oil and the aqueous washing buffer in the downstream filtration unit. As the device was fabricated with 3.5 mm thick PDMS, both computational simulation and experimental results demonstrated that the crosslinking chamber allowed enough time for crosslinking microgels through the thickness of the PDMS.

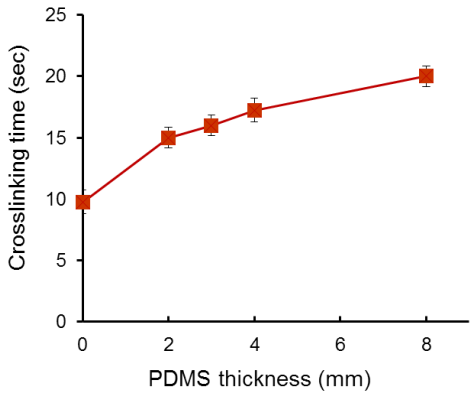


**Figure 2-7. GelMA crosslinking time under different thicknesses of PDMS pieces.**

The photoinitiator, VA-086, used in this research has an absorption peak of 385 nm, which is close to the wavelength of the laser diode.[174] This permits the initiation of crosslinking via visible light range with a relatively short crosslinking time (< 20 sec), avoiding the usage of harmful UV light. Concentrations up to 1.5% w/v were widely tested and proven to be biocompatible.[175–177] However, we found that 1.5% was not enough to completely crosslink GelMA microgels, resulting in that the microgels were escaped through

the filter microposts or dissolved in the washing buffer while transiting from oil the phase. This is due to that in microscale the inhibition effect of crosslinking chain reaction due to the existence of oxygen is more critical.[178,179] This happens even in the enclosed microfluidic chamber because of the oxygen permeability of the PDMS.[180,181] Therefore, we have used the concentration of 2% w/v to ensure full crosslinking of the microgels. VA-086 is known to be more biocompatible than other commonly used photoinitiators in tissue engineering.[176,182] However, it was previously reported that VA-086-based photocrosslinking process in a macroscale level generates nitrogen gas bubbles within the hydrogels, which makes it unfavorable for tissue engineering applications.[127] This does not happen on the microscale since the small droplet size allows the gas to rapidly diffuse out, preventing the formation of bubbles (Figure 2-6B). It is also worth noting that the laser diode is also much more cost-effective light source than the high-intensity UV light, which is widely used in tissue engineering.

Figure 2-6C shows the transfer of the microdroplets from the oil phase to the aqueous washing buffer phase in the presence of tween 80, while Figure 2-6D shows the accumulation of microdroplets in the oil phase due to the absence of tween 80 in the washing buffer. The low angle (1°) of the arrayed micropost rail to the filter channel helps the microgels move parallel to the flow direction of the oil and washing buffer smoothly, minimizing turbulence possibly caused by the hindrance of the microposts. Both the microposts and the addition of a water-based surfactant in the washing buffer enable smooth separation of the microdroplets from the oil. The water-based surfactant reduced the interfacial tension between the oil and the aqueous washing buffer phases. Tween 80 was selected due to its proven biocompatibility with many cell types for up to 24 hours of

contact.[183,184] An effective flow rate (150 μL/min) of the washing buffer was determined by the flow rate and the viscosity of the coming oil phase at the entrance of the filter unit, and the viscosity of the washing buffer phase. Considering these factors, the filter unit was designed to be three times wider (1.5 mm) than the input channels (0.5 mm) to reduce the oil flow rate and be able to gently separate the soft hydrogel microdroplets without affecting their integrity. Figure 2-6E shows the complete separation of the microdroplets in the aqueous washing buffer phase from the oil phase, which goes to the waste outlet at the exit of the filter unit. To confirm complete oil removal, we collect the droplets in a petri dish and check under the microscope. If the oil is not completely removed, we are able to see that the solution containing droplets is cloudy and then we wash the collected droplets on a cell strainer (mesh size of 75 μm) using the washing buffer for three times. Without filtration, oil removal manually is impossible, and thus the centrifugation is mandatory.

## 2.7 Cell Encapsulation and Biocompatibility Assessment

Cells tend to agglomerate together forming clumps, resulting in a larger size droplet and encapsulating a larger number of cells in a droplet than others. The fabricated microgels around 250 μm in diameter were chosen to be optimum for encapsulating enough cells to promote cell-cell communication. In addition, 250 μm is the size of droplets that is easily generated with the current flow-focusing nozzle design (250 μm width and 300 μm height). On the one hand, bigger droplets are squeezed by the channel walls, which affects the stability of droplet generation process. To fabricate the devices with the wider and taller nozzle and channel, microfabrication process becomes more complex and challenging. On the other hand, generating smaller droplets requires higher flow rate of the oil phase, which subsequently affects all the downstream processes (i.e., photocrosslinking and oil filtration)

and causes insufficient crosslinking and filtering microgels. With smaller droplets, less number of cells are encapsulated, which makes cell proliferation delayed. Moreover, microscale tissues are also beneficial for easy oxygen exchange of the encapsulated cells from surrounding environments, enhancing long-term cell viability and proliferation. However, cell encapsulation during the microdroplet generation process causes the instability and inconsistency of droplet generation motion, leading to heterogeneous droplet size and non-uniform cell distribution. Since cell-laden microgels are often employed as building blocks for fabricating macroscale tissues, the number of cells per a building block governs the total cell density in the resultant constructs.[185] The cell density and cell-to-cell distance are crucial factors to determine the structural and functional characteristics of the engineered tissues.[44] All these considerations are necessary to control the number and uniformity of encapsulated cells per microdroplet with consistent and reproducible results. By treating BSA for cells and adding a magnetic mixer setup on the platform as shown in Figure 2-5, we could fabricate monodisperse microgels with a uniform number of cell distribution.

As shown in Figure 2-8A, the platform was tested with 4 different cell concentrations ($2.5\times10^6$ cells/ml, $5\times10^6$ cells/ml, $10\times10^6$ cells/ml, and $20\times10^6$ cells/ml) mixed the GelMA prepolymer solution. Highly controllable cell encapsulation with the desired number of cells per microdroplet was demonstrated without affecting the stability of the droplet generation process and with a monodispersity of the microdroplet size (Figure 2-8B and C).

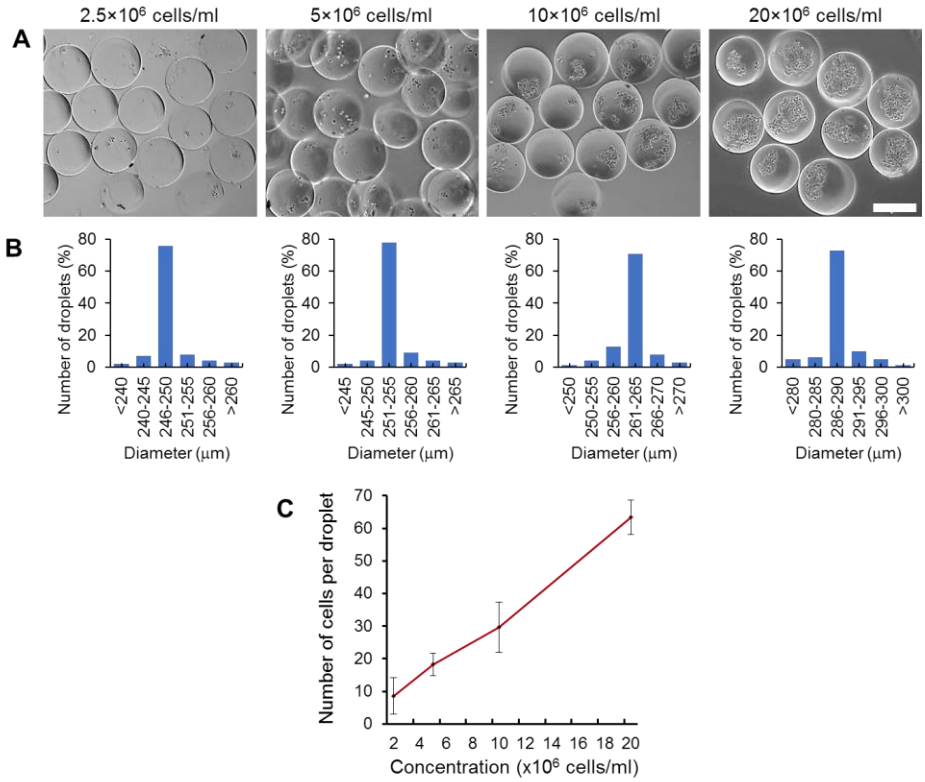


**Figure 2-8. Characterization of the fabricated cell-laden microdroplets. (A) Micrographic images of the cell-laden microgels with different cell concentrations on day 1 demonstrate that the numbers of encapsulated cells are controllable in accordance with cell concentrations. Scale bar = 250 μm. (B) Plots show that around 80% of the fabricated microgels are in the same size range for each cell concentration. (C) A plot represents the average number of cells/microgel with different cell concentrations.**

As shown in Figure 2-9, with the $2.5\times10^6$ cells/ml concentrations, cells needed 7 days for elongation, while the cells with the other 3 concentrations were elongated and formed 3D networks within 5 days. The lower cell concentration required a longer time for cell attachment and elongation due to the lack of cell-cell interactions. For encapsulating cells in microgels, there is a temporary loss of cell-cell contact and cell-matrix interactions during and after the droplet generation process since the cells are suspended in the hydrogel prepolymer solution. As a result, the cells maintain their round shape within the microgels for the first few days after encapsulation. During culturing, the cells are elongated to re-

establish attachment on the matrix and reform the cell-cell 3D networks in accordance with the degradation of hydrogels. The cells that were not elongated within a few days would lack essential cell-cell and cell-matrix signaling, and lose their functionality, resulting in de-differentiation or anoikis.[44] Therefore, controlling the number of encapsulated cells per microdroplet with consistent and reproducible results is necessary.

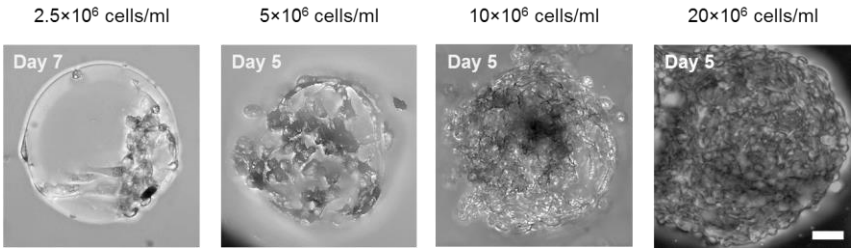


**Figure 2-9. Micrographic images of representative microgels per each concentration show the effect of the initial cell encapsulation concentration on the required time for the cell spreading and proliferation. Scale bar = 50 μm.**

We found that $20\times10^6$ cells/ml was the best concentration as it allows the greatest number of cells to be encapsulated in a 250 μm droplet without affecting the crosslinkability of GelMA hydrogel. Encapsulating more cells, while maintaining both the cell-laden microdroplet size and its monodispersity, is necessary to increase the efficiency of fabricating cell-laden microgels. Although the higher the cell concentration is, the more the cells are encapsulated in a droplet; this is limited by the cell to hydrogel ratio for effective crosslinking to maintain the integrity of cell-laden microgels.

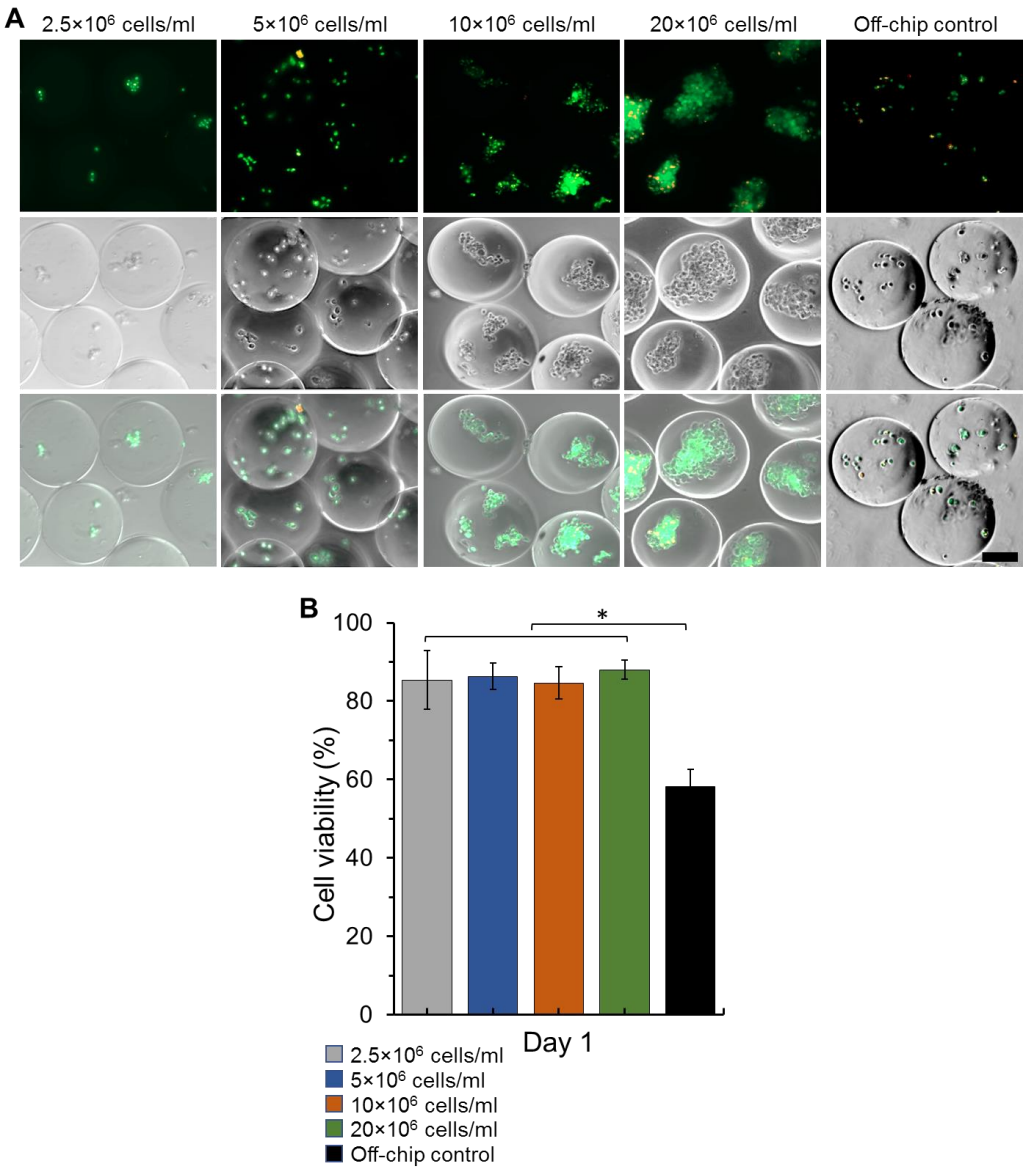


**Figure 2-10. Live/dead cell viability assay results for the on-chip filtration of cell-laden GelMA microgels with 4 different cell concentrations vs. the off-chip oil filtration with the concentration of $5\times10^6$ cells/ml at day 1. (A) Representative fluorescent, phase contrast, and merged images of live/dead assayed samples (live cells: green and dead cells: red). Scale bar = 100 µm. (B) Cell viability quantification data at day 1 shows that the cell viability of off-chip oil filtration is significantly lower than the on-chip filtration. *$p<0.05$.**

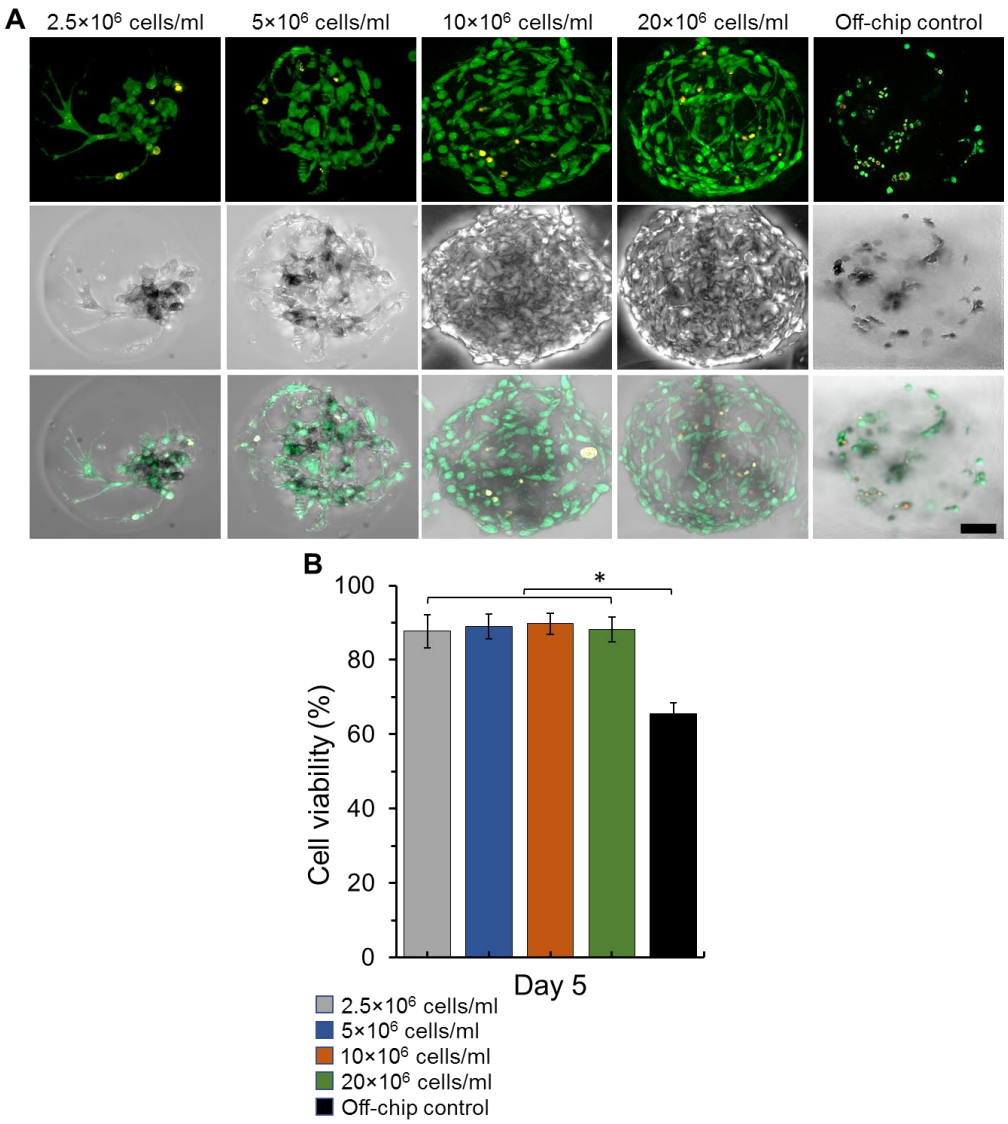


**Figure 2-11. Live/dead cell viability assay results for the on-chip filtration of cell-laden GelMA microgels with 4 different cell concentrations vs. the off-chip oil filtration with the concentration of $5\times10^6$ cells/ml at day 5. (A) Representative fluorescent, phase contrast, and merged images of live/dead assayed samples (live cells: green and dead cells: red). Scale bar = 100 µm. (B) Cell viability quantification data at day 5 shows that the cell viability is maintained for five days. *p<0.05.**

As shown in Figure 2-10 and 2-11, the cell viability was around 85% for day 1 (Figure 2-10) and was maintained for 5 days (Figure 2-11), demonstrating the high cytocompatibility of the platform. The viability is the combined result of cell proliferation, cell migration from the microspheres, and cell death. A control group of the cell-laden microdroplets using cycles

of centrifugation and washing was also tested to examine the effect of the off-chip separation and washing method. The cell viability at day 1 and day 5 was around 60%, which was significantly lower than droplets filtered from the on-chip filter unit. The fabricated cell-laden GelMA microdroplets with high viability demonstrated that the developed microfluidic platform is suitable for the in vitro fabrication of injectable microtissues with high-throughput.

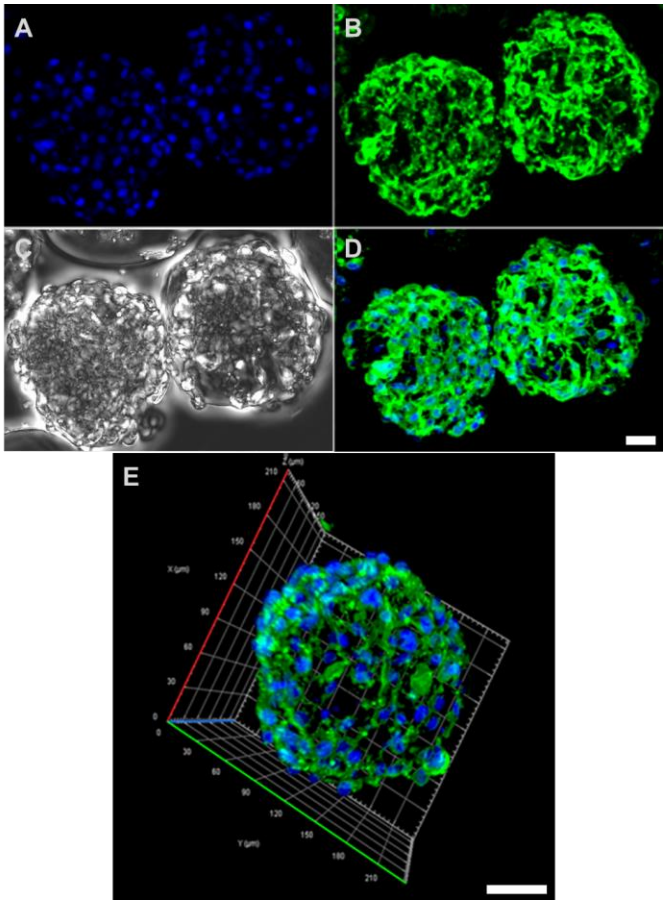


**Figure 2-12. Immunostaining of cells encapsulated in GelMA microgels at day 5. Fluorescent microscopy images of (A) nucleolus labeled by DAPI (blue) and (B) actin labeled by phalloidin (green), respectively. (C) Phase-contrast image of the same microgels. (D) Combined image showing both nuclei and actin. (E) 3D constructed image of cells in the microgels. Scale bar = 50 µm.**

In addition to the cell viability, the ability of spreading, proliferating, and migrating are known to determine the biocompatibility of the microgels for tissue engineering

applications.[186] Therefor, cell morphology and 3D tissue network structures were investigated using F-actin and nucleolus staining. Figure 2-12 shows that the cells were integrated well with the GelMA hydrogel microstructure and exhibited a characteristic polarized, polygonal morphology. Cells spread and proliferated inside the microgels over the culturing period, having the cell concentration increased gradually as shown in Figure 2-13. In addition, the degradability of the microgels is directly related to the number of encapsulated cells and their proliferation, as cells secrete protease enzymes for degrading GelMA at the metalloproteinase active sites[168,169] rather than the crosslinkability of the microgels. As microgels degrade, the cells are able to form their 3D network to actively communicate together. The average time for full droplet degradation was around 11 days. Cells that cannot establish these networks may undergo apoptosis after certain time. Based on our observations, for the $2.5\times10^6$ cells/ml, the microgels required around 2 weeks for complete degradation. On the other hand, for the 3 other concentrations ($5\times10^6$ cells/ml, $10\times10^6$ cells/ml, and $20\times10^6$ cells/ml), it took around 10 days for them to be completely degraded. As the GelMA hydrogel degraded, the cells migrated from the interior of the microgels to the surrounding tissue culture plastic surface, demonstrating that the cell-laden microgels were able to fuse into surrounding tissues after implantation as shown in Figure 2-14. Many cells migrated to the boundary of the microgels on day 8 and that the big number of growing cells could reach confluency on a petri dish on day 10. This is a central precondition for the active participation of cells in any regeneration activity and demonstrates that the produced microenvironment is suitable and sufficient for the cells to preserve their innate characteristics.

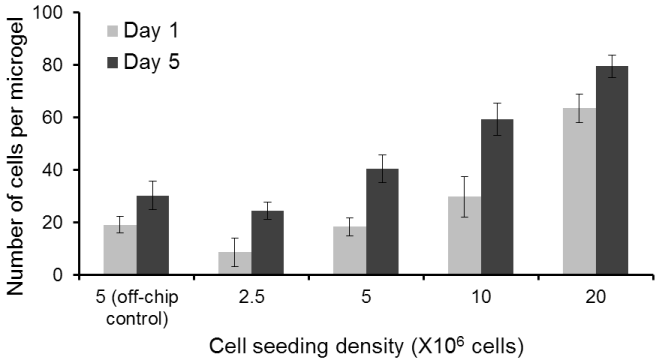


**Figure 2-13. A plot to show cell concentration changes in microgels with different cell seeding densities in GelMA on day 1and day 5.**

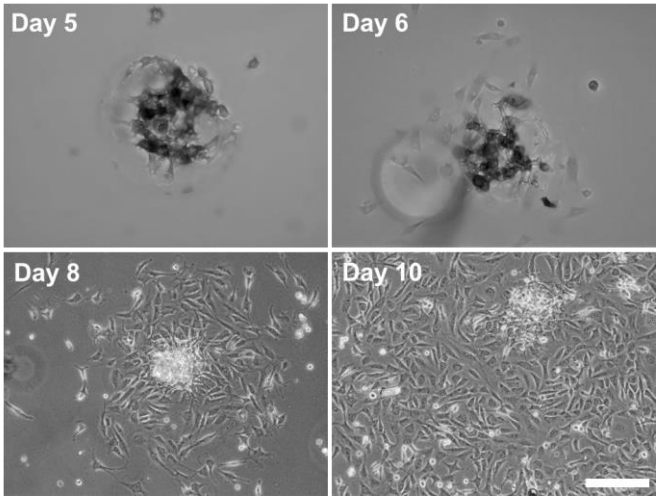


**Figure 2-14. Cell migration study shows that the cells migrated out from microgels to the surrounding area on the tissue culture plastic over time and confluent for ten days of culturing. Scale bar = 100 µm.**

The effect of GelMA concentration on cell spreading was also investigated. With the same initial concentration of $10\times10^6$ cells/ml, 7.5% w/v and 10% w/v GelMA prepolymer solutions were used to fabricate cell-laden microgels. Figure 2-15 shows that after 5 days of culture, the cells encapsulated in the 7.5% w/v GelMA show noticeably greater elongation and proliferation than 10% w/v GelMA. This is possibly due to the smaller pore size and

lower degradation rate of 10% GelMA than 7.5%. In summary, the analyses of cell viability and 3D tissue structure demonstrates that the developed platform is capable of producing cell-laden GelMA microgels with high functionality. The microgels can actively contribute to the process of tissue regeneration. This result can be attributed to the combined approaches of the on-chip photocrosslinking with the cell-compatible laser beam and the on-chip oil filtration unit using the biocompatible washing buffer, which enable cells to minimize contact time with the oil phase and avoid excessive centrifugation after fabrication.

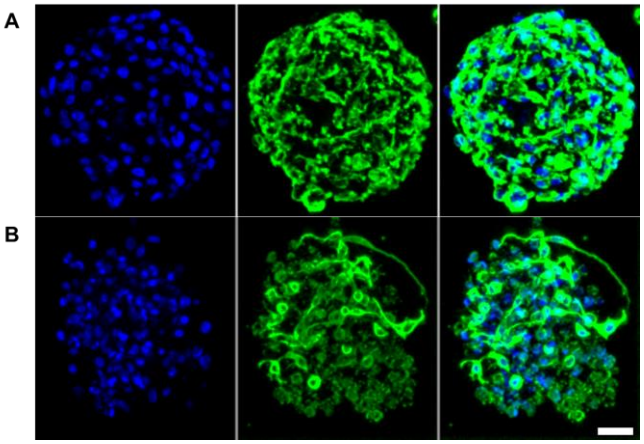


**Figure 2-15. Effect of GelMA concentration on cell spreading within the microgels. Representative fluorescent images of immunostained cell nuclei and actin with (A) 7.5% w/v GelMA microgel and (B) 10% w/v GelMA microgel. Scale bar = 50 µm. Cells are more spread out in 7.5% w/v GelMA to form a 3D network.**

Therefore, there are two main advantages of the integrated microfluidic device to fabricate cell-laden microgels. First, integrating the off-chip handling steps into a single step could provide high practical efficiency and low operational difficulty. This is because multiple manipulation steps induce the loss of many fabricated microgels and the reduced cell viability (as proven by the control group experiment and previously reported in [90,91,94]). Second, the device enabled us to encapsulate cells in microdroplets without causing any

turbulence and fabricate monodisperse cell-laden microgels with high cell viability. This is coupled with the encapsulation of a high, well-distributed number of viable cells.

## 2.8 Summary

In this chapter, cell-laden hydrogel droplet generation with a continuous high-throughput was established with a practical cellular distribution among uniformly sized microgel droplets over 4 different cellular encapsulation densities. This is by applying the approaches of having enough channels' height, pre-treating the cells with BSA, and applying the magnetic mixer in the dispersed phase. On-chip manipulation strategies, photocrosslinking and removal of carrier oil were successfully integrated into the microfluidic device improving the quality of hydrogel microcapsules and the encapsulated cells' viability. Up to our knowledge, this is the first study to integrate all the fabrication steps into a single chip. The synthesized microgels provide a good platform for 3D in vitro cell culture. Their miniaturized homogeneous size across different cell seeding densities and controllable structures enable them for success in vitro cell culture. Numerous cellular activities, such as cell growth, proliferation, and cell interaction, have been shown. The analyses of cell viability and 3D tissue structure demonstrate that the developed platform is capable of producing cell-laden GelMA microgels with high utility that can actively contribute to the process of tissue engineering. This can be attributed to the combined approaches of the on-chip fast photocrosslinking with the cell-compatible visible wavelength of the laser beam, and the on-chip oil filtration unit using a biocompatible washing buffer to minimize the contact time of cells with the oil phase to avoid excessive centrifugation after fabrication. This technology holds the promise for widespread applications in tissue engineering with enhancements in overall efficiency.

# Chapter 3 : Rapid, High Yield, and Sterilized Synthesis of GelMA

The development of well-performing, sterile, and reproducible hydrogels is in great demand, especially due to recent advances in biofabrication of living tissues. Due to their biocompatibility, biodegradability, and porosity, gelatin methacryloyl (GelMA) hydrogels have been widely used in various biofabrication applications. However, the synthesis process for GelMA remains uncharacterized and displays high batch-to-batch variation. Moreover, the process is highly time-consuming and lasts up to 2 weeks and produces a small yield. Contemporary synthesis methods make use of toxic reagents like glycidyl methacrylate (GMA) and methacrylic anhydride (MAA) that require lengthy dialysis purification to be eliminated. In this chapter, we present our method for successfully synthesizing high-quality GelMA, which was achieved by employing a combined approach consisting of ion-pairing and desolvation in an aprotic solvent medium of low relative permittivity. It is also worth mentioning that the process was accomplished within a few hours and did not require the use of excess organic solvents. This rapid, scalable, sterile, and high-yield process is a candidate for being the standard GelMA synthesis process and could be of great benefit to studies and applications in regenerative medicine, tissue engineering, and 3D cell culturing.

## 3.1 Materials and Methods

### 3.1.1 GelMA Synthesis

GelMA hydrogel synthesis was carried out based on 4 different protocols. The conventional dialysis based GelMA was synthesized as described previously.[137,140]Briefly, a 10% W/V gelatin solution was prepared in either one of dimethyl sulfoxide (DMSO), or phosphate-buffered saline (PBS) at 50 °C and stirred. 0.6 %W/V of 4-dimethylaminopyridine (d-map) was then added gradually as a catalyst, only to the gelatin solution in DMSO and not to the

PBS solution. Finally, 4 %V/V of glycidyl methacrylate (GMA) was added to the mixture containing DMSO, while 10% V/V of methacrylic anhydride (MAA) was added to the mixture with PBS, in a dropwise manner. The DMSO mixture was stirred for 48 hours at 50 °C, while the PBS mixture was stirred for 1 to 3 hours. The reaction mixtures were then diluted and dialyzed against reverse osmosis (RO) water using dialysis membranes (MWCO: 12-14 kDa, Spectrum Labs, Rancho Dominguez, CA, USA). The dialysis was conducted for a week at 40°C, during which the water was changed twice a day in order to remove unreacted toxic chemicals. Subsequently, dried GelMA was obtained after freeze-drying the mixture for 7 days.

For the more efficient approach, a 10% W/V gelatin solution was prepared in DMSO at 50 °C, to which 0.6 %W/V of d-map was added. Then 18 %V/V of GMA was gradually added to the mixture. The reaction ran for 2 hours at 50 °C, after which 0.154% W/V sodium chloride was added to the GelMA-containing reaction mixture. This mixture is then dropped onto 3 volumes of ethanol at -200 C, with moderate stirring. The precipitate was found to be in the form of small pellets due to the drop-by-drop addition (Video 3.1), which simplifies the subsequent steps of collecting, washing, dissolving, and drying of the resultant product. The precipitates are then collected by centrifugation at 5000 RPM for 5 minutes and washed in an equal volume of Reagent Alcohol by vortexing for 2 minutes. The process of washing was repeated twice. The precipitated and washed GelMA was then dissolved in 10-15X of sterile type 1 water that was poured into 50 ml petri dishes to form a thin layer that was a few millimeters thick, followed by snap freezing in liquid nitrogen and freeze-drying. The dry weight of the GelMA was then recorded. The yield of the methacrylation procedure was calculated as the ratio of the final dry weight of GelMA to the initial dry weight of gelatin.

All materials were purchased from Sigma-Aldrich (St. Louis, MO, USA) unless otherwise specified.

The degree of methacrylation of each sample is investigated using proton nuclear magnetic resonance (1H-NMR) spectroscopy. Briefly, 20 mg of the lyophilized GelMA or the gelatin reference was dissolved in 1.5 ml of deuterium oxide (Sigma, St. Louis, MO, USA). The spectra were collected at 35 °C using a 400 MHz spectrometer (Bruker, Billerica, MA, USA). MestReNova software (Mestrelab Research, Spain) was used for phase correction, baseline subtraction, and integration of the acquired spectra. The degree of methacrylation of each sample is measured as:

$$\text{Degree of Methacrylation} = 100\% \times \left(1 - \frac{\text{Lysine integration signal of GelMA}}{\text{Lysine integration signal of gelatin}}\right)$$

### 3.1.2 Characterization of Material Properties

For preparing photo-crosslinkable hydrogels, 5%, 7.5%, and 10% w/v of the freeze-dried GelMA was dissolved in PBS containing 0.5% w/v of 2-Hydroxy-4′-(2-hydroxyethoxy)-2-methylpropiophenone (Igacure2959, CIBA Chemicals) photoinitiator. For the characterization of the elastic modulus of GelMA, 1 ml of GelMA prepolymer solution was pipetted into cylindrical PDMS molds that were of 8 mm diameter and 6 mm height. The sample was then exposed to a 375 nm UV light for 5 min. The disk samples were compressed by a mechanical testing system (MACH-1TM V500C, Biomomentum, Laval, QC, Canada). The slopes of the linear portion of the stress-strain curves were used to calculate the compressive elastic modulus of each sample.

Four cylindrical specimens from each sample were used to evaluate the mass swelling ratio. The excess water content was wiped out using a tissue paper, and then the swollen

weight was measured. After freeze-drying under -50˚C, the dry weight was also measured. The mass swelling ratio was calculated as:

$$\text{The mass swelling ratio} = \frac{\text{The swollen weight of the sample}}{\text{The dry weight of the sample}}$$

The prepared hydrogel samples were incubated in PBS at 37˚C for a month. At predetermined specific time points, the samples were collected, rinsed with RO water, freeze-dried and weighed. The mass remaining % was evaluated as:

$$\text{Mass remaining \%} = 100 \times \frac{\text{The dry weight of the sample}}{\text{The initial sample dry weight}}$$

GelMA hydrogels were left in RO water overnight, and subsequently, snap frozen in liquid nitrogen. Then, the frozen samples were lyophilized. The dried samples were sputter-coated with 10 nm thick gold-palladium layers and imaged with a scanning electron microscope (SEM) (Mira3 XMU, TESCAN, Brno, Czech Republic).

### 3.1.3 Biocompatibility Analysis

With the same initial concentration of $7\times10^6$ cells/ml, 5% w/v, 7.5% w/v and 10% w/v GelMA prepolymer solutions were prepared and crosslinked as described above. The viability of the cells inside the hydrogels was examined after culturing for 1 day and 5 days by using the LIVE⁄DEAD® cell viability assay (Biotium, Fremont, CA, USA) containing fluorescent dyes, calcein-AM (green) for live cells and ethidium homodimer-1 (red) for dead cells. The encapsulated cells were washed twice with PBS and were stained with the viability assay via incubation at 37 °C for 20 minutes. Green live cells and red dead cells were imaged by using an inverted fluorescent microscope (Axio Observer 7, Carl Zeiss Canada Ltd.,

Toronto, ON, Canada). The obtained images of live and dead cells were quantified by using ImageJ software (NIH, Bethesda, MD, USA). Cell viability was measured as follows.

$$\text{Cell Viability} = \frac{\text{Number of live cells}}{\text{Number of live and dead cells}}$$

To investigate 3D cell culturing, the nucleus and F-actin of the cells were fluorescently labeled at day 7 of culturing. Briefly, the hydrogels were washed with PBS twice, after which the cells were fixed by 3.7% paraformaldehyde for 20 minutes. The fixed samples were washed with PBS three times, and cell membranes permeabilized by 0.1% Triton X-100 (VWR, Radnor, PA, USA) for 5 minutes. Subsequently, the samples were incubated at room temperature in a dark location for 45 minutes, followed by the addition of 1 mL of 100 nM Phalloidin 488 solution (Cytoskeleton, Denver, CO, USA). The stained samples were washed with PBS three times. Finally, DAPI mounting media (Fluoroshield with DAPI, Sigma Aldrich, St. Louis, MO. USA) was added. The fluorescently labeled cell images were taken immediately, under an inverted fluorescent microscope.

Two structures were fabricated using a stereolithography 3D bioprinting system, as described earlier[187]. A prepolymer solution was prepared using 10% w/v GelMA in PBS and adding visible light photoinitiator. The photoinitiator comprised of 0.02mM 2′,4′,5′,7′-tetrabromofluorescein disodium salt (Eosin Y), 0.02% w/v triethanolamine (TEA) and 37 nM 1-vinyl-2-pyrrolidinone (NVP). The bioink was obtained by adding NIH-3T3 fibroblasts ($5x10^6$ cells/mL) to the pre-polymer solution. Next, 850 µL of bioink was dispensed in a Petri dish (60 mm diameter) to form a uniform layer of 300µm thickness. The patterns of UBC logo and miniature bone were projected, respectively. Each structure comprised of 3 layers to achieve a total thickness of 900µm. Upon completion of the bioprinting process, the

samples were washed trice with PBS and then cultured in an incubator. The cell morphology in the samples was examined after 5 days of culture by actin/nuclei staining using phalloidin/DAPI. The stained samples were imaged using a fluorescent microscope (Axio Observer 7, Carl Zeiss Canada Ltd.) with DAPI and EGFP channels. Objective lenses of magnification 5X, 10X and 20X were used with z-stack and tile modes.

### 3.1.4 Statistical Analysis

A one-way analysis of variance function in Microsoft Excel was used to analyze the data statistically. Results are shown as the average ± standard deviation. Statistical significance was accepted at $p < 0.05$.

## 3.2 Analysis of Synthesis Process and Yield Rate

In polar solutions, proteins embrace a structure that exposes their hydrophilic region to the surrounding media, allowing the formation of a hydration (solvation) layer that prevents protein-protein interactions. Disrupting this hydration layer usually causes protein precipitation.[188] As shown in Figure 3-1, towards the end of the reaction, NaCl salt is directly added to the reaction mixture in DMSO before precipitation with ethanol. This inclusion was mainly intended for enhancing the precipitation of GelMA at lower volumes of the more expensive organic solvent, and consequently increased the efficiency of the production process. The effect of NaCl on the precipitation efficiency of GelMA in ethanol can be described using the model of ion-pairing.[189–191] Ion-pairing shields the repulsive electrostatic forces, which are responsible for maintaining protein solubility.

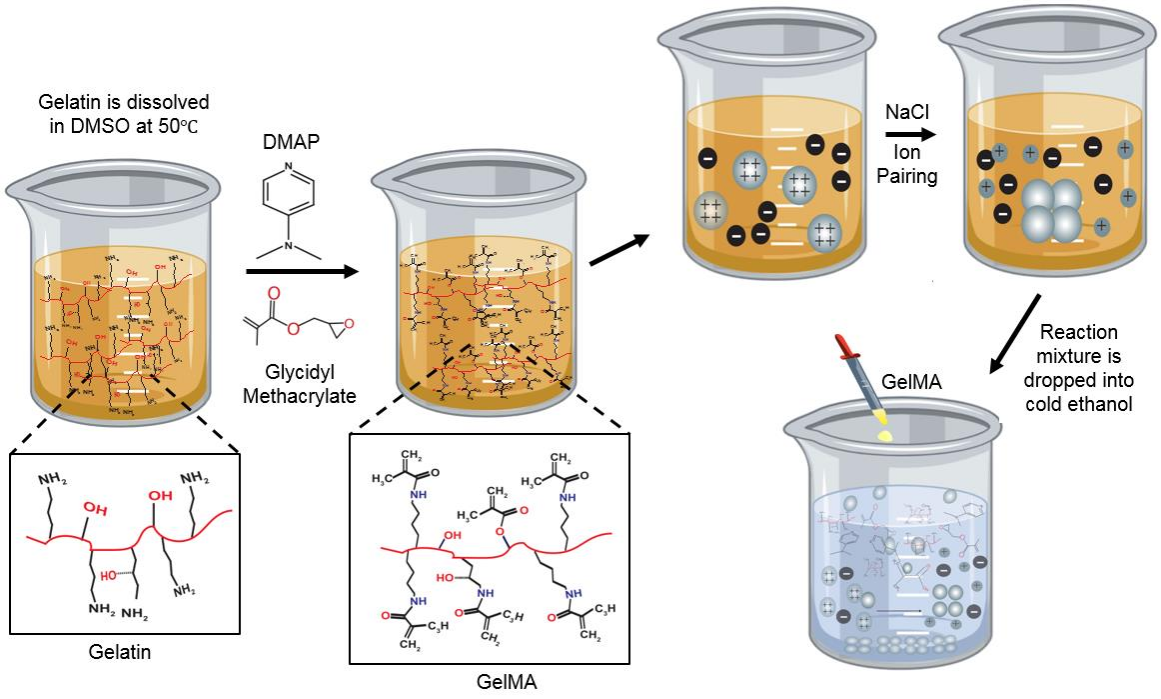


**Figure 3-1. Schematic representation for the efficient production approach. Precipitation-gelatin methacryloyl (ppt-GelMA) is produced by reacting gelatin dissolved in dimethyl sulfoxide (DMSO) with high glycidyl methacrylate (GMA) concentration (18% V/V) in the presence of dimethylaminopyridine (DMAP) as a catalyst. Sodium Chloride (NaCl) is then added for de-shielding the charges from the surfaces of the protein. GelMA is then purified by adding to cold ethanol which dissolves all the reaction by-products and the excess GMA.**

Despite the fact that sodium chloride is a 1:1 salt that is hydrated when added to water (permittivity~80 at 20°C),[192–194]preventing ion pairing, the low dielectric constant of DMSO (permittivity~40 at 20°C)[192–194] facilitates ion-pairing between $Na^+$ or $Cl^-$ and charges on the protein surface. Additionally, the presence of the dissolved protein in DMSO affects its dielectric constant. This allows it to attain enough ionic strength for shielding the protein charges, which in turn makes it possible to achieve high yield protein precipitation at a relatively low sodium chloride concentration.[195] Taking into consideration NaCl solubility in both DMSO (0.4%W/V) and ethanol (0.65 g/Kg),[196–198] a sodium chloride concentration of 0.154 %W/V of the initial reaction mixture was introduced. This concentration was

specifically used to achieve sufficient ionic strength for successful precipitation, in a mixture of solvents of relatively low permittivity (∼24 for ethanol and ∼ 40 for DMSO at 20◦C)[192–194], while maintaining the salt solubility in the final mixture, thus avoiding any impurities in the final GelMA product.

This shielding of the charges on the protein increases the likelihood of aggregation due to the hydrophobic interactions between proteins, upon the addition of ethanol (permittivity∼24 at 20◦C),[192–194] which further reduces the polarity of the medium. There is, therefore, a synergistic effect between the NaCl ion pairing, the low DMSO permittivity, and the Ethanol desolvation effect. With a reduced number of hydration layers, solvent-induced precipitation can be described according to Coulomb's law, which relates the magnitude of the electrostatic force to the dielectric constant of the medium. Solvents with reduced dielectric strength, increase the interactions between hydrophobic protein parts causing protein aggregation.[199,200]

The choice of the precipitating agent used in our approach was based on the following criteria: The agent must display hydrophobicity (low dielectric constant), enough to allow for a high and reproducible precipitation yield of the hydrophilic GelMA protein. At the same time, it should be characterized by superior solubility of all the reaction by-products and unreacted chemicals. It is also essential for it to maintain strong antibacterial properties in order to integrate sterilization with the production and purification processes. Based on these criteria, ethanol was selected as the organic solvent of choice carrying out three roles in this method.

As a precipitating agent, ethanol reduces the dielectric constant (polarity) of the solvent of the methacrylation reaction, which renders the GelMA less soluble and therefore

precipitates it with high yield in a reduced volume (3X). This is because ethanol has a low dielectric constant (~24 at 20°C)[192–194] As shown in figure 3-1, ethanol-miscible gelatin aprotic solvent of low relative permittivity (Dimethyl Sulfoxide) works better with this approach. This is because precipitating from solvents of low relative permittivity (of around 40)[201] requires smaller volumes of the organic solvent volume, which is also more efficient. Subsequently, glycidyl methacrylate is the preferred methacrylate group donor in our approach as it permits the usage of a sufficient concentration of NaCl without its precipitation as any impurity. This is due to the relatively higher solubility of NaCl in ethanol (0.65g/Kg) as compared to other organic solvents.[198] Figure 3-2 illustrates the different stages of the GelMA synthesis process.

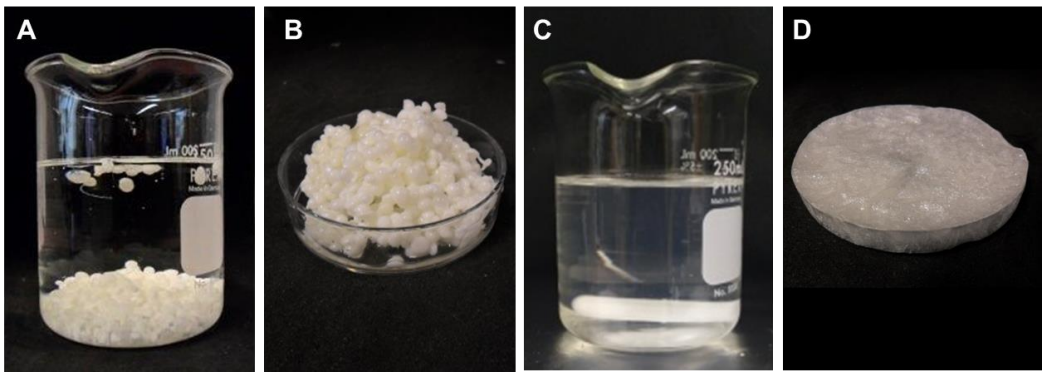


**Figure 3-2. Images depicting the different stages of the ppt-GelMA production process. (A) Pelleted GelMA precipitated in cold ethanol. (B) Washed pelleted GelMA. (C) Fast dissolution of the pelleted GelMA in sterile type 1 water. (D) Freeze-dried GelMA. (E) Yield of the different gelatin methacrylation production approaches (*p < 0.05, ***p < 0.001, n = 3).**

Figure 3-3 shows the yield of the reactions of the GelMA produced by various methacrylation protocols; the yield differs widely between the groups. The dialysis-reliant purification approaches, either using MAA or GMA in PBS or DMSO respectively, produced a yield (~60% - 70%), which is higher than the salt-free ethanol precipitation method but

significantly lower than the ion pairing-aided precipitation (ppt + NaCl) group (~90%). It is noteworthy that these dialysis-reliant methods showed poor yield reproducibility as demonstrated by their standard deviations and also as previously reported.[144] The direct-ethanol precipitation group, with no addition of salt (ppt – NaCl) showed the lowest yield (~50%). This finding might be related to the absence of charge shielding, which makes the precipitation less efficient. Alternately, the precipitation was conducted in volumes much larger (10 folds) of the initial reaction mixture volume, but this has not been observed to enhance the yield significantly.

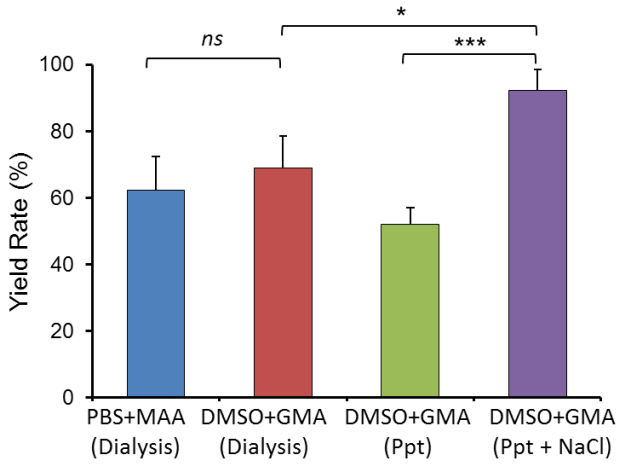


**Figure 3-3. Yield of the different gelatin methacrylation production approaches (*p < 0.05, ***p < 0.001, n = 3).**

Proteins have poor solubility at pHs that are equal to their isoelectric points (IEPs) because of shielding the electrostatic repulsions. However, gelatin, and subsequently GelMA, is a heterogeneous mixture of proteins derived from collagen by either alkaline or acidic hydrolysis. Therefore, gelatins have an IEP range rather than a definite point. Type A gelatin (derived from acid-cured tissue) has an IEPs range of 7.0-9.0, whereas type B (derived from lime-cured tissue) has an IEPs range of 4.7-5.2.[202–204] Moreover, the charges on the gelatin

moiety, which determines its isoelectric point, are primarily a function of its side chains.[205,206] For this reason, each produced GelMA batch has an unknown IEP due to the difference in reagents used and degrees of substitution on these side chains, which mandates IEP range determination for every batch. Adjusting the pH of the GelMA solution would be an impractical approach to enhance the precipitation efficiency. This is not only due to the fact that the precipitation of a complex protein mixture would not be feasible at a single pH since the IEP varies throughout the sample, but also due to the IEP of each GelMA being unknown. These alternative approaches increase the cost and technical difficulty of the purification process as compared to the simple addition of the pre-calculated amount of NaCl.

As shown in Figure 3-3, increasing the initial concentration of GMA to 18% V/V and applying ion-pairing-aided precipitation has resulted in the highest reproducible yield of GelMA in a much shorter time. Also, this increased GMA concentration has led to a methacrylation rate comparable to conventionally used methods (Figure 3-4A). Ethanol acts as a purifying agent in which a reaction impurities and toxic materials are soluble. Glycidyl methacrylate, its by-products, and the toxic d-map catalyst have better solubility in ethanol than they have in water.[192,207] As glycidyl methacrylate is very soluble in the ethanol and only moderately soluble in water,[192,207] its volume % could be increased up to 18% V/V of the initial gelatin methacrylation reaction mixture to further catalyze the reaction and reduce the reaction time from 2 days to 2 hours, while producing a highly substituted GelMA ((≃ 75 - 80%), as shown in Figure 3-4A and B. This makes the elimination of the glycidyl methacrylate easier and thorough. Furthermore, for long, ethanol has been recognized for its use as a bactericidal, tuberculocidal, fungicidal, and virucidal agent.[208] Therefore ethanol is

used as a disinfecting agent sterilizing the GelMA during the precipitation and the washing steps. It is necessary to handle GelMA as sterile from this step onward and during freeze-drying.

The freeze-drying process is also time-consuming and ensues high capital equipment costs, which is a primary motivation for minimizing process times.[142] Conventionally, the water content of the final GelMA hydrogel precursor is more than 97% due to many dilutions during the synthesis process combined with the subsequent step of dialysis. In our approach, the solvent content is much lower and more controllable, which enables faster freeze-drying.[142,149,151] The water content (10X to 15X of the precipitate volume) was kept within the effective limits for fast drying (within few hours) and for maintaining the porosity, allowing for efficient drying with no packing, which might result into difficult subsequent dissolution of GelMA. Additionally, the relatively fast drying step was aided by increasing the surface area to volume ratio that was achieved by performing the freeze-drying process in wide petri dishes.

## 3.3 Results of Material Properties Characterization

### 3.3.1 Degree of Substitution

Four sets of GelMA were produced using the various synthesis and purification methods and are discussed above. Their degrees of methacrylation were then comparatively studied using $^{1}$H-NMR. Representative $^{1}$H-NMR spectra are shown in Figure 3-4B. The degree of methacrylation can be defined by comparing the amino lysine integration signal (the component “b” in Figure 3-4B) of the gelatin and GelMA spectra to those of the phenylalanine signal of the gelatin spectrum (the component “a” in Figure 3-4B) as an

internal reference. All the groups showed similar methacrylation rates of around 70% to 80% with no statistically significant difference, as shown in Figure 3-4A. These results demonstrate that the proposed protocol of increasing the GMA initial concentration to 18% V/V and running the reaction for only 1-3 hours is able to produce GelMA pre-polymer with a degree of methacrylation similar to that produced by conventional methods consisting of MAA in PBS for 1-3hours, or GMA in DMSO for 48 hours.

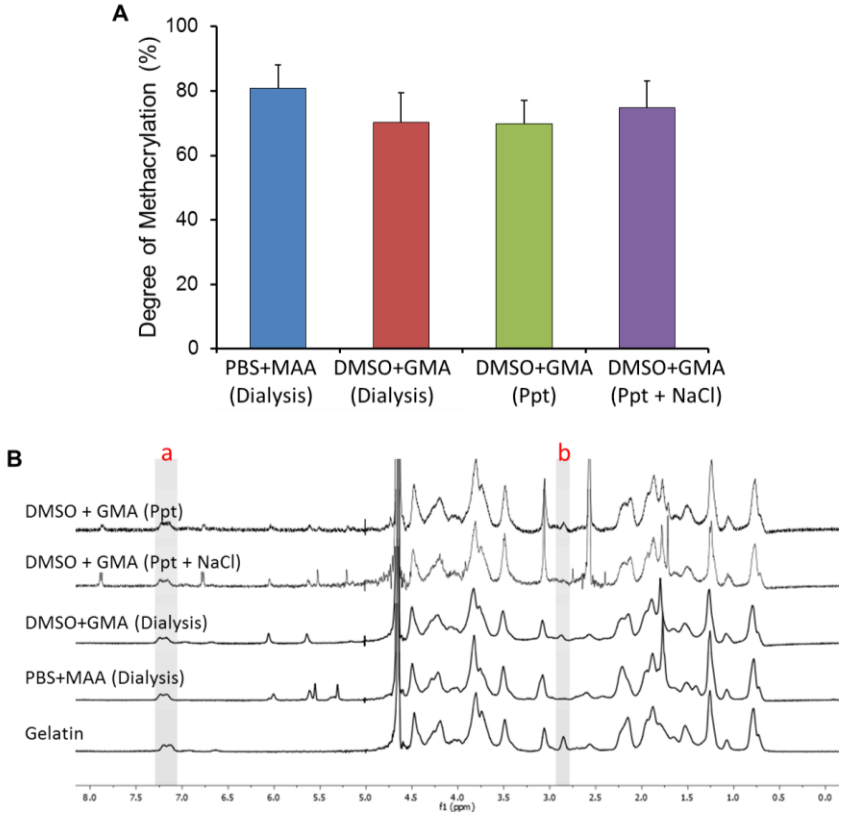


**Figure 3-4. Degree of substitution results (A) Quantification of the degree of gelatin methacrylation. (B) $^{1}$H-NMR spectra of GelMA produced by different approaches in reference to gelatin. (a) Denotes the gelatin internal reference, and (b) denotes the unsubstituted primary amines used to calculate the degree of methacrylation. (Ppt = precipitation).**

### 3.3.2 Mechanical Property

Upon exposure to UV light, the GelMA prepolymer solution formed a crosslinked network. Previously, the mechanical properties of a hydrogel matrix environment have been shown to

influence cell function, proliferation, and differentiation.[209,210] It was, therefore, important to characterize the mechanical properties of GelMAs at differing concentrations. An unconfined compression test was performed on samples composed of 5%, 7.5%, and 10% GelMA concentrations to assess the effect of the pre-polymer concentration on the mechanical properties of the hydrogels.

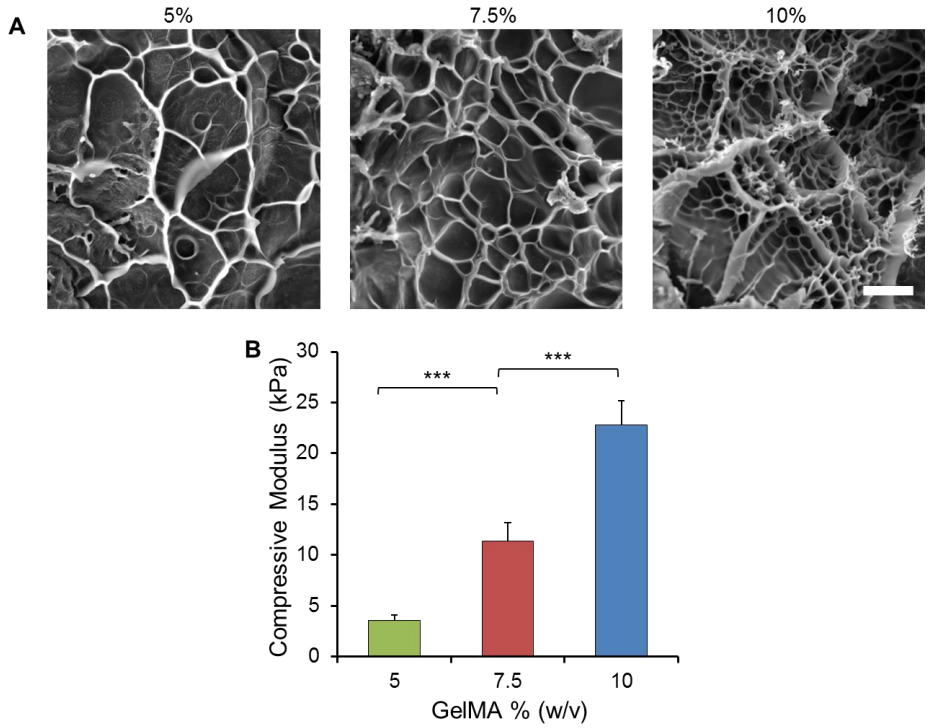


**Figure 3-5. Mechanical properties of the ppt-GelMA hydrogel at various GelMA % (w/v). (A) SEM pictures depicting the crosslinked hydrogel microstructures. Scale bar = 50 µm. (B) Compressive modulus (*P < 0.001, n = 5).**

Figure 3-5A shows an increase in the density of crosslinking with the increase in GelMA concentration, in an agreement with previous reports.[211,212] Figure 3-5B demonstrates a direct association between GelMA concentrations and the respective compressive moduli, ranging from less than 5 kPa (5% GelMA) to ~23 kPa (10% GelMA). While on one hand, despite the fact that stiffness increases with the density of the microstructure, this may be a

negative effect on cell spreading and proliferation inside the hydrogels. However, some applications, such as keratinocyte culturing, need high compressive moduli for favorable adhesion, growth, and proliferation on the hydrogel for skin tissue engineering.[212,213]

### 3.3.3 Swelling Ratio

The swelling behavior of a hydrogel network is another important property that may predict its mechanical and surface properties, degradation rate, solute diffusion, and cell behavior.[214–216] The mass swelling ratio is dependent on the pore size of the network microstructure and the solvent-polymer interaction.[215,217] As shown in Figure 3-6A, the change in the mass swelling ratio of ppt-GelMA was investigated at different hydrogel concentrations, 5%, 7.5%, and 10%, and found to be 14.8, 10.7, and 9.4, respectively. Thus, the mass swelling ratio decreased significantly with increasing hydrogel concentrations. This limits the amount and rate of water uptake into the hydrogel and consequently slows down its degradation.[218] From Figure 3-6B, the change in hydrogel degradation rate of the three ppt-GelMA concentrations can be observed and seen to have exhibited a similar trend as was observed for the swelling ratio. The mass remaining (%) of ppt-GelMA over time was considered as a measure of degradation. The 5% ppt-GelMA displayed a much faster degradation with 100% mass loss at 2 weeks compared to 3 weeks and 4 weeks for the 7.5% and the 10%, respectively. In summary, the above results have proven that the tunable mechanical behavior and degradability of the ppt GelMA hydrogel demonstrate its broad spectrum of properties and also renders it an ideal candidate for a wide range of applications.

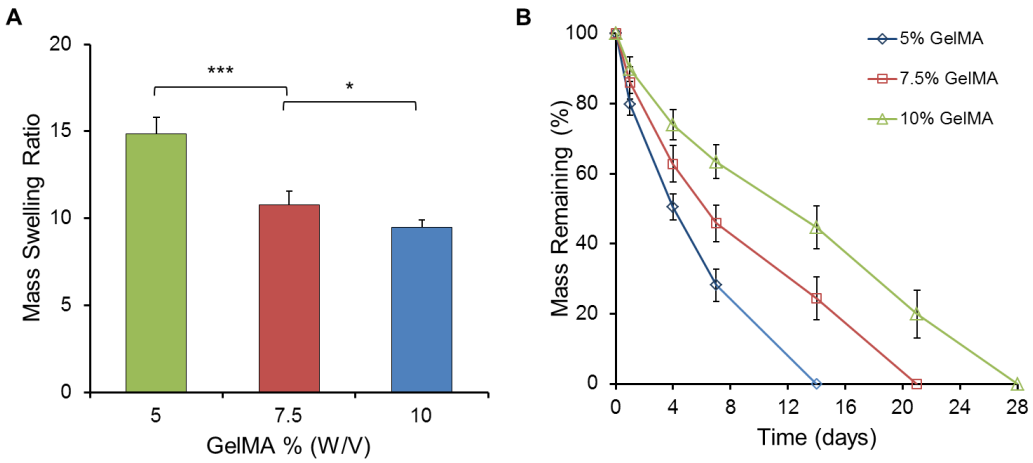


**Figure 3-6. Swelling characteristics (A) Mass swelling ratio (*p < 0.05, ***p < 0.001, n = 4). (B) Mass retention during *in vitro* degradation.**

### 3.3.4 Biocompatibility

The ability of cells to integrate and grow within the hydrogel 3D microstructure is of utmost importance for tissue engineering. For the evaluation of cell viability, NIH-3T3 cells were encapsulated into ppt-GelMA hydrogels composed of differing concentrations. Cell viabilities were quantified based on the counting of live-green and red-dead cells. As shown in Figure 3-7, cell viabilities were found to be higher than 90% at days 1 and 5 for all ppt-GelMA concentrations. On the fifth-day of culturing, the cells were elongated and displayed a characteristic spindle-shaped morphology in the 5% GelMA (Figure 3-7A). Cells did not elongate or spread to the same extent in the 7.5% or the 10% concentrations. It is documented that cell elongation relates inversely with the gel concentration. However individual elongated cells could be identified in the 7.5% group, demonstrating that increasing the hydrogel concentration does not inhibit the process entirely. These observations motivated further investigation into cell spreading and networking within the 5% ppt-GelMA 3D microenvironment.

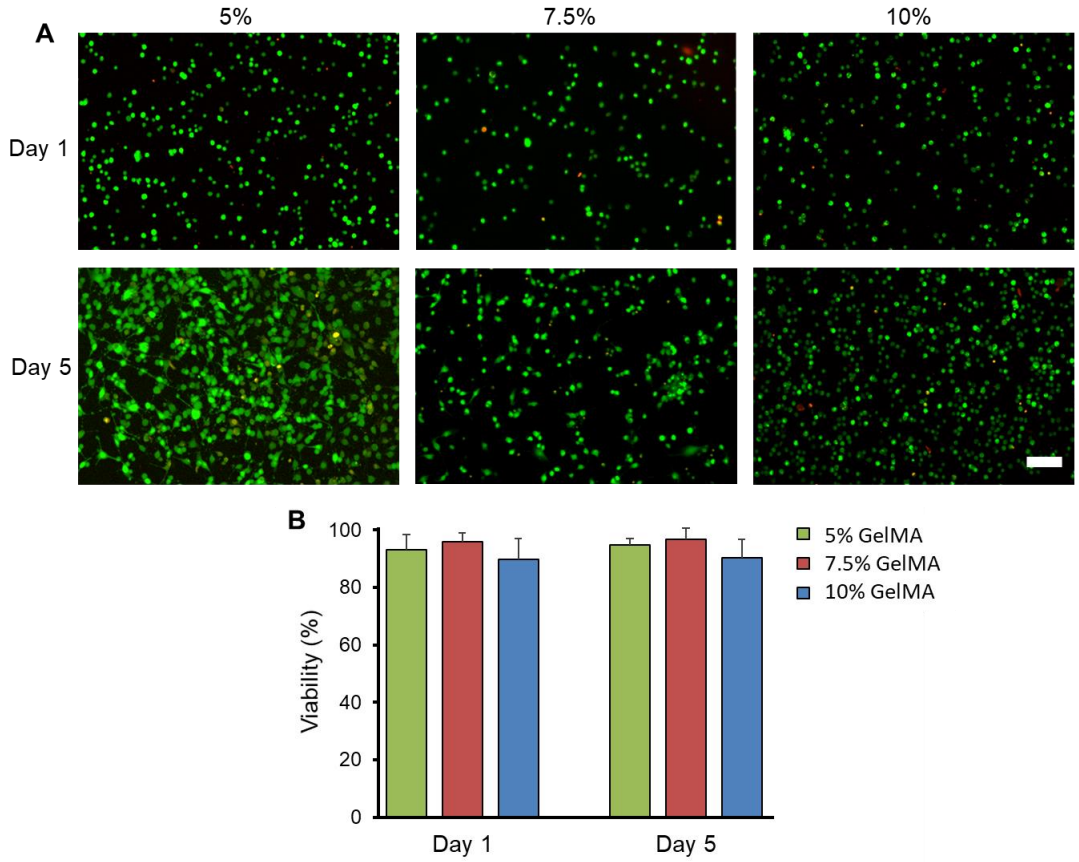


**Figure 3-7. Biocompatibility results of the cell-laden ppt-GelMA (A, B) Live/dead cell viability assay results for the cell-laden ppt-GelMA at varying GelMA concentrations at days 1 and 5. (A) Representative fluorescent images of live/dead assayed samples (live cells: green and dead cells: red). Scale bar = 100 µm. (B) Quantification of cell viability shows high cell survival.**

To investigate the cell behavior in 3D microenvironments, the cell's F-actin and nucleolus were fluorescently stained at day 7 of culture. A series of z-stack images were obtained from the cell-laden samples, after which they were projected orthogonally to form a 2D view (Figure 3-8A) and reconstructed to form the 3D isometric view image (Figure 3-8B). As shown in Figure 3-8, cells were well distributed in the z-direction, elongated, migrated and successfully formed 3D interconnected networks with neighboring cells. These results demonstrate the innate cytocompatibility of the ppt-GelMA hydrogel and of our highly efficient production process.

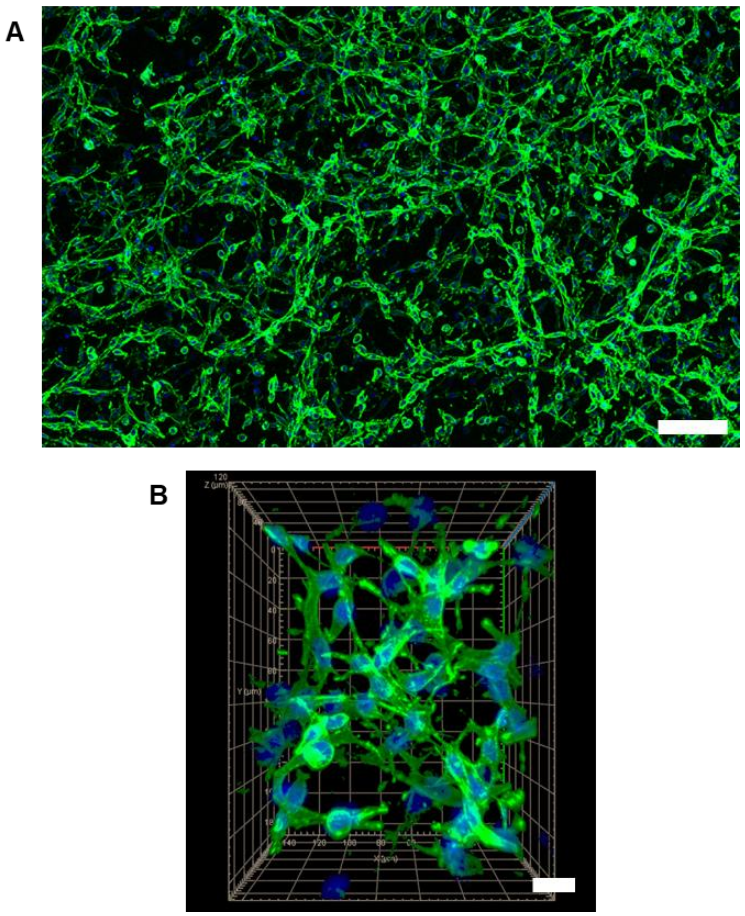


**Figure 3-8. Nuclei/F-actin immunostaining of cells encapsulated in 5% GelMA at day 7. (A) Orthogonally projected 2D fluorescent microscopy images (scale bar = 100 µm). (B) 3D constructed image of cells in GelMA (scale bar = 20 µm). The nucleolus is labeled by DAPI (blue), and actin is labeled by phalloidin (green).**

## 3.4 3D Bioprinting Experimental Results

To demonstrate the applicability of the synthesized GelMA in 3D bioprinting, we fabricated two different structures using the stereolithography bioprinting system[219]. Two patterns with variable complexities were selected – (i) UBC logo and (ii) bone with rectangular pores. Both patterns were printed with well-resolved features and structural integrity (Figure 3-9). Figures 3-9A (i) and B (i) show the printed structures on day 0 stained with blue dye for visualization. Figure 3-9A (ii) shows the fluorescent image of the printed UBC logo formed by stitching tile images. The waviness of the boundary indicates the softening of the hydrogel

in culture which is expected as the hydrogel undergoes enzymatic degradation in the presence of living cells. Uniformity of the fluorescence signal also demonstrates that the cells integrated with the GelMA scaffold throughout the domain. Figure 3-9A (iii) shows a zoomed-in representative image of the region marked in Figure 3-9A (ii). The cells exhibit elongated morphology forming a network among the cells. These observations demonstrate that the GelMA scaffold provides a highly biocompatible environment for the cells to grow and integrate. Figure 3-9B (ii) shows the bioprinted bone structure with a uniform distribution of cells throughout. The square pores are also distinctively marked by the boundaries demonstrating the capability of the bioprinting system and the biomaterial to output high-resolution internal features. A close-up view of the region marked in Figure 3-9B (ii) is shown in Figure 3-9B (iii). A further zoomed-in view of the marked region in Figure 3-9B (iii) is shown in Figure 3-9C. Parts (i), (ii), and (iii) of Figure 3-9C show the stained nuclei with DAPI, stained cytoskeleton with phalloidin, and combined DAPI/Phalloidin images. Closer examination of cellular morphology shows the formation of interconnected networks among cells with highly elongated cytoskeleton. These observations highlight the excellent biocompatibility and integration of cells with the scaffold. Overall, the synthesized GelMA presented in this work is found to be suitable for 3D bioprinting applications.

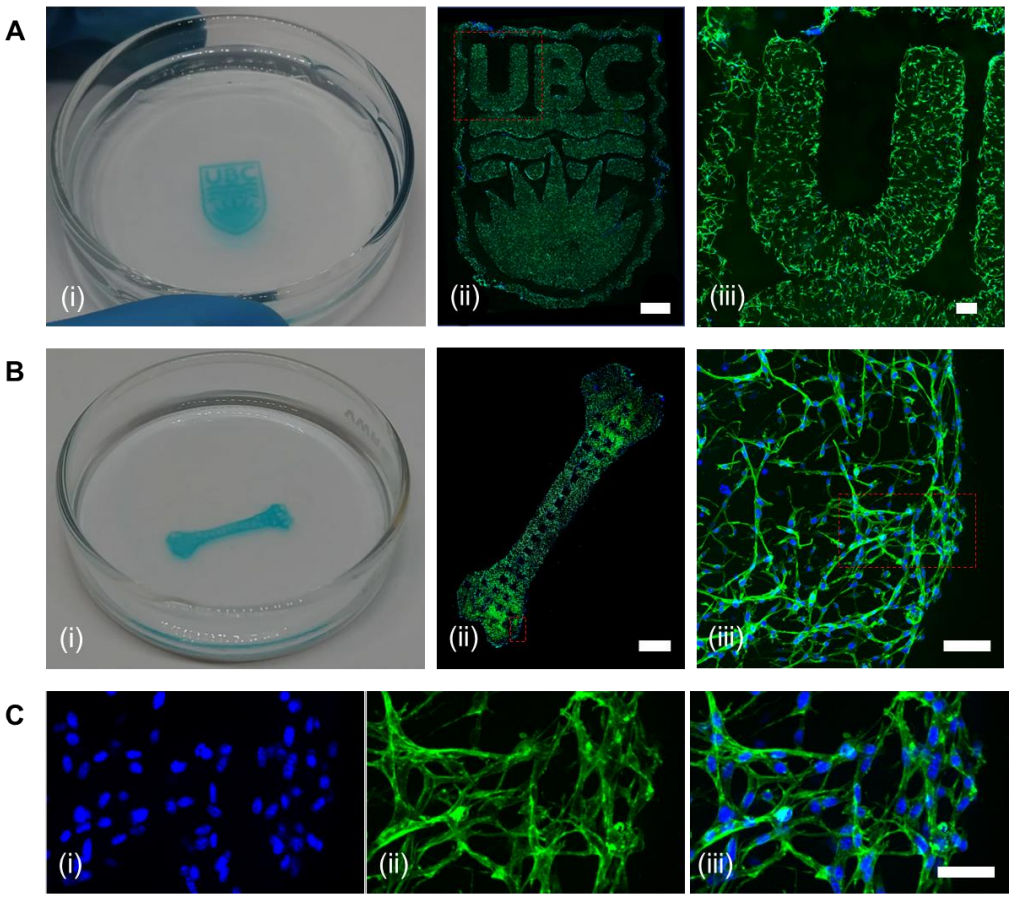


**Figure 3-9. Stereolithographic (SLA) three-dimensional (3D) bioprinting with GelMA. (A)(i) Printed UBC logo stained with blue dye. (ii) DAPI (blue)/Phalloidin (green) stained bioprinted UBC logo after 5 days of culture. Scale bar = 1 mm. (iii) Zoomed-in view of the cell morphology in the bioprinted UBC logo after 5 days of culture. Scale bar = 200 µm. (B) (i) Printed bone pattern stained with blue dye. (ii) DAPI (blue)/Phalloidin (green) stained bioprinted bone pattern after 5 days of culture. Scale bar = 2 mm. (iii) Zoomed-in view of the cell morphology in the bioprinted bone pattern after 5 days of culture. Scale bar = 100 µm. (C) Zoomed view of section of bioprinted bone pattern showing (i) nuclei stained with DAPI, (ii) cytoskeleton stained with phalloidin, and (iii) combined DAPI/Phalloidin image. Scale bar = 50 µm.**

Finally, because of the controllable and relatively low water content of the pre-drying samples developed by the current methodology, we recommend that future studies should focus on other drying alternatives that have not been possible before due to the very high water content of the pre-drying samples, such as Spray drying (SD), drum drying, or pulse combustion drying.[220] By the high production costs and long drying times of FD, it can be

concluded that SD could be a good alternative.[152,153] FD efficiency per kilogram of material is about 10 times lower than SD.[154] So, in contrast to FD, SD is a higher throughput process that is simpler, scalable, and can produce powders suitable for direct processing without milling or other secondary processing.[152,155]

## 3.5 Summary

We have presented a method that enables GelMA production with a highly reproducible yield with efficient purification and sterilization through a combined ion pairing and precipitation-based approach. Specific reaction conditions were selected for the GelMA synthesis process, which ensured its compatibility with the applied extraction and purification principles, while the reagents were chosen to ensure the simplified integration of all the production phases. In this approach, we have used an aprotic solvent (DMSO) as the reaction medium to allow, in the subsequent steps, the usage of an appropriate concentration of a neutral salt (NaCl) and a hydrophobic organic solvent (ethanol) for thorough precipitation of the protein (GelMA) at lower volumes of the precipitating agent. Additionally, ethanol has a superior dissolution power of the used organic reagents and their by-products, which has allowed for the usage of higher GMA concentration, thus reducing the reaction time considerably. For the first time, methods of GelMA hydrogel synthesis and production have been compared for their yields and degrees of methacrylation. The currently proposed method showed the highest and most reproducible yield of a highly substituted GelMA product.

The characteristics of this newly produced GelMA hydrogel were also thoroughly investigated. In brief, the ppt-GelMA showed excellent performance in consideration of both physical properties (compressive modulus, swelling properties, and degradability) and

biological properties (cell viability, and 3D cell spreading and elongation). The authors envision that the developed method for synthesizing the ppt-GelMA hydrogel can be of great benefit for tissue engineering and regenerative medicine applications, especially since it has demonstrated cell-response behaviors identical to conventionally produced GelMA hydrogels.

# Chapter 4 : Dehydration-free, High Efficiency Synthesis of GelMA

The process of synthesizing GelMA remains vastly uncharacterized and has been plagued with inconsistent batch to batch properties, low yields, and long process times. Additionally, after lengthy detoxification, this method necessitates a dehydration step, which is achieved via drying. Drying methods are usually expensive, time-consuming, laborious, and hinder the large-scale application of the synthesis process. In this work, we have outlined an approach that makes use of toluene as a detoxifying, precipitating, and sterilizing agent. In addition, toluene, by virtue of its immiscibility with water and a strong ability to precipitate, enables to directly obtain high purity GelMA (which we named as direct-GelMA or d-GelMA) without the need for an additional drying step. Using this method, we were able to produce sterile d-GelMA within 4-8 hours, which is a significantly shorter time frame as compared to conventional synthesis methods that take up to 2 weeks to complete.

## 4.1 Materials and Methods

### 4.1.1 d-GelMA Synthesis

Type A porcine skin gelatin (G-2500, Sigma-Aldrich, St Louis, MO, USA) was added to dimethyl sulfoxide (DMSO) aprotic solvent (Fisher Scientific, Ottawa, ON, Canada) at a temperature of 50°C and stirred at 400 rpm until fully dissolved to form a solution of 10% w/v. In a pellet-by-pellet fashion, the catalyst N, N-Dimethyl-4-aminopyridine (DMAP) (Sigma-Aldrich, St Louis, MO, USA) was added to attain a final concentration of 0.6 % W/V of the original DMSO volume. 1.8 ml of glycidyl methacrylate (Alfa Aesar, Tewksbury, MA, USA) per gram of dissolved gelatin were then dropped gradually onto this solution mixture while stirring. The reaction was left to run for at least 45 minutes. Either the reaction mixture or toluene (Fisher Scientific, Ottawa, ON, Canada) at three times (3X) the used initial

volume of DMSO was poured or dropped onto each other at room temperature with no stirring. The methacrylated gelatin product of the reaction is obtained as the precipitate from the resulting solution. The supernatant solution, of the other reaction's by-products, the catalyst, and any excess unreacted reactants in toluene, is decanted away from the GelMA product. Optionally, the GelMA product can be washed with more toluene. The precipitate is left to dry for at least 15 minutes. Aseptically, GelMA is to be dissolved directly into a suitable aqueous medium: phosphate-buffered saline for direct usage, or sterile reverse osmosis (RO) water to form a 20% stock solution. Any residual toluene will float on the surface of the aqueous medium and evaporates. The GelMA solution is stored at -80°C until further usage.

### 4.1.2 Yield Rate Analysis

To determine the optimal volume of toluene required for maximizing the retrieval of GelMA from the reaction mixture solution, we added toluene to the reaction mixture in increments of 1X (a similar volume to the originally used DMSO volume). After each addition, the supernatant is decanted into a new container where the subsequent 1X of toluene is added. The precipitate of all containers is then individually dissolved in pure, sterile RO water. The synthesized d-GelMA solution in pure water was frozen for 24 hours at-20°C, and then the dried d-GelMA product was recovered via lyophilization in a freeze dryer (Labconco, Kansas City, MO, USA). The dried GelMA weights are recorded. The yield of the production method was calculated as the percentage of the d-GelMA dry weight at the end of each drying process to the initially used gelatin weight.

### 4.1.3 Characterization of Material Properties

The d-GelMA stock solution, a 3% w/v stock solution of the 2-Hydroxy-4′-(2-hydroxyethoxy)-2-methylpropiophenone (Irgacure2959, CIBA Chemicals, Basel, Switzerland) photoinitiator, and sterile PBS were used in relevant amounts to prepare workable concentrations. 5%, 7.5%, and 10% w/v photocrosslinkable Df-GelMA hydrogel solutions having a final concentration of 0.5% w/v of the photoinitiator were prepared for the material characterization. The d-GelMA's degree of methacrylation, mechanical properties, and the cell viability biocompatibility assessment were performed as previously described in Chapters 3.1.1, 3.1.2, and 3.1.3, respectively.

## 4.2 Experimental Results

### 4.2.1 d-GelMA Synthesis Analysis

This study intended to produce high quality, high yield, sterile and biocompatible gelatin methacryloyl (GelMA) prepolymer through a highly efficient synthesis process, and primarily for use in tissue engineering and regenerative medicine-based applications. As shown in Figure 4-1, our production process was based on a dialysis-free and drying-free approach, comprising of the direct precipitation of the synthesized GelMA from an aprotic solvent using a water-immiscible organic solvent. Through this process, the time taken to produce ready-to-use GelMA was around 4 to 8 hours. The GelMA synthesis reaction under the conditions described above in chapter 3 takes about 1 to 3 hours. The strong precipitative ability of toluene coupled with the ability of impurities (all except GelMA) to dissolve resulted in the elimination of the dialysis step, which was instead replaced by a simple 30-minute-long dissolution and decantation procedure. Additionally, the immiscibility of toluene

with water eliminated the additional drying step. An extra hour was reserved for air-drying the GelMA, which was followed by its dissolution in an aqueous medium, leaving enough time for the light and immiscible toluene to effectively evaporate from the surface of the aqueous solution. Thus, completing a highly efficient method that demonstrates a reduction in material costs by around 90%, and the production time by more than 95% from up to 2 weeks in current methods down to a maximum of 8 hours.

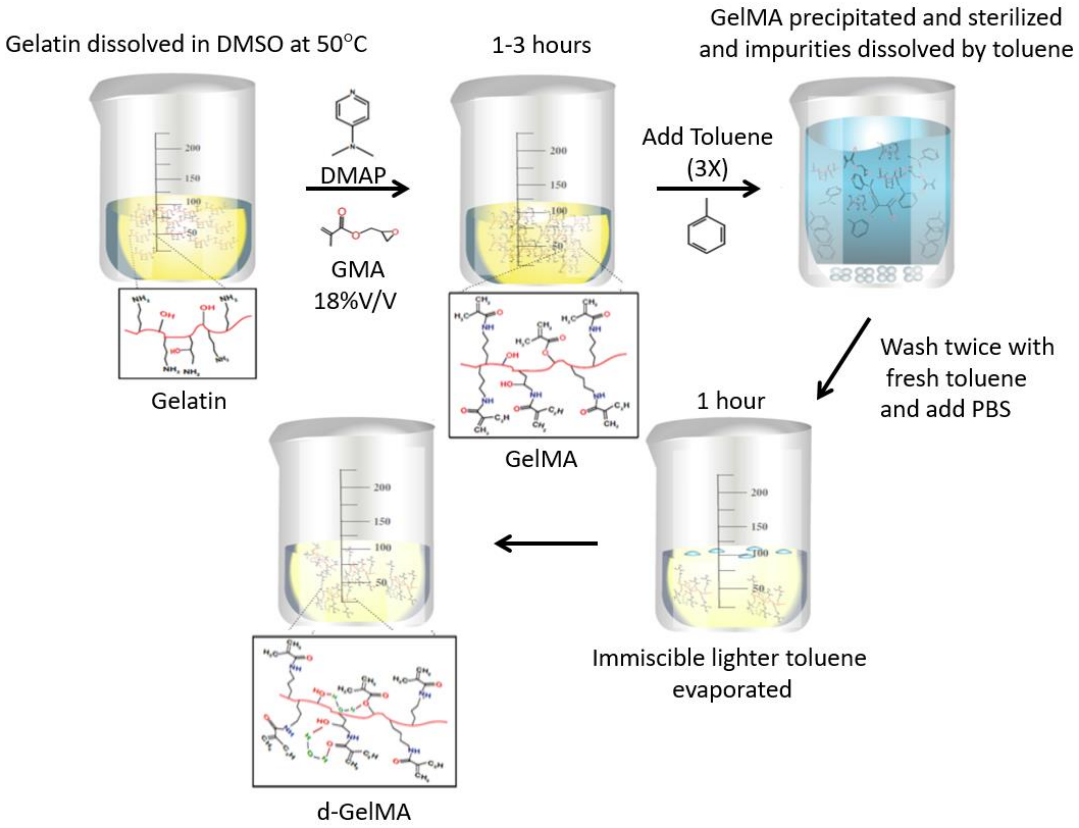


**Figure 4-1. Schematic representation of the direct GelMA (d-GelMA) production steps.**

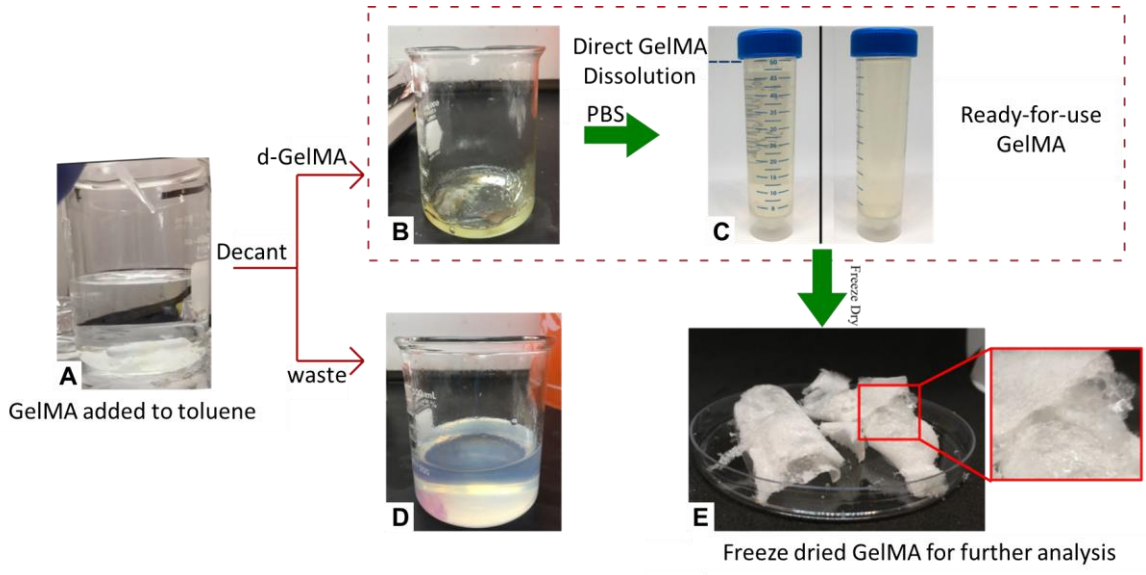


**Figure 4-2. Images depicting the d-GelMA production major process steps.**

Major steps in producing d-GelMA are highlighted in Figure 4-2. In this approach, DMSO was used as the aprotic reaction medium-solvent while toluene was used to precipitate GelMA out of the reaction mixture. Since DMSO is miscible with both aqueous and hydrophobic organic solvents, it could dissolve the reagents readily, allowing the reaction to take place. Upon the addition of toluene, in which GelMA is insoluble, both the DMSO and the reagents were removed easily. Furthermore, since proteins denature quicker in the presence of water, the absence of water in this reaction mixture prevented protein denaturation.[208] Eventually, due to the extreme hydrophobicity of the toluene, the precipitate adhered to the bottom surface of the glass beaker, allowing the considerably easy handling and washing of the resultant product. Following this, the supernatant was simply decanted, while the precipitate was washed in fresh toluene. Then, PBS was added to attain the required GelMA concentration based on the known reproducible yield of the manufacturing method. The water simply dissolved the GelMA while the lighter and more volatile toluene

floated onto the surface, evaporating and in the process, leaving behind a pure and sterile GelMA solution.[221] While this produced GelMA was ready for use or packaging, d-GelMA could now also be dissolved in pure water and dried for carrying out yield and degree of substitution measurements. As compared to the ethanol-based ppt-GelMA production methodology, the d-GelMA synthesis process can be conducted at room temperatures without the need for the addition of any other salt and/or chemical. More importantly, there is no longer a requirement for an additional drying step.

### 4.2.2 Yield Optimization

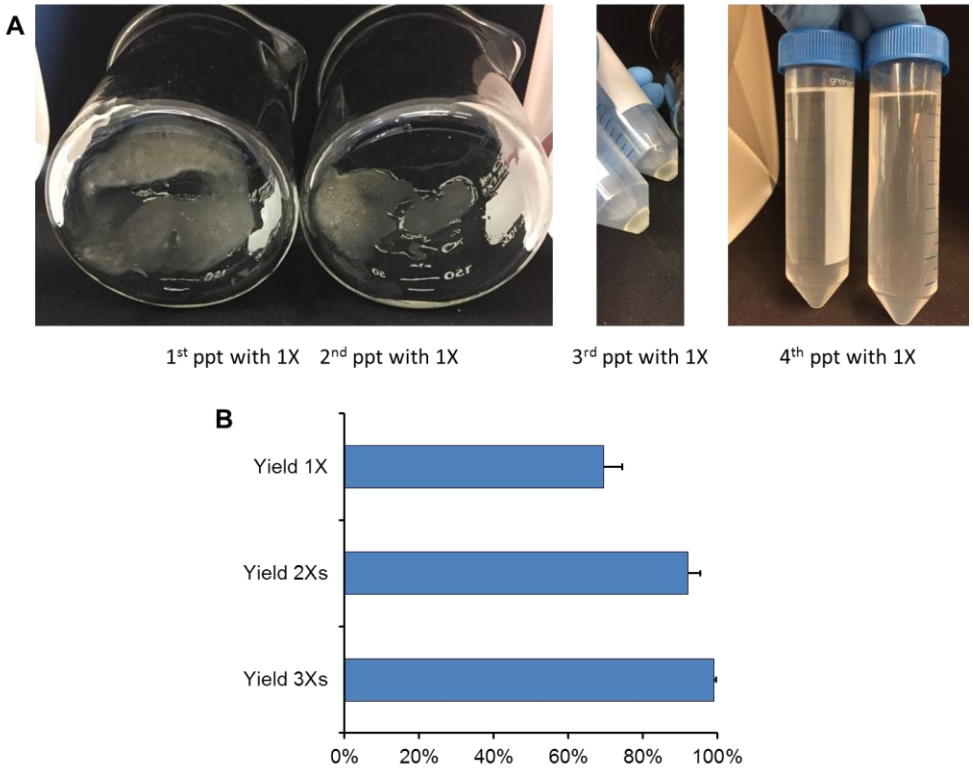


**Figure 4-3. Yield optimization strategy. (A) Images showing the d-GelMA yields after incremental additions of toluene. (1X = the volume of the used dimethyl sulfoxide in the reaction mixture). (B) Yield quantification shows that the highest d-GelMA precipitation is obtained upon adding 3X of toluene.**

Figure 4-3A highlights images depicting the optimized d-GelMA recovery process with the incremental addition of 1-fold (1X) of a toluene volume that equals to the DMSO volume

used in the reaction mixture. Figure 4-3B demonstrates that the highest yield of GelMA precipitation is obtained upon adding a maximum of 3-folds (3X) toluene volumes. With each addition of an increment of toluene, the yield was seen to increase, but this relation was not proportional. The most effective volume was the first fold of toluene that produced a yield of about 70%. Upon the addition of the second fold, the yield increased by about 20 %. With the third increment, a nearly complete recovery of the hydrogel monomers was attained. A fourth increment had no effect, thus exhibiting that there was little to no more GelMA remaining to precipitate. This was especially important in determining the minimum amount of organic solvent required for the efficient precipitation of the pre-hydrogel. The step-precipitation of the GelMA can be attributed to the mixed length of monomers that is a characteristic of GelMA and its gelatin precursor, and the variation in ionic strength that is observed at different volumes of toluene, which also has a low dielectric constant. The large GelMA protein chains could be precipitated first at relatively higher polarities of the medium as they were heavier and tended to have more hydrophobic interactions that allowed them to settle, thus forming the precipitate. With an additional reduction of medium polarity upon the addition of extra toluene, smaller chains were precipitated. For this reason, various gelatin sources with diverse average molecular weights and bloom numbers will also display varying precipitation behaviors. It should be noted that the GelMA monomers were not exposed to water during the entire process. They were, however, subjected to moderate heat ($50^0$ C, for a maximum duration of 4 hours), without the need for any additional warm dialysis. Therefore, most of the GelMA was precipitated with the first increment of toluene.

### 4.2.3 d-GelMA Characterization

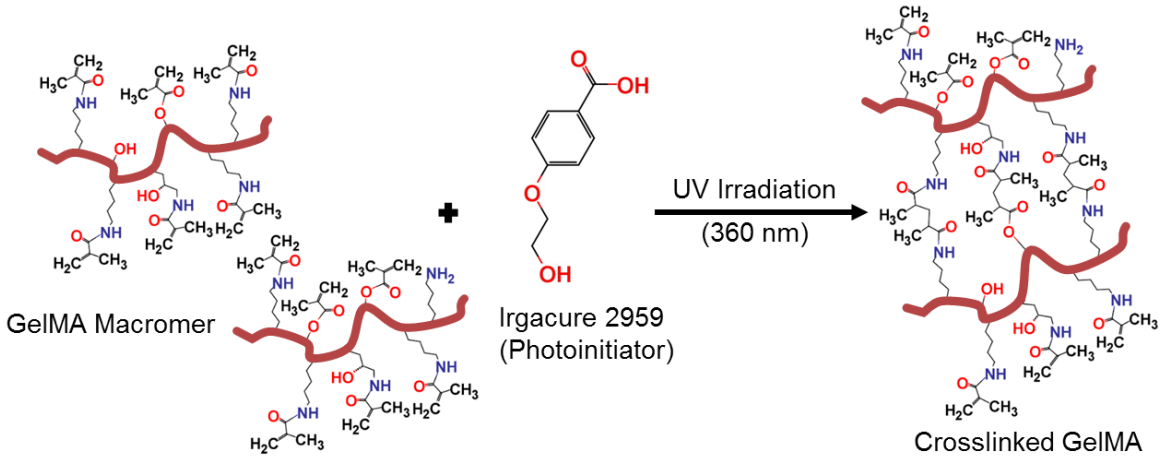


**Figure 4-4. Schematic of the GelMA photocrosslinking reaction under 360 nm ultraviolet light irradiation in the presence of Irgacure 2959 photoinitiator.**

GelMA monomers polymerize into a hydrogel via a chain photocrosslinking reaction that is initiated by the release of free radicals from the photoinitiator, irgacure 2959 upon its exposure to ultraviolet light (Figure 4-4). Characterization of the d-GelMA is illustrated in Figure 4-5. Figure 4-5A shows representative $^{1}$H-NMR spectra of the d-GelMA and gelatin as a reference for determining the degree of methacrylation. The GelMA and gelatin spectra component "*b*" (the amino lysine integration signal) is compared to the component "*a*" internal reference (the phenylalanine signal). Methacrylating gelatin with 18% V/V GMA in the presence of a DMAP catalyst for 2 hours results in a degree of methacrylation of around 80%.

At this point, it is possible to use the d-GelMA directly for an additional assessment of its mechanical properties and biocompatibility. By skipping the dialysis and drying steps, the d-GelMA was directly dissolved in the biocompatible buffer, PBS. Due to the immiscibility of toluene in water, with stirring, residual toluene formed an emulsion-like appearance

initially, Figure 4-5B. At the end of the dissolution process, the toluene had already evaporated from the surface of the aqueous solution, rendering it clear. The bioactivity of a hydrogel network, in terms of cellular attachment, morphology, and function, is highly guided by its mechanical properties, which in turn is directly correlated with the monomer concentration that is used.[209,210] Therefore, the unconfined compressive young's moduli at 3 different concentrations, 5%, 7.5%, and 10% W/V, of the d-GelMA monomers were examined. As predicted, an increase in the mechanical stiffness of the hydrogel was directly proportional to an increase in the monomer concentration, Figure 4-5C.

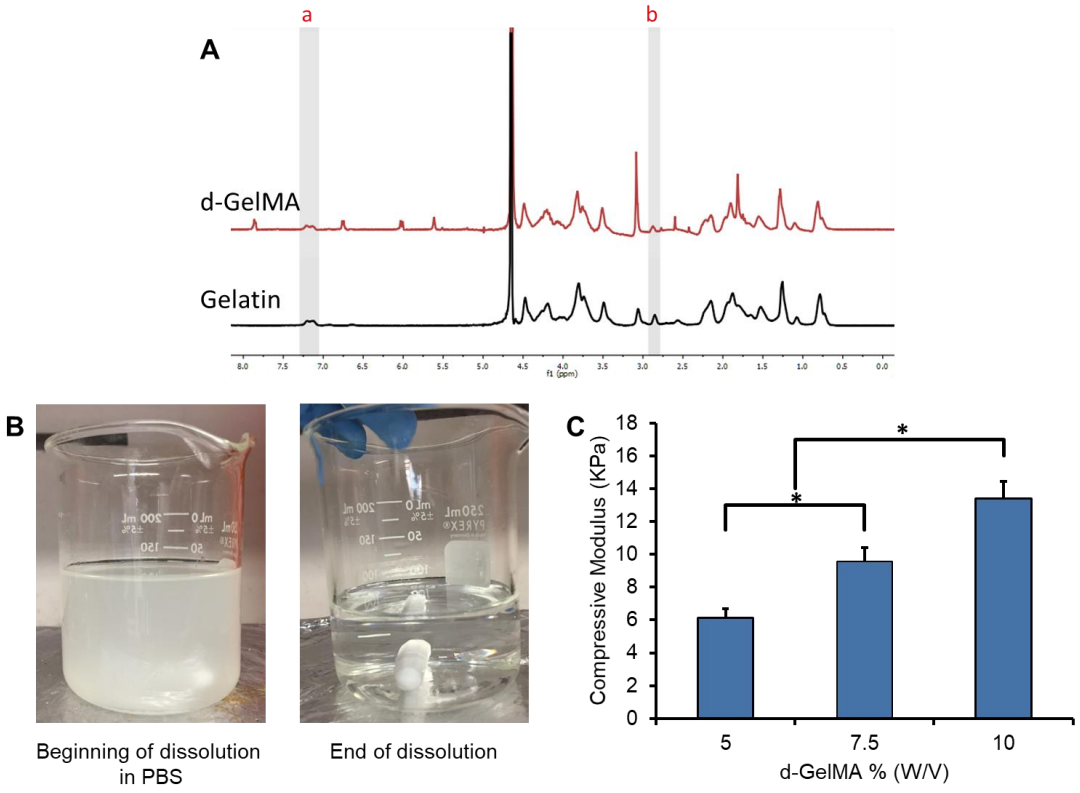


**Figure 4-5. Physical properties of the d-GelMA. (A) 1H-NMR spectra of the d-GelMA in reference to gelatin, a connotes the internal reference of the gelatin backbone, and b connotes the unsubstituted primary amines. (B) Toluene evaporation upon the dissolution of GelMA in PBS. (C) A plot represents the compressive moduli at various d-GelMA concentrations.**

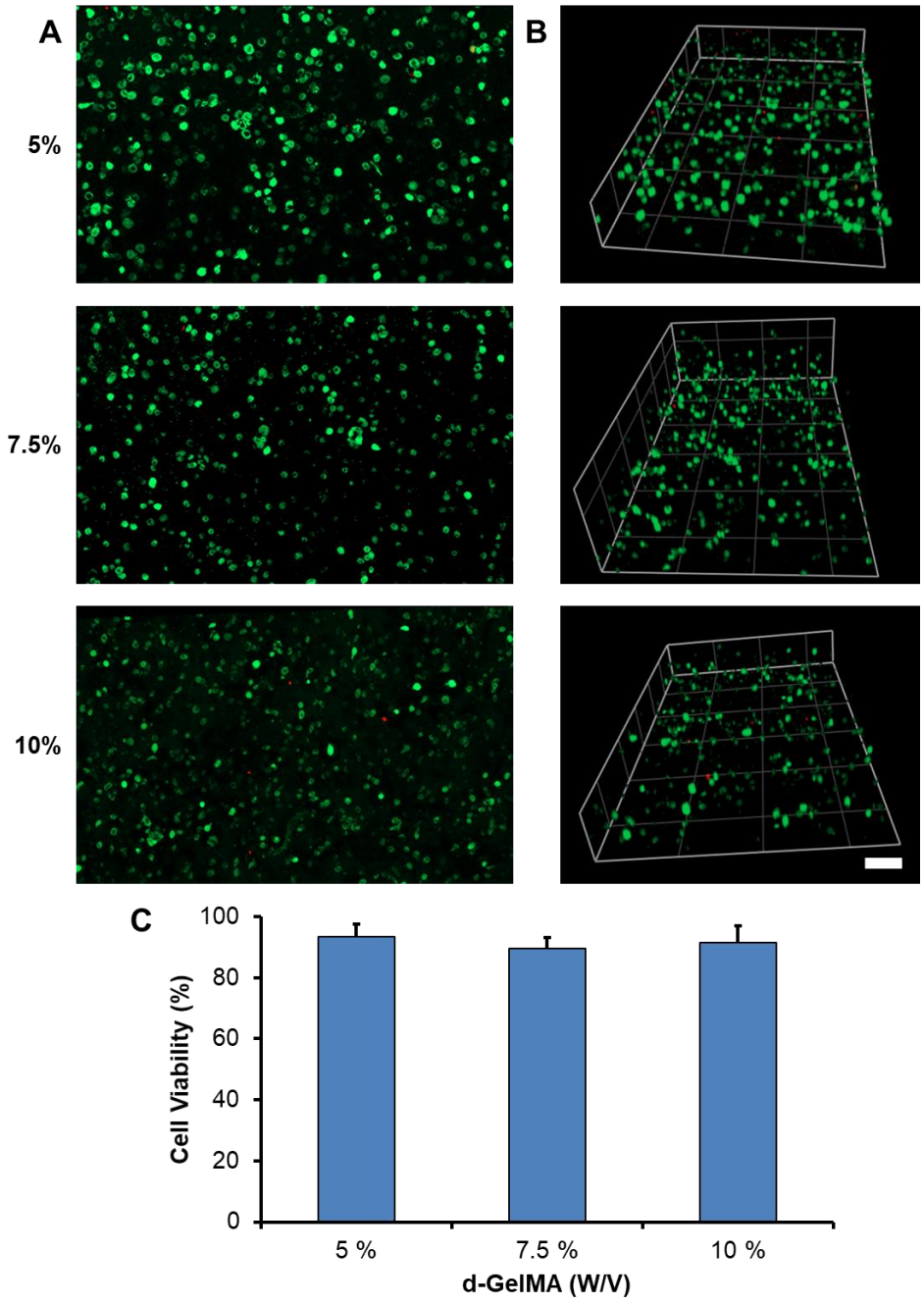


**Figure 4-6. Viability of cells encapsulated in 5%, 7.5%, and 10% d-GelMA on day 1. (A) Live/dead 2D fluorescent images. (B) 3D constructed images (green: live cells, red: dead cells). Scale bar = 100 µm. (C) Cell viability quantification.**

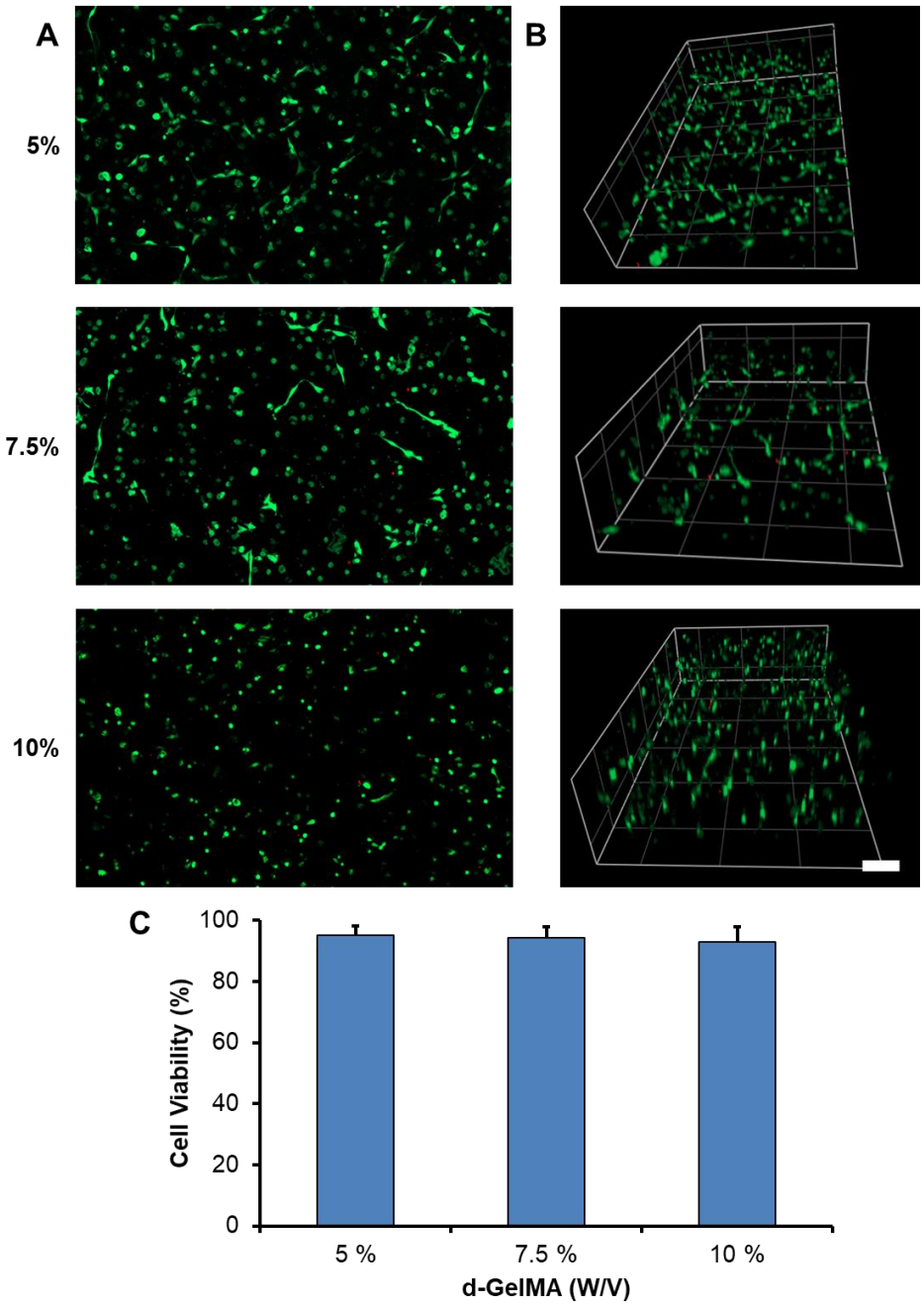


**Figure 4-7. Viability of cells encapsulated in d-GelMA on day 5. (A) Live/dead 2D fluorescent images. (B) 3D constructed images (green: live cells, red: dead cells). Scale bar = 100 µm. (C) Cell viability quantification.**

Biofabrication largely depends on the capacity of the hydrogel to provide a cell-friendly 3D microenvironment. Figures 4-6 and 4-7 show the viability of the 3D encapsulated NIH-3T3 fibroblasts viability over days 1 and 5, respectively, in the three

different d-GelMA hydrogel concentrations that were mentioned above. Viable cells emit green fluorescence, whereas dead cells emit red fluorescence. Cell viabilities around 90% were maintained for 5 days of culturing the cells. The cells also started to display their characteristic spindle-shaped elongations on day 5. The cell-cell interaction, as a function of the mixed cell density, is a fundamental factor to control the structural and functional properties of a given engineered tissue.[222] An optimum concentration of cells, $10X10^6$ per ml, was used to maintain proper cellular interactions.[222] Different degrees of elongations are shown in Figure 4-7. The degree of elongation was found to be inversely proportional to the hydrogel concentration. On day 5, the cells were forming highly interconnected networks and occupied more space within cell-laden 3D hydrogels constructs in the 5% and 7.5% GelMA concentrations, but to a lesser extent in the 10% concentration.

### 4.3 Discussion

Solvents with reduced dielectric strengths increase the attractive forces between oppositely charged protein parts, causing protein aggregation by attractive electrostatic and dipole forces.[199,200] At the isoelectric point, the relationship between the dielectric constant and protein solubility is given by:

$$\log S = k/e^2 + \log S^0 \quad (4\text{-}1)$$

, where $S^0$ is an extrapolated value of S, e is the dielectric constant of the mixture, and k is a constant that relates to the dielectric constant of water. This study presents a dialysis-free rying-free direct approach for high-purity high-yield sterile GelMA rapid production. The basis for this method is the quick and easy elimination of toluene, which enables the simultaneous precipitation of protein and the dissolution of impurities. An array of organic solvents was considered for meeting some specific characteristics complementary to the

requirements of the reaction. In addition to the hydrophobicity, antimicrobial activity, and impurities dissolution abilities of the projected organic solvent, the ideal solvent must be water immiscible with lighter density and volatile. Water-immisciblity is a physical factor that restricts the solvent's access to the hydrophilic GelMA, and subsequently inhibits protein hydrolysis. The precipitating agent is required to be volatile and lighter than water to enable its easy removal by evaporation upon the addition of the aqueous PBS solution for dissolving the GelMA. In this approach, water miscible organic solvents were excluded due the following reasons. [193,194,207,223–225] First, they have no enough hydrophobicity for high yield precipitation of GelMA. The dielectric constant (ε) at room temperature ranges between 17 to 24, while this of toluene is around 2. Second, ethanol and isopropanol are the only 2 most widely used relatively safe disinfectants. Third, the currently applied GelMA synthesis reaction impurities' dissolution power of this group widely differs. For example, ethanol has good dissolution power of the impurities but less hydrophobicity (ε= 24) than acetone (ε= 20) or isopropanol (ε= 17), which have almost no purification ability of the reaction by-products. Fourth, despite the majority are volatile, getting rid of them without lyophilization is not possible due to their miscibility with water.

Toluene was selected as the organic solvent of choice since it met all of the above-mentioned conditions while also having a superior safety profile for working personnel as compared to other similar solvents, such as benzene, carbon tetrachloride, dichloroethane and dichloromethane that exhibit small permissible exposure limits.[226–231] Table 4-1 summarizes and compares the properties of different organic solvents and their suitability for the current approach. An attempt was made to make this list of candidate solvents as comprehensive as possible. In fact, any solvent that could meet the above-stated criteria could be deemed

suitable for use in this method. However, to the best of our knowledge, toluene is the most suitable choice. For instance, benzene, dichloroethane, dichloromethane, butanol, butanone, ethyl acetate, alkanes (pentane, hexane, cyclohexane, heptane, and octane), diethyl ether, or carbon tetrachloride either show limited or no antimicrobial effects.[232] Also, dichloroethane, dichloromethane, butanol, butanone, ethyl acetate, diethyl ether, and chloroform are less hydrophobic as compared to toluene.[194,223–225] Similarly, dichloroethane, dichloromethane, carbon tetrachloride, and chloroform have a higher density than water. As well, if any of these criteria is missing, the replacement approaches would make the process less economical. For example, for solvents with no antimicrobial activity, a sterilization step (such as syringe filtration) would be needed. If the solvent was found to be less hydrophobic, there would be a need to add larger volumes for reducing the overall polarity of the media down to appropriate values. However, safety is still a difficult issue that is needed to be addressed.

As a precipitating agent, toluene fulfills the following roles; since it is highly hydrophobic and miscible in DMSO, it reduces the dielectric constant (polarity) of the solvent of the methacrylation reaction making the GelMA less soluble and therefore precipitates it. Toluene is also used to increase the production yield as it is extremely hydrophobic and has a very low dielectric constant (relative permittivity) (= 2)[194,223,225] and is better for completely precipitating the GelMA in high yield at a reduced volume (3 X) at room temperature (Figure 4-3). Additionally, toluene has a zero HLB (Hydrophile-Lipophile Balance) (a value that expresses the relationship of the strength of hydrophilic to hydrophobic moieties of a chemical).[233] The extreme hydrophobicity displayed by toluene protects GelMA against hydrolysis since, in this medium, it has restricted access to water. As

a purifying agent, toluene dissolves all reaction impurities and toxic materials. Glycidyl methacrylate, its by-products, and the d-map catalyst are highly soluble in toluene.[192,207] Toluene has also long been recognized for its use as an antimicrobial and a sterilizing agent.[234] Toluene is a bacteriostatic agent that interferes with the microbial protein production.[235] Examples of other commonly known bacteriostatic antibiotics classes are tetracyclines, sulfonamides, spectinomycin, trimethoprim, chloramphenicol, macrolides, and lincosamides. Therefore, toluene is also used as a disinfecting agent for sterilizing the GelMA during the precipitation and the washing steps at room temperature.

By virtue of their miscibility with toluene and low relative permittivities (of around 40),[194,223,225] that reduces the solubility of the pre-gel monomer, thereby enabling a more efficient purification, aprotic solvents are chosen as the suitable reaction media for this approach. DMSO is less toxic as compared to other aprotic solvents. For instance, as per the International Agency for Research on Cancer (IARC), dimethylformamide is a possible carcinogen and causes liver disease.[236,237] It has also been reported as a reproductive toxin that could damage the developing fetus in animals. Meanwhile, pyridine, triethylamine, or any other tertiary nitrogen base could be used as a catalyst as an alternative to diaminopyridine. While these catalysts have been in use since the turn of the 20th century, D-MAP is a newer catalyst that is stronger and could enhance the rate of acylation by a factor of approximately 10,000.[238,239] All these catalysts are relatively toxic but are used in small quantities for our reaction.[238,240,241]

**Table 4-1. Summary of various organic solvents properties and comparison of their suitability for the dehydration-free method.**

| Organic Solvents/Required Solvent Properties | Hydrophobicity (for GelMA ppt) | Antimicrobial Property (for sterilization) | By-products Dissolution Power (for purification) | Volatility (needs to be volatile at room temperature) | Density (needs to be lighter than water) | Relative Safety | Ref |
|---|---|---|---|---|---|---|---|
| Dichloroethane and Dichloromethane | Less Hydrophobic (ε ~ 10) | X | NA | ✓ | Heavier than water | X permissible exposure limit (25 - 50 ppm) | 194,223–225,231,242 |
| Butanol and butanone | Less hydrophobic (ε= 6.02) | X | NA | ✓ | ✓ | ✓ permissible exposure limit (100 - 200 ppm) | 194,223–225,243,244 |
| Ethyl Acetate | Less hydrophobic (ε ~ 17) | Limited | NA | ✓ | ✓ | ✓ permissible exposure limit (400 ppm) | 194,223–225,245,246 |
| Alkanes (Pentane, hexane, cyclohexane, heptane, octane) | ✓ (ε ~ 2) | X | NA | ✓ | ✓ | ✓ permissible exposure limit (~500 ppm) | 194,223–225,247–251 |
| Diethyl ether | Less hydrophobic (ε= 4.33) | X | NA | ✓ | ✓ | ✓ permissible exposure limit (400 ppm) | 191, 227–229, 250 |
| Carbon tetrachloride | ✓ (ε= 2.24) | X | NA | ✓ | Heavier than water | X permissible exposure limit (10 ppm) | 191, 224, 227–229 |
| Chloroform | Less hydrophobic (ε= 4.81) | ✓ | NA | ✓ | Heavier than water | ✓ permissible exposure limit (50 ppm) | 191, 227–229, 251 |
| Benzene | ✓ (ε= 2.27) | X | ✓ | ✓ | ✓ | X permissible exposure limit (1 ppm) | 191, 223, 227–229 |
| Toluene | ✓ | ✓ | ✓ | ✓ | ✓ | ✓ permissible exposure limit (200 ppm) | 191, 220, 227–229 |

## 4.4 Summary

The dialysis and freeze-drying steps comprising the GelMA synthesis process are significant hurdles that have prevented it from being time-efficient, economical, and reproducible. Also, currently popular methods are plagued with irreproducible yields, despite maintaining similar reaction conditions from batch to batch. In our approach, we have used an aprotic solvent as the reaction medium to allow the use of an extremely hydrophobic organic solvent. This subsequently enables the complete precipitation of the protein when lower volumes of the precipitating agent are used, thus producing high and reproducible yields. Of all the used reagents, the precipitating agent displays a superior dissolution ability by virtue of its high hydrophobicity. The immiscibility of the precipitating agent with water[221] coupled with its lightness and volatility allows it to be purified easily via evaporation, eliminating any need for an additional drying process, thus ensuring the purity of the final product. Additionally, using the extremely hydrophobic toluene, which does not have access to the polar GelMA, prevents protein denaturation and so enables properties of GelMA that are reproducible. Thus, using the specifically designed toluene-based GelMA precipitation method has enabled: 1- The elimination of two primary causes of irreproducibility; dialysis and freeze-drying. 2- The integration of the purification and sterilization steps to enable a reduction of the production time, and finally, 4- A reduction in the cost of materials by about 90% and production time by about 95%.

# Chapter 5 : Conclusion and Future Works

## 5.1 Concluding Remarks

Many challenges still face the efficient production of cell-laden microgels that are subject to extensive study. For tissue engineering applications, current microfluidics-based technologies are still considered as being low throughput and, thus, unfeasible. The cell distribution among the generated microdroplets needs to be controlled, and the off-chip steps of gelation and oil extraction need to be replaced by more innovative techniques. In addition, the hydrogel component manufacturing represents another low-yield and a non-cost-effective process.

In this research, the required steps of microgel production are parallelized by integrating droplet generation with simultaneous cell encapsulation, droplet photocrosslinking, and oil filtration within one chip. This automates the bio-manufacturing process of cell-laden microgels as a serial, parallel, and continually operational approach that fully eliminates the need for any off-chip handling of the generated microdroplets. Bypassing the off-chip crosslinking and filtration steps increases the total yield and efficiency of manufacturing, while also improving the viability of encapsulated cells. Over 4 different cellular seeding densities, monodisperse hydrogel microdroplets loaded with cells in a reasonable uniformity were generated in high-throughput. The BSA cellular pre-treatment, using the dispersed phase magnetic mixer and manufacturing the device with a relatively elevated channel height, resulted in a stable droplets-generation process. The microgels produced under this platform conditions were able to serve as excellent microenvironments for 3D cell culture. The encapsulated cells were investigated for healthy cellular activities and exhibited normal growth, proliferation, and formation of intercellular connections. The cells could also migrate from the degrading gels over time and integrated effectively with

their surrounding tissue culture environment. This result confirms that the developed microfluidic platform could indeed fabricate biocompatible micro-3D environments. This is owing to the on-chip rapid photogelation under a visible light wavelength laser, and to the rapid elimination of the oil phase in the microfilter that is integrated to the same device. With these functionalities, this platform can greatly increase the efficiency of microgel-based tissue engineering.

For inefficiencies concerning hydrogel manufacturing, this thesis presents a novel method for GelMA detoxification and purification. Tackling these hurdles enabled a rapid, highly reproducible yield process along with the integration of the sterilization step within the purification phase. This was based on the concept of applying a combined approach integrating the properties of desolvation and ion-pairing for effective dialysis-free purification of the photocrosslinkable hydrogel. The reaction conditions were manipulated to reduce the methacrylation reaction time in a manner that is compatible with the proposed detoxification process and simultaneously permitted the complete integration of all the production stages.

A medium polarity reaction milieu was initially created by using DMSO aprotic solvent. This allowed for easier desolvation of the produced GelMA protein upon the combined addition of small amounts of the NaCl salt and the hydrophobic ethanol solvent in the following steps. In addition, all the other reaction components and impurities except GelMA display high solubilities in ethanol. This property permitted the usage of higher concentrations of the methacrylating agent GMA, which was not possible before. Consequently, the reaction was forward faster and was completed sooner. As a part of this study, the yield and the extent of methacrylation in GelMA batches produced by various

protocols were also compared. This precipitation-based method exhibited the highest yield with a similar degree of substitution of methacrylate groups. Moreover, ppt-GelMA demonstrated mechanical and biological properties similar to conventionally produced GelMA to the extent that it could be applied for tissue engineering applications such as 3D bioprinting, as shown in this thesis.

Post-extraction dehydration of proteins, among other chemicals, is essential for determining the quantities of the isolated protein to specify its reconstructed concentration. This is mainly due to the highly variable and mostly low yield production of general protein extraction processes. The inherent properties of each protein, preparation conditions, and/or isolation methods define the subsequent drying and reconstitution approaches. In case a protein is synthesized in a chemical reaction, the physical and chemical properties of each of the reagents, products, and by-products need to be considered before and during executing the purification and drying approaches. In the case of GelMA, it is commonly synthesized in a chemical reaction that requires dialysis for detoxification and a subsequent freeze-drying step to produce a highly diluted dialysis-product. Freeze-drying and spray drying are the most widely used dehydration methods; however, they are, in general, either expensive, time-consuming, or expose the protein to some risk of destabilization and loss of yield.

With careful analysis and contemplation upon the options and conditions expected during the methacrylation reaction, we could tailor specifications of the used reaction media, reagents, and their relative concentrations for efficient purification that did not require an additional drying step. This depends on the production of a high reproducible known yield that allows for the direct reconstitution of the protein immediately after detoxification. Depending on the adjusted reaction conditions, thorough consideration of organic solvents

was conducted with a predetermined set of criteria including; high hydrophobicity, dissolution power of the selected reagents and their by-products, antimicrobial properties, densities, immiscibility with water, and safety. It was found that toluene met these pre-set criteria to the greatest extent and so was used as the solvent of choice for the reaction. This approach could effectively produce a purified, sterile GelMA through a reproducible, high yield, and dehydration-free manufacturing process. Table 5-1 compares the two precipitation GelMA synthesis methods with the conventional method.

**Table 5-1. Comparison of the GelMA synthesis methods.**

| | Standard GelMA (Dialysis + Freeze Drying) | Ppt-GelMA (Precipitation in Ethanol + NaCl) | d-GelMA (Precipitation in Toluene) |
|---|---|---|---|
| **Yield** | 60 – 70% | 90% | 99% |
| **Production Time** | 2 weeks | 3 – 4 days | 8 hours |
| **Production Cost** | High | Medium | Low |
| **Reproducibility** | X | ✓ | ✓ |
| **Sterility** | X | ✓ | ✓ |

## 5.2 Significance of Contributions

Advances in biofabrication technologies for tissue engineering require the development of highly efficient and reproducible technologies that can be translated clinically to regenerate or replace injured tissues. The microscale tissue engineering approach aims to create biomimetic engineered microtissues by manipulating the microscale structural features.

Hydrogel-based solutions, that can encapsulate various cell-types and bioactive molecules, are used as matrices in microgels and 3D bioprinting biofabrication approaches. However, the cell-laden microgels biofabrication has a limited throughput, and the hydrogel component manufacturing is a low-yield and a non-cost-effective process. This represented significant hurdles against exploring the maximum potential of these biofabrication techniques. This thesis intended to resolve these efficiency challenges. The contributions of this thesis to research include,

1. The novel on-chip platform integrating several steps for the microfluidics-based fabrication of the cell-laden microgels has been developed. This platform allowed for a high-throughput process of fabricating microgels by eliminating any off-chip requirements for handling the microgels.
2. A dialysis-free detoxification and purification method for GelMA production without the need of excess volumes of organic solvents has been developed. The synthesis protocol demonstrated a high yield GelMA and the resulting GelMA was sterile, reproducible, showed acceptable physical properties, and was highly biocompatible. The yield of different GelMA production protocols was a knowledge gap that has been addressed along with their methacrylation rates.
3. Furthermore, this thesis research has developed the tailoring of a dehydration-free GelMA production method that uses toluene to eliminate the labor-intensive and time-consuming drying step, in addition to the dialysis and product sterilization steps. This is an efficient novel method to directly produce high yield GelMA within a few hours.

## 5.3 Recommendations for Future Work

There are a few recommended future works. First, the integration of multiple microgel fabrication chips onto a single chip for a parallel operation will enable to realize scale-up production of microgels for practical tissue regeneration applications as shown in Figure 5-1.

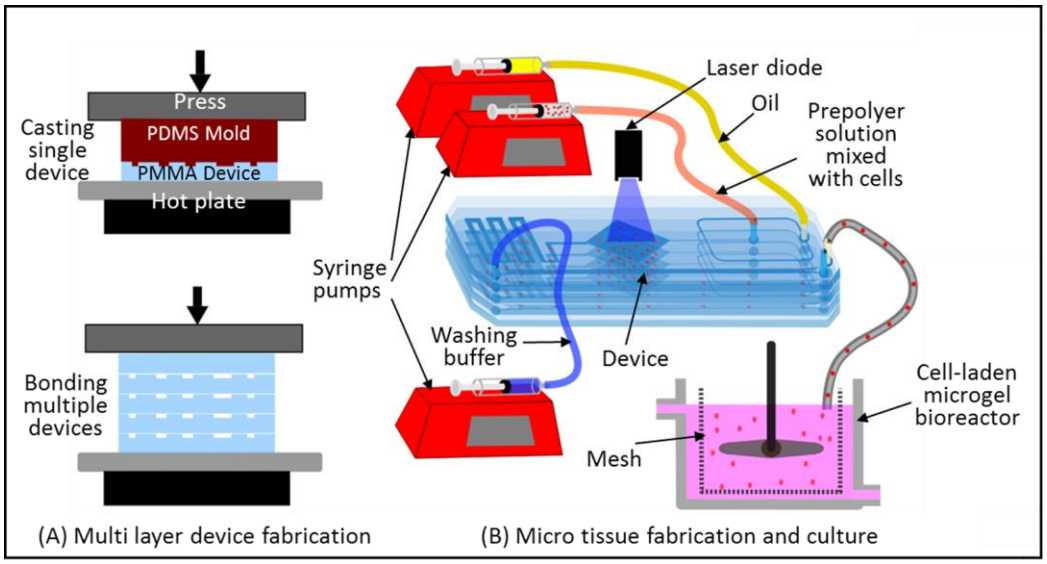


**Figure 5-1. Schematic of mass production process for cell-laden microgels**

The integrated microfluidic channels will be stacked onto the same chip with only a single set of inputs and outputs. The horizontal parallelization layout of several chips necessitates large dead-volumes due to long distribution channels.[254] While vertically packing microfluidic chips on top of each other would permit a higher density of microfluidic chips per area and volume with reduced device structure complexity. Current fabrication techniques, such as micromachining and soft-lithography, confine the structures to two-dimensional, precluding common use of parallelized devices.[255,256] Rapid prototyping based on additive fabrication principles is required to enable the production of complex three-dimensional structures at low cost, and design freedom. Hot embossing and bonding

techniques of several polymethyl methacrylate (PMMA)-based chips can be used for parallelization and stacking of the integrated platform.

Second, we believe that GelMA production will be fully automated in the near future. The reported novel methods for GelMA production eliminate the requirement for any devices or excessive equipment. The selective precipitation approach in water immiscible organic solvent for GelMA manufacturing do not require separate purification steps, such as dialysis and dehydration steps (e.g., freeze-drying or spray-drying). Having a single-compartment container for the multistep process opens the door for the development of an automated synthesis system. Automated GelMA synthesis will significantly reduce material handling time to facilitate the concept of highly efficient biofabrication of cell-laden hydrogel tissues for real clinical applications.

## Bibliography


1. Engineering T. *Tissue Engineering*. (Pallua N, Suscheck C V., eds.). Berlin, Heidelberg: Springer Berlin Heidelberg; 2011. doi:10.1007/978-3-642-02824-3

2. Howard D, Buttery LD, Shakesheff KM, Roberts SJ. Tissue engineering: Strategies, stem cells and scaffolds. *J Anat*. 2008. doi:10.1111/j.1469-7580.2008.00878.x

3. Hong J, Shin Y, Kim S, Lee J, Cha C. Complex Tuning of Physical Properties of Hyperbranched Polyglycerol-Based Bioink for Microfabrication of Cell-Laden Hydrogels. *Adv Funct Mater*. 2019;29(13):1808750. doi:10.1002/adfm.201808750

4. Chang TM. Semipermeable Microcapsules. *Science*. 1964;146(3643):524-525. doi:10.1126/science.146.3643.524

5. Rabanel JM, Banquy X, Zouaoui H, Mokhtar M, Hildgen P. Progress technology in microencapsulation methods for Cell therapy. *Biotechnol Prog*. 2009;25(4):946-963. doi:10.1002/btpr.226

6. Groll J, Boland T, Blunk T, et al. Biofabrication: Reappraising the definition of an evolving field. *Biofabrication*. 2016;8(1). doi:10.1088/1758-5090/8/1/013001

7. Pavlovich MJ, Hunsberger J, Atala A. Biofabrication: a secret weapon to advance manufacturing, economies, and healthcare. *Trends Biotechnol*. 2016;34(9):679-680. doi:10.1016/j.tibtech.2016.07.002

8. Costa PF. Translating Biofabrication to the Market. *Trends Biotechnol*. October 2019. doi:10.1016/j.tibtech.2019.04.013

9. Nichol JW, Khademhosseini A. Modular tissue engineering: engineering biological tissues from the bottom up. *Soft Matter*. 2009;5(7):1312. doi:10.1039/b814285h

10. Ikada Y. Challenges in tissue engineering. *J R Soc Interface*. 2006;3(10):589-601. doi:10.1098/rsif.2006.0124

11. Khademhosseini A, Langer R, Borenstein J, Vacanti JP. Microscale technologies for tissue engineering and biology. *Proc Natl Acad Sci*. 2006;103(8):2480-2487. doi:10.1073/pnas.0507681102

12. McGuigan AP, Sefton M V. Design and fabrication of sub-mm-sized modules containing encapsulated cells for modular tissue engineering. *Tissue Eng*. 2007;13(5):1069-1078.

13. Pathak A, Kumar S. Biophysical regulation of tumor cell invasion: moving beyond matrix stiffness. *Integr Biol (Camb)*. 2011;3(4):267-278. doi:10.1039/c0ib00095g

14. Atala A, Lanza R, Thomson JA, Nerem R. *Principles of Regenerative Medicine*.

Academic Press; 2010.

15. Choi CH, Jung JH, Rhee YW, Kim DP, Shim SE, Lee CS. Generation of monodisperse alginate microbeads and in situ encapsulation of cell in microfluidic device. *Biomed Microdevices*. 2007;9(6):855-862. doi:10.1007/s10544-007-9098-7

16. Caprini D, Sinibaldi G, Marino L, Casciola CM. A T-junction device allowing for two simultaneous orthogonal views: application to bubble formation and break-up. *Microfluid Nanofluidics*. 2018;22(8):85. doi:10.1007/s10404-018-2101-1

17. Li X, He L, Gu H, Sun F, Liu M. Numerical study of droplet formation in the T-junction microchannel with wall velocity slip. *Energy Procedia*. 2019;158:5459-5464. doi:10.1016/J.EGYPRO.2019.01.601

18. Ma P, Fu T, Zhu C, Ma Y. Asymmetrical breakup and size distribution of droplets in a branching microfluidic T-junction. *Korean J Chem Eng*. 2019;36(1):21-29. doi:10.1007/s11814-018-0165-y

19. Liang D, Ma R, Fu T, et al. Dynamics and formation of alternating droplets under magnetic field at a T-junction. *Chem Eng Sci*. 2019;200:248-256. doi:10.1016/J.CES.2019.01.053

20. Chakraborty I, Ricouvier J, Yazhgur P, Tabeling P, Leshansky AM. Droplet generation at Hele-Shaw microfluidic T-junction. *Phys Fluids*. 2019;31(2):022010. doi:10.1063/1.5086808

21. Sun L, Fan M, Li P, et al. Microbubble characteristic in a T-junction microchannel in microfluidic chip. *Mol Phys*. February 2019:1-11. doi:10.1080/00268976.2019.1572926

22. Tan WH, Takeuchi S. Monodisperse alginate hydrogel microbeads for cell encapsulation. *Adv Mater*. 2007;19(18):2696-2701. doi:10.1002/adma.200700433

23. Um E, Lee D-S, Pyo H-B, Park J-K. Continuous generation of hydrogel beads and encapsulation of biological materials using a microfluidic droplet-merging channel. *Microfluid Nanofluidics*. 2008;5(4):541-549. doi:10.1007/s10404-008-0268-6

24. Sabhachandani P, Sarkar S, Mckenney S, Ravi D, Evens AM, Konry T. Microfluidic assembly of hydrogel-based immunogenic tumor spheroids for evaluation of anticancer therapies and biomarker release. *J Control Release*. 2019;295:21-30. doi:10.1016/J.JCONREL.2018.12.010

25. Kumachev A, Greener J, Tumarkin E, Eiser E, Zandstra PW, Kumacheva E. High-throughput generation of hydrogel microbeads with varying elasticity for cell encapsulation. *Biomaterials*. 2011;32(6):1477-1483. doi:10.1016/j.biomaterials.2010.10.033

26. Highley CB, Song KH, Daly AC, Burdick JA. Jammed Microgel Inks for 3D Printing

Applications. *Adv Sci*. 2019;6(1):1801076. doi:10.1002/advs.201801076

27. Wang H, Liu H, Liu H, Su W, Chen W, Qin J. One-Step Generation of Core-Shell Gelatin Methacrylate (GelMA) Microgels Using a Droplet Microfluidic System. *Adv Mater Technol*. January 2019:1800632. doi:10.1002/admt.201800632

28. Mohamed MGA, Kheiri S, Islam S, Kumar H, Yang A, Kim K. An integrated microfluidic flow-focusing platform for on-chip fabrication and filtration of cell-laden microgels. *Lab Chip*. 2019. doi:10.1039/C9LC00073A

29. Benavente-Babace A, Haase K, Stewart DJ, Godin M. Strategies for controlling egress of therapeutic cells from hydrogel microcapsules. *J Tissue Eng Regen Med*. March 2019:term.2818. doi:10.1002/term.2818

30. Gañán-Calvo A. Generation of Steady Liquid Microthreads and Micron-Sized Monodisperse Sprays in Gas Streams. *Phys Rev Lett*. 1998;80(2):285-288. doi:10.1103/PhysRevLett.80.285

31. Seemann R, Brinkmann M, Pfohl T, Herminghaus S. Droplet based microfluidics. *Reports Prog Phys*. 2011;75(1):016601. doi:10.1088/0034-4885/75/1/016601

32. Wang Z, Samanipour R, Gamaleldin M, Sakthivel K, Kim K. An automated system for high-throughput generation and optimization of microdroplets. *Biomicrofluidics*. 2016;10(5):054110. doi:10.1063/1.4963666

33. Mohamed M, Kumar H, Wang Z, et al. Rapid and Inexpensive Fabrication of Multi-Depth Microfluidic Device using High-Resolution LCD Stereolithographic 3D Printing. *J Manuf Mater Process*. 2019;3(1):26. doi:10.3390/jmmp3010026

34. Samanipour R, Wang Z, Ahmadi A, Kim K. Experimental and computational study of microfluidic flow-focusing generation of gelatin methacrylate hydrogel droplets. *J Appl Polym Sci*. 2016;133(29). doi:10.1002/app.43701

35. Sun Y, Cai B, Wei X, et al. A valve-based microfluidic device for on-chip single cell treatments. *Electrophoresis*. 2019;40(6):961-968. doi:10.1002/elps.201800213

36. Cai B, Ji T-T, Wang N, et al. A microfluidic platform utilizing anchored water-in-oil-in-water double emulsions to create a niche for analyzing single non-adherent cells. *Lab Chip*. 2019;19(3):422-431. doi:10.1039/C8LC01130C

37. Edd JF, Di Carlo D, Humphry KJ, et al. Controlled encapsulation of single-cells into monodisperse picolitre drops. *Lab Chip*. 2008;8(8):1262-1264. doi:10.1039/b805456h

38. Kim C, Lee KS, Kim YE, et al. Rapid exchange of oil-phase in microencapsulation chip to enhance cell viability. *Lab Chip*. 2009;9(9):1294-1297. doi:10.1039/b819044e

39. Kim C, Chung S, Kim YE, et al. Generation of core-shell microcapsules with three-dimensional focusing device for efficient formation of cell spheroid. *Lab Chip*.

2011;11(2):246-252. doi:10.1039/c0lc00036a

40. Wu L, Chen P, Dong Y, Feng X, Liu BF. Encapsulation of single cells on a microfluidic device integrating droplet generation with fluorescence-activated droplet sorting. *Biomed Microdevices*. 2013;15(3):553-560. doi:10.1007/s10544-013-9754-z

41. Capretto L, Mazzitelli S, Luca G, Nastruzzi C. Preparation and characterization of polysaccharidic microbeads by a microfluidic technique: Application to the encapsulation of Sertoli cells. *Acta Biomater*. 2010;6(2):429-435. doi:10.1016/j.actbio.2009.08.023

42. Allazetta S, Hausherr TC, Lutolf MP. Microfluidic synthesis of cell-type-specific artificial extracellular matrix hydrogels. *Biomacromolecules*. 2013;14(4):1122-1131. doi:10.1021/bm4000162

43. Köster S, Angilè FE, Duan H, et al. Drop-based microfluidic devices for encapsulation of single cells. *Lab Chip*. 2008;8(7):1110. doi:10.1039/b802941e

44. Jiang W, Li M, Chen Z, et al. Cell-laden microfluidic microgels for tissue regeneration. *Lab Chip*. 2016;16(23):4482-4506. doi:10.1039/C6LC01193D

45. Baharvand H, Hashemi SM, Kazemi Ashtiani S, Farrokhi A. Differentiation of human embryonic stem cells into hepatocytes in 2D and 3D culture systems in vitro. *Int J Dev Biol*. 2006;50(7):645-652. doi:10.1387/ijdb.052072hb

46. Baker BM, Chen CS. Deconstructing the third dimension - how 3D culture microenvironments alter cellular cues. *J Cell Sci*. 2012;125(13):3015-3024. doi:10.1242/jcs.079509

47. Ronaldson-Bouchard K, Vunjak-Novakovic G. Organs-on-a-Chip: A Fast Track for Engineered Human Tissues in Drug Development. *Cell Stem Cell*. 2018;22(3):310-324. doi:10.1016/J.STEM.2018.02.011

48. Wang Z, Samanipour R, Kim K. Organ-on-a-Chip Platforms for Drug Screening and Tissue Engineering. In: *Biomedical Engineering: Frontier Research and Converging Technologies*. Springer International Publishing; 2015:209-233.

49. Zhang Q, Sito L, Mao M, He J, Zhang YS, Zhao X. Current advances in skin-on-a-chip models for drug testing. *Microphysiological Syst*. 2018;1:1-1. doi:10.21037/mps.2018.08.01

50. Jung J, Oh J. Cell-induced flow-focusing instability in gelatin methacrylate microdroplet generation. *Biomicrofluidics*. 2014;8(3):036503. doi:10.1063/1.4880375

51. Ma S, Natoli M, Liu X, et al. Monodisperse collagen–gelatin beads as potential platforms for 3D cell culturing. *J Mater Chem B*. 2013;1(38):5128. doi:10.1039/c3tb20851f

52. Headen DM, Aubry G, Lu H, García AJ. Microfluidic-based generation of size-controlled, biofunctionalized synthetic polymer microgels for cell encapsulation. *Adv Mater*. 2014;26(19):3003-3008. doi:10.1002/adma.201304880

53. Bajaj P, Schweller RM, Khademhosseini A, West JL, Bashir R. 3D Biofabrication Strategies for Tissue Engineering and Regenerative Medicine. *Annu Rev Biomed Eng*. 2014;16:247-276. doi:10.1146/annurev-bioeng-071813-105155

54. van Duinen V, Trietsch SJ, Joore J, Vulto P, Hankemeier T. Microfluidic 3D cell culture: from tools to tissue models. *Curr Opin Biotechnol*. 2015;35:118-126. doi:10.1016/j.copbio.2015.05.002

55. Annabi N, Tamayol A, Uquillas JA, et al. 25th anniversary article: Rational design and applications of hydrogels in regenerative medicine. *Adv Mater*. 2014;26(1):85-124. doi:10.1002/adma.201303233

56. Utech S, Prodanovic R, Mao AS, Ostafe R, Mooney DJ, Weitz D a. Microfluidic Generation of Monodisperse, Structurally Homogeneous Alginate Microgels for Cell Encapsulation and 3D Cell Culture. *Adv Healthc Mater*. 2015;4(11):1628-1633. doi:10.1002/adhm.201500021

57. Sheikhi A, de Rutte J, Haghniaz R, et al. Microfluidic-enabled bottom-up hydrogels from annealable naturally-derived protein microbeads. *Biomaterials*. 2019;192:560-568. doi:10.1016/J.BIOMATERIALS.2018.10.040

58. Matsunaga YT, Morimoto Y, Takeuchi S. Molding cell beads for rapid construction of macroscopic 3D tissue architecture. *Adv Mater*. 2011;23(12):90-94. doi:10.1002/adma.201004375

59. Kato-Negishi M, Morimoto Y, Onoe H, Takeuchi S. Millimeter-sized neural building blocks for 3D heterogeneous neural network assembly. *Adv Healthc Mater*. 2013;2(12):1564-1570. http://www.ncbi.nlm.nih.gov/pubmed/23828857. Accessed January 20, 2016.

60. Hoch E, Tovar GEM, Borchers K. Bioprinting of artificial blood vessels: current approaches towards a demanding goal. *Eur J Cardiothorac Surg*. 2014;(JUNE):1-12. doi:10.1093/ejcts/ezu242

61. Bertassoni LE, Cecconi M, Manoharan V, et al. Hydrogel bioprinted microchannel networks for vascularization of tissue engineering constructs. *Lab Chip*. 2014;14(13):2202-2211. doi:10.1039/c4lc00030g

62. Choi S-W, Zhang Y, Yeh Y-C, Lake Wooten a., Xia Y. Biodegradable porous beads and their potential applications in regenerative medicine. *J Mater Chem*. 2012;22(23):11442. doi:10.1039/c2jm16019f

63. Chung HJ, Park TG. Injectable Cellular Aggregates Prepared from Biodegradable Porous Microspheres for Adipose Tissue Engineering. *TISSUE Eng PART A*.

2009;15(6).

64. Chung HJ, Kim IK, Kim TG, Park. TG. Highly Open Porous Biodegradable Microcarriers: In Vitro Cultivation of Chondrocytes for Injectable Delivery. *TISSUE Eng PART A*. 2008;14(5).

65. Huang H, Yu Y, Hu Y, et al. Generation and manipulation of hydrogel microcapsules by droplet-based microfluidics for mammalian cell culture. *Lab Chip*. 2017;2:1-11. doi:10.1039/C7LC00262A

66. Kim C, Bang JH, Kim YE, Lee JH, Kang JY. Stable hydrodynamic trapping of hydrogel beads for on-chip differentiation analysis of encapsulated stem cells. *Sensors Actuators B Chem*. 2012;166-167:859-869. doi:10.1016/J.SNB.2012.02.008

67. Alessandri K, Feyeux M, Gurchenkov B, et al. A 3D printed microfluidic device for production of functionalized hydrogel microcapsules for culture and differentiation of human Neuronal Stem Cells (hNSC). *Lab Chip*. 2016;16(9):1593-1604. doi:10.1039/C6LC00133E

68. Zhao X, Liu S, Yildirimer L, et al. Injectable Stem Cell-Laden Photocrosslinkable Microspheres Fabricated Using Microfluidics for Rapid Generation of Osteogenic Tissue Constructs. *Adv Funct Mater*. 2016;26(17):2809-2819. doi:10.1002/adfm.201504943

69. Ma Y, Neubauer MP, Thiele J, Fery A, Huck WTS. Artificial microniches for probing mesenchymal stem cell fate in 3D. *Biomater Sci*. 2014;(2). doi:10.1039/c4bm00104d

70. Chan HF, Zhang Y, Ho Y-P, Chiu Y-L, Jung Y, Leong KW. Rapid formation of multicellular spheroids in double-emulsion droplets with controllable microenvironment. *Sci Rep*. 2013;3(1):3462. doi:10.1038/srep03462

71. Maguire T, Novik E, Schloss R, Yarmush M. Alginate-PLL microencapsulation: effect on the differentiation of embryonic stem cells into hepatocytes. *Biotechnol Bioeng*. 2006;93(3):581-591. doi:10.1002/bit.20748

72. Richardson T, Kumta PN, Banerjee I. Alginate Encapsulation of Human Embryonic Stem Cells to Enhance Directed Differentiation to Pancreatic Islet-Like Cells. *Tissue Eng Part A*. 2014;20(23-24):3198-3211. doi:10.1089/ten.tea.2013.0659

73. Agarwal P, Zhao S, Bielecki P, et al. One-step microfluidic generation of pre-hatching embryo-like core-shell microcapsules for miniaturized 3D culture of pluripotent stem cells. *Lab Chip*. 2013;13(23):4525-4533. doi:10.1039/c3lc50678a

74. Siltanen C, Yaghoobi M, Haque A, et al. Microfluidic fabrication of bioactive microgels for rapid formation and enhanced differentiation of stem cell spheroids. *Acta Biomater*. 2016;34:125-132. doi:10.1016/j.actbio.2016.01.012

75. Zhao H, Chen Y, Shao L, et al. Airflow-Assisted 3D Bioprinting of Human

Heterogeneous Microspheroidal Organoids with Microfluidic Nozzle. *Small*. 2018;14(39):1802630. doi:10.1002/smll.201802630

76. Allazetta S, Lutolf MP. Stem cell niche engineering through droplet microfluidics. *Curr Opin Biotechnol*. 2015;35:86-93. doi:10.1016/j.copbio.2015.05.003

77. Colosi C, Shin SR, Manoharan V, et al. Microfluidic Bioprinting of Heterogeneous 3D Tissue Constructs Using Low-Viscosity Bioink. *Adv Mater*. 2016;28(4):677-684. doi:10.1002/adma.201503310

78. Tumarkin E, Tzadu L, Csaszar E, et al. High-throughput combinatorial cell co-culture using microfluidics. *Integr Biol*. 2011;3(6):653. doi:10.1039/c1ib00002k

79. Shepherd RF, Conrad JC, Rhodes SK, et al. Microfluidic assembly of homogeneous and Janus colloid-filled hydrogel granules. *Langmuir*. 2006;22(21):8618-8622. doi:10.1021/la060759+

80. Chung BG, Lee K-H, Khademhosseini A, Lee S-H. Microfluidic fabrication of microengineered hydrogels and their application in tissue engineering. *Lab Chip*. 2012;12(1):45. doi:10.1039/c1lc20859d

81. Jung J, Oh J. Cell-induced flow-focusing instability in gelatin methacrylate microdroplet generation. *Biomicrofluidics*. 2014;8(3):036503. doi:10.1063/1.4880375

82. Ceyhan E, Xu F, Gurkan UA, et al. Prediction and control of number of cells in microdroplets by stochastic modeling. *Lab Chip*. 2012;12(22):4884. doi:10.1039/c2lc40523g

83. Demirci U, Montesano G. Single cell epitaxy by acoustic picolitre droplets. *Lab Chip*. 2007;7(9):1139-1145. doi:10.1039/b704965j

84. Cheng E, Yu H, Ahmadi A, Cheung KC. Investigation of the hydrodynamic response of cells in drop on demand piezoelectric inkjet nozzles. *Biofabrication*. 2016;8(1):015008. doi:10.1088/1758-5090/8/1/015008

85. Wu X-Z, Kato T, Terada S. Real-time noninvasive monitoring of UV light-induced cell death by the deflection of a probe beam. *Anal Sci*. 2014;30(10):1023-1025. http://www.ncbi.nlm.nih.gov/pubmed/25312635. Accessed January 18, 2018.

86. Armstrong BK, Kricker A. The epidemiology of UV induced skin cancer. *J Photochem Photobiol B*. 2001;63(1-3):8-18. http://www.ncbi.nlm.nih.gov/pubmed/11684447. Accessed January 18, 2018.

87. Wang S, Jeon O, Shankles PG, et al. In-situ photopolymerization of monodisperse and discoid oxidized methacrylated alginate microgels in a microfluidic channel. *Biomicrofluidics*. 2016;10(1):011101. doi:10.1063/1.4941339

88. Tan WHW -H., Takeuchi S. Monodisperse alginate hydrogel microbeads for cell

encapsulation. *Adv Mater*. 2007;19(18):2696-2701. doi:10.1002/adma.200700433

89. Liu K, Ding H-J, Liu J, Chen Y, Zhao X-Z. Shape-controlled production of biodegradable calcium alginate gel microparticles using a novel microfluidic device. *Langmuir*. 2006;22(22):9453-9457. doi:10.1021/la061729+

90. Deng Y, Zhang N, Zhao L, et al. Rapid purification of cell encapsulated hydrogel beads from oil phase to aqueous phase in a microfluidic device. *Lab Chip*. 2011;11(23):4117. doi:10.1039/c1lc20494g

91. Hong S, Hsu H-J, Kaunas R, Kameoka J. Collagen microsphere production on a chip. *Lab Chip*. 2012;12(18):3277. doi:10.1039/c2lc40558j

92. Choi C-H, Wang H, Lee H, et al. One-step generation of cell-laden microgels using double emulsion drops with a sacrificial ultra-thin oil shell. *Lab Chip*. 2016;16(9):1549-1555. doi:10.1039/C6LC00261G

93. Huang H, He X. Interfacial tension based on-chip extraction of microparticles confined in microfluidic Stokes flows. *Appl Phys Lett*. 2014;105(14):143704. doi:10.1063/1.4898040

94. Zhang H, Tumarkin E, Sullan RMA, Walker GC, Kumacheva E. Exploring Microfluidic Routes to Microgels of Biological Polymers. *Macromol Rapid Commun*. 2007;28(5):527-538. doi:10.1002/marc.200600776

95. Hospodiuk M, Dey M, Sosnoski D, Ozbolat IT. The bioink: A comprehensive review on bioprintable materials. *Biotechnol Adv*. 2017;35(2):217-239. doi:10.1016/J.BIOTECHADV.2016.12.006

96. Gungor-Ozkerim PS, Inci I, Zhang YS, Khademhosseini A, Dokmeci MR. Bioinks for 3D bioprinting: an overview. *Biomater Sci*. 2018;6(5):915-946. doi:10.1039/C7BM00765E

97. Brannon-Peppas L, Harland RS. *Absorbent Polymer Technology*. Elsevier; 2012.

98. Wan J. Microfluidic-based synthesis of hydrogel particles for cell microencapsulation and cell-based drug delivery. *Polymers (Basel)*. 2012;4(2):1084-1108. doi:10.3390/polym4021084

99. Orive G, Hernández RM, Rodríguez Gascón A, et al. History, challenges and perspectives of cell microencapsulation. *Trends Biotechnol*. 2004;22(2):87-92. doi:10.1016/j.tibtech.2003.11.004

100. Balakrishnan B, Banerjee R. Biopolymer-based hydrogels for cartilage tissue engineering. *Chem Rev*. 2011;111(8):4453-4474. doi:10.1021/cr100123h

101. Choi B, Loh XJ, Tan A, et al. Introduction to In Situ Forming Hydrogels for Biomedical Applications. In: ; 2015. doi:10.1007/978-981-287-152-7_2

102. Jin R. In-Situ Forming Biomimetic Hydrogels for Tissue Regeneration. In: *Biomedicine*. InTech; 2012. doi:10.5772/38852

103. Zimmermann H, Ehrhart F, Zimmermann D, et al. Hydrogel-based encapsulation of biological, functional tissue: fundamentals, technologies and applications. *Appl Phys A*. 2007;89(4):909-922.

104. Drury JL, Mooney DJ. Hydrogels for tissue engineering: scaffold design variables and applications. *Biomaterials*. 2003;24(24):4337-4351. doi:10.1016/S0142-9612(03)00340-5

105. Slaughter B V, Khurshid SS, Fisher OZ, Khademhosseini A, Peppas NA. Hydrogels in regenerative medicine. *Adv Mater*. 2009;21(32-33):3307-3329.

106. Watanabe T, Motohiro I, Ono T. Microfluidic Formation of Hydrogel Microcapsules with a Single Aqueous Core by Spontaneous Cross-Linking in Aqueous Two-Phase System Droplets. *Langmuir*. 2019;35(6):2358-2367. doi:10.1021/acs.langmuir.8b04169

107. Rossow T, Heyman J a., Ehrlicher AJ, et al. Controlled Synthesis of Cell-Laden Microgels by Radical-Free Gelation in Droplet Microfluidics. *J Am Chem Soc*. 2012;134(10):4983-4989. doi:10.1021/ja300460p

108. Tan J, Gemeinhart RA, Ma M, Saltzman WM. Improved cell adhesion and proliferation on synthetic phosphonic acid-containing hydrogels. *Biomaterials*. 2005;26(17):3663-3671. http://www.ncbi.nlm.nih.gov/pubmed/15621257. Accessed January 21, 2016.

109. Liu X, Toprakcioglu Z, Dear AJ, et al. Fabrication and Characterization of Reconstituted Silk Microgels for the Storage and Release of Small Molecules. *Macromol Rapid Commun*. March 2019:1800898. doi:10.1002/marc.201800898

110. Daniele MA, Adams AA, Naciri J, North SH, Ligler FS. Interpenetrating networks based on gelatin methacrylamide and PEG formed using concurrent thiol click chemistries for hydrogel tissue engineering scaffolds. *Biomaterials*. 2014;35(6):1845-1856. http://www.ncbi.nlm.nih.gov/pubmed/24314597. Accessed January 21, 2016.

111. Kim SH, Yeon YK, Lee JM, et al. Precisely printable and biocompatible silk fibroin bioink for digital light processing 3D printing. *Nat Commun*. 2018;9(1):1620. doi:10.1038/s41467-018-03759-y

112. Xie M, Gao Q, Zhao H, et al. Electro-Assisted Bioprinting of Low-Concentration GelMA Microdroplets. *Small*. 2019;15(4):1804216. doi:10.1002/smll.201804216

113. Tan H, Marra KG. Injectable, Biodegradable Hydrogels for Tissue Engineering Applications. *Materials (Basel)*. 2010;3(3):1746-1767. http://www.mdpi.com/1996-1944/3/3/1746. Accessed October 9, 2015.

114. Huang RYM, Pal R, Moon GY. Characteristics of sodium alginate membranes for the pervaporation dehydration of ethanol–water and isopropanol–water mixtures. *J Memb Sci*. 1999;160(1):101-113. http://www.sciencedirect.com/science/article/pii/S037673889900071X. Accessed January 21, 2016.

115. Bajpai SK, Sharma S. Investigation of swelling/degradation behaviour of alginate beads crosslinked with Ca2+ and Ba2+ ions. *React Funct Polym*. 2004;59(2):129-140. http://www.sciencedirect.com/science/article/pii/S1381514804000161. Accessed November 18, 2015.

116. Kang A, Park J, Ju J, Jeong GS, Lee SH. Cell encapsulation via microtechnologies. *Biomaterials*. 2014;35(9):2651-2663. doi:10.1016/j.biomaterials.2013.12.073

117. de Rutte JM, Koh J, Di Carlo D. Scalable High-Throughput Production of Modular Microgels for In Situ Assembly of Microporous Tissue Scaffolds. *Adv Funct Mater*. March 2019:1900071. doi:10.1002/adfm.201900071

118. Ferreira L, Gil MH, Dordick JS. Enzymatic synthesis of dextran-containing hydrogels. *Biomaterials*. 2002;23(19):3957-3967. http://www.ncbi.nlm.nih.gov/pubmed/12162328. Accessed January 21, 2016.

119. Patterson J, Hubbell JA. Enhanced proteolytic degradation of molecularly engineered PEG hydrogels in response to MMP-1 and MMP-2. *Biomaterials*. 2010;31(30):7836-7845. http://www.ncbi.nlm.nih.gov/pubmed/20667588. Accessed October 12, 2015.

120. Li S, Molina I, Bueno Martinez M, Vert M. Hydrolytic and enzymatic degradations of physically crosslinked hydrogels prepared from PLA/PEO/PLA triblock copolymers. *J Mater Sci Mater Med*. 2002;13(1):81-86. doi:10.1023/A:1013651022431

121. Lévesque SG, Shoichet MS. Synthesis of enzyme-degradable, peptide-cross-linked dextran hydrogels. *Bioconjug Chem*. 2007;18(3):874-885. doi:10.1021/bc0602127

122. Lee KY, Bouhadir KH, Mooney DJ. Controlled degradation of hydrogels using multi-functional cross-linking molecules. *Biomaterials*. 2004;25(13):2461-2466. doi:10.1016/j.biomaterials.2003.09.030

123. De Isla N, Huseltein C, Jessel N, et al. Introduction to tissue engineering and application for cartilage engineering. In: *Bio-Medical Materials and Engineering*. ; 2010. doi:10.3233/BME-2010-0624

124. O'brien FJ. *Biomaterials and Scaffolds for Tissue Engineering*.; 2011. https://epubs.rcsi.ie/anatart/38.

125. Loessner D, Meinert C, Kaemmerer E, et al. Functionalization, preparation and use of cell-laden gelatin methacryloyl–based hydrogels as modular tissue culture platforms. *Nat Protoc*. 2016;11(4):727-746. doi:10.1038/nprot.2016.037

126. Yue K, Trujillo-de Santiago G, Alvarez MM, Tamayol A, Annabi N, Khademhosseini A. Synthesis, properties, and biomedical applications of gelatin methacryloyl (GelMA) hydrogels. *Biomaterials*. 2015;73:254-271. doi:10.1016/J.BIOMATERIALS.2015.08.045

127. Wang Z, Jin X, Dai R, Holzman JF, Kim K. An ultrafast hydrogel photocrosslinking method for direct laser bioprinting. *RSC Adv*. 2016;6(25):21099-21104. doi:10.1039/C5RA24910D

128. Wang Z, Tian Z, Jin X, Holzman JF, Menard F, Kim K. Visible light-based stereolithography bioprinting of cell-adhesive gelatin hydrogels. In: *2017 39th Annual International Conference of the IEEE Engineering in Medicine and Biology Society (EMBC)*. IEEE; 2017:1599-1602. doi:10.1109/EMBC.2017.8037144

129. Kessler L, Gehrke S, Winnefeld M, et al. Methacrylated gelatin/hyaluronan-based hydrogels for soft tissue engineering. *J Tissue Eng*. 2017;8:2041731417744157. doi:10.1177/2041731417744157

130. Cha C, Oh J, Kim K, et al. Microfluidics-Assisted Fabrication of Gelatin-Silica Core–Shell Microgels for Injectable Tissue Constructs. *Biomacromolecules*. 2014;15(1):283-290. doi:10.1021/bm401533y

131. Celikkin N, Mastrogiacomo S, Jaroszewicz J, Walboomers XF, Swieszkowski W. Gelatin methacrylate scaffold for bone tissue engineering: The influence of polymer concentration. *J Biomed Mater Res - Part A*. 2018. doi:10.1002/jbm.a.36226

132. Arya AD, Hallur PM, Karkisaval AG, et al. Gelatin Methacrylate Hydrogels as Biomimetic Three-Dimensional Matrixes for Modeling Breast Cancer Invasion and Chemoresponse in Vitro. *ACS Appl Mater Interfaces*. 2016. doi:10.1021/acsami.6b06309

133. Bajaj P, Schweller RM, Khademhosseini A, West JL, Bashir R. 3D Biofabrication Strategies for Tissue Engineering and Regenerative Medicine. *Annu Rev Biomed Eng*. 2014. doi:10.1146/annurev-bioeng-071813-105155

134. Lai JY, Li YT, Cho CH, Yu TC. Nanoscale modification of porous gelatin scaffolds with chondroitin sulfate for corneal stromal tissue engineering. *Int J Nanomedicine*. 2012. doi:10.2147/IJN.S28753

135. Nichol JW, Koshy ST, Bae H, Hwang CM, Yamanlar S, Khademhosseini A. Cell-laden microengineered gelatin methacrylate hydrogels. *Biomaterials*. 2010. doi:10.1016/j.biomaterials.2010.03.064

136. Pei B, Wang W, Fan Y, Wang X, Watari F, Li X. Fiber-reinforced scaffolds in soft tissue engineering. *Regen Biomater*. 2017. doi:10.1093/rb/rbx021

137. Loessner D, Meinert C, Kaemmerer E, et al. Functionalization, preparation and use of cell-laden gelatin methacryloyl–based hydrogels as modular tissue culture platforms.

*Nat Protoc*. 2016;11(4):727-746. doi:10.1038/nprot.2016.037

138. Ludwig PE, Huff TJ, Zuniga JM. The potential role of bioengineering and three-dimensional printing in curing global corneal blindness. *J Tissue Eng*. 2018;9:2041731418769863. doi:10.1177/2041731418769863

139. Product Name Gelatin methacryloyl | Sigma-Aldrich. https://www.sigmaaldrich.com/catalog/search?term=Gelatin+methacryloyl&interface=Product Name&N=0+&mode=mode matchpartialmax&lang=en&region=CA&focus=productN=0 220003048 219853286 219853082. Accessed July 13, 2018.

140. Wang Z, Tian Z, Menard F, Kim K. Comparative study of gelatin methacrylate hydrogels from different sources for biofabrication applications. *Biofabrication*. 2017;9(4):044101. doi:10.1088/1758-5090/aa83cf

141. Japan Chemical Industry Ecology-Toxicology & Information Center., Japan. Tsūshō Sangyōshō., Chemicals Inspection & Testing Institute (Japan). *Biodegradation and Bioaccumulation Data of Existing Chemicals Based on the CSCL Japan*. Japan Chemical Industry Ecology-Toxicology & Information Center; 1992. https://pubchem.ncbi.nlm.nih.gov/compound/7837#section=Flash-Point. Accessed November 6, 2018.

142. Pikal MJ. Use of laboratory data in freeze drying process design: heat and mass transfer coefficients and the computer simulation of freeze drying. *J Parenter Sci Technol*. 1985;39(3):115-139. http://www.ncbi.nlm.nih.gov/pubmed/3839016. Accessed October 26, 2018.

143. An I. Van Den Bulcke †, Bogdan Bogdanov †, Nadine De Rooze †, Etienne H. Schacht *,†, Maria Cornelissen ‡ and, Berghmans§ H. Structural and Rheological Properties of Methacrylamide Modified Gelatin Hydrogels. 2000. doi:10.1021/BM990017D

144. Martineau L, Peng HT, Shek PN. Development of a novel biomaterial: Part II. Evaluation of a photo cross-linking method Defence R&D Canada-Toronto DEFENCE DÉFENSE & 2005. http://cradpdf.drdc-rddc.gc.ca/PDFS/unc48/p524644.pdf. Accessed July 19, 2018.

145. Thongboonkerd V, Mcleish KR, Arthur JM, Klein JB. Proteomic analysis of normal human urinary proteins isolated by acetone precipitation or ultracentrifugation. *Kidney Int*. 2002;62(4):1461-1469. doi:10.1111/J.1523-1755.2002.KID565.X

146. Crowell AMJ, Wall MJ, Doucette AA. Maximizing recovery of water-soluble proteins through acetone precipitation. *Anal Chim Acta*. 2013;796:48-54. doi:10.1016/j.aca.2013.08.005

147. Mortimer RG. *Physical Chemistry*. Academic Press/Elsevier; 2008.

148. Rey L, May JC (Joan C. *Freeze Drying/Lyophilization of Pharmaceutical and Biological Products*. Informa Healthcare; 2010. https://www.crcpress.com/Freeze-DryingLyophilization-of-Pharmaceutical-and-Biological-Products/Rey/p/book/9781439825754. Accessed September 13, 2019.

149. Rasetto V, Marchisio DL, Fissore D, Barresi AA. *Model Based-Monitoring of a Non-Uniform Batch in a Freeze-Drying Process*.; 2008. http://folk.ntnu.no/skoge/prost/proceedings/escape18/Topic_2/Poster/FP_00210.pdf. Accessed October 26, 2018.

150. Pikal MJ, Lukes AL, Lang JE. Thermal decomposition of amorphous beta-lactam antibacterials. *J Pharm Sci*. 1977;66(9):1312-1316. http://www.ncbi.nlm.nih.gov/pubmed/903872. Accessed October 26, 2018.

151. Yalkowsky SH, Patel SD. Acceleration of Heat Transfer in Vial Freeze-Drying of Pharmaceuticals. II. A Fluid Cushion Device. *Pharm Res*. 1992;09(6):753-758. doi:10.1023/A:1015847420642

152. Wisniewski R. Spray Drying Technology Review. July 2015. https://ttu-ir.tdl.org/ttu-ir/handle/2346/64598. Accessed July 13, 2018.

153. Spray drying versus freeze drying. https://www.manufacturingchemist.com/news/article_page/Spray_drying_versus_freeze_drying/109261. Accessed July 13, 2018.

154. Freeze Drying vs Spray Drying: is it essentially quality vs cost? – Biopharma. https://biopharma.co.uk/blog/2017/03/15/freeze-drying-vs-spray-drying-is-it-essentially-quality-vs-cost/. Accessed July 13, 2018.

155. Patel BB, Patel JK, Chakraborty S. Review of patents and application of spray drying in pharmaceutical, food and flavor industry. *Recent Pat Drug Deliv Formul*. 2014;8(1):63-78. http://www.ncbi.nlm.nih.gov/pubmed/24720661. Accessed July 13, 2018.

156. Abdul-Fattah AM, Kalonia DS, Pikal MJ. The Challenge of Drying Method Selection for Protein Pharmaceuticals: Product Quality Implications. *J Pharm Sci*. 2007;96(8):1886-1916. doi:10.1002/jps.20842

157. Maa YF, Hsu CC. Protein denaturation by combined effect of shear and air-liquid interface. *Biotechnol Bioeng*. 1997;54(6):503-512. doi:10.1002/(SICI)1097-0290(19970620)54:6<503::AID-BIT1>3.0.CO;2-N

158. Adler M, Unger M, Lee G. Surface composition of spray-dried particles of bovine serum albumin/trehalose/surfactant. *Pharm Res*. 2000;17(7):863-870. doi:10.1023/a:1007568511399

159. Lee SH, Heng D, Ng WK, Chan H-K, Tan RBH. Nano spray drying: A novel method for preparing protein nanoparticles for protein therapy. *Int J Pharm*. 2011;403(1-

2):192-200. doi:10.1016/J.IJPHARM.2010.10.012

160. Rabbani NR, Seville PC. The influence of formulation components on the aerosolisation properties of spray-dried powders. *J Control Release*. 2005;110(1):130-140. doi:10.1016/J.JCONREL.2005.09.004

161. Li X, Anton N, Arpagaus C, Belleteix F, Vandamme TF. Nanoparticles by spray drying using innovative new technology: The Büchi Nano Spray Dryer B-90. *J Control Release*. 2010;147(2):304-310. doi:10.1016/J.JCONREL.2010.07.113

162. Ståhl K, Claesson M, Lilliehorn P, Lindén H, Bäckström K. The effect of process variables on the degradation and physical properties of spray dried insulin intended for inhalation. *Int J Pharm*. 2002;233(1-2):227-237. doi:10.1016/S0378-5173(01)00945-0

163. Bittner B, Morlock M, Koll H, Winter G, Kissel T. Recombinant human erythropoietin (rhEPO) loaded poly(lactide-co-glycolide) microspheres: influence of the encapsulation technique and polymer purity on microsphere characteristics. *Eur J Pharm Biopharm*. 1998;45(3):295-305. doi:10.1016/S0939-6411(98)00012-5

164. Maury M, Murphy K, Kumar S, Shi L, Lee G. Effects of process variables on the powder yield of spray-dried trehalose on a laboratory spray-dryer. *Eur J Pharm Biopharm*. 2005;59(3):565-573. doi:10.1016/J.EJPB.2004.10.002

165. Bowey K, Swift BE, Flynn LE, Neufeld RJ. Characterization of biologically active insulin-loaded alginate microparticles prepared by spray drying. *Drug Dev Ind Pharm*. 2013;39(3):457-465. doi:10.3109/03639045.2012.662985

166. Zhu C, Shoji Y, McCray S, et al. Stabilization of HAC1 Influenza Vaccine by Spray Drying: Formulation Development and Process Scale-Up. *Pharm Res*. 2014;31(11):3006-3018. doi:10.1007/s11095-014-1394-3

167. Baba K, Nishida K. Calpain inhibitor nanocrystals prepared using Nano Spray Dryer B-90. *Nanoscale Res Lett*. 2012;7(1):436. doi:10.1186/1556-276X-7-436

168. Yue K, Trujillo-de Santiago G, Alvarez MM, Tamayol A, Annabi N, Khademhosseini A. Synthesis, properties, and biomedical applications of gelatin methacryloyl (GelMA) hydrogels. *Biomaterials*. 2015;73:254-271. doi:10.1016/j.biomaterials.2015.08.045

169. Nichol JW, Koshy ST, Bae H, Hwang CM, Yamanlar S, Khademhosseini A. Cell-laden microengineered gelatin methacrylate hydrogels. *Biomaterials*. 2010;31(21):5536-5544. doi:10.1016/j.biomaterials.2010.03.064

170. Hu X, Ma L, Wang C, Gao C. Gelatin hydrogel prepared by photo-initiated polymerization and loaded with TGF-beta1 for cartilage tissue engineering. *Macromol Biosci*. 2009;9(12):1194-1201. doi:10.1002/mabi.200900275

171. Cha C, Oh J, Kim K, et al. Microfluidics-assisted fabrication of gelatin-silica core-

shell microgels for injectable tissue constructs. *Biomacromolecules*. 2014;15(1):283-290. doi:10.1021/bm401533y

172. Jose BM, Cubaud T. Droplet arrangement and coalescence in diverging/converging microchannels. *Microfluid Nanofluidics*. 2012;12(5):687-696. doi:10.1007/s10404-011-0909-z

173. Sochol RD, Li S, Lee LP, Lin L. Continuous flow multi-stage microfluidic reactors via hydrodynamic microparticle railing. *Lab Chip*. 2012;12(20):4168-4177. doi:10.1039/c2lc40610a

174. Occhetta P, Sadr N, Piraino F, Redaelli A, Moretti M, Rasponi M. Fabrication of 3D cell-laden hydrogel microstructures through photo-mold patterning. https://re.public.polimi.it/retrieve/handle/11311/759296/22067/ark_2013_Occhetta_Biofabrication.pdf. Accessed January 18, 2018.

175. Billiet T, Gevaert E, De Schryver T, Cornelissen M, Dubruel P. The 3D printing of gelatin methacrylamide cell-laden tissue-engineered constructs with high cell viability. *Biomaterials*. 2014;35(1):49-62. doi:10.1016/J.BIOMATERIALS.2013.09.078

176. Occhetta P, Visone R, Russo L, Cipolla L, Moretti M, Rasponi M. VA-086 methacrylate gelatine photopolymerizable hydrogels: A parametric study for highly biocompatible 3D cell embedding. *J Biomed Mater Res Part A*. 2015;103(6):2109-2117. doi:10.1002/jbm.a.35346

177. Rouillard AD, Berglund CM, Lee JY, et al. Methods for Photocrosslinking Alginate Hydrogel Scaffolds with High Cell Viability. *Tissue Eng Part C Methods*. 2011;17(2):173-179. doi:10.1089/ten.tec.2009.0582

178. Dendukuri D, Panda P, Haghgooie R, Kim JM, Hatton TA, Doyle PS. Modeling of Oxygen-Inhibited Free Radical Photopolymerization in a PDMS Microfluidic Device. *Macromolecules*. 2008;41(22):8547-8556. doi:10.1021/ma801219w

179. Dendukuri D, Gu SS, Pregibon DC, Hatton TA, Doyle PS. Stop-flow lithography in a microfluidic device. *Lab Chip*. 2007;7(7):818. doi:10.1039/b703457a

180. Stern SA, Shah VM, Hardy BJ. Structure-permeability relationships in silicone polymers. *J Polym Sci Part B Polym Phys*. 1987;25(6):1263-1298. doi:10.1002/polb.1987.090250607

181. Oh S-J, Zurawsky WP. Gas permeation through poly(dimethylsiloxane)-plasma polymer composite membranes. *J Memb Sci*. 1996;120(1):89-99. doi:10.1016/0376-7388(96)00139-1

182. Rouillard AD, Berglund CM, Lee JY, et al. Methods for photocrosslinking alginate hydrogel scaffolds with high cell viability. *Tissue Eng Part C Methods*. 2011;17(2):173-179. doi:10.1089/ten.TEC.2009.0582

183. Czajkowska-Kośnik A, Wolska E, Chorążewicz J, Sznitowska M. Comparison of cytotoxicity in vitro and irritation in vivo for aqueous and oily solutions of surfactants. *Drug Dev Ind Pharm*. 2015;41(8):1232-1236. doi:10.3109/03639045.2014.938656

184. Arechabala B, Coiffard C, Rivalland P, Coiffard LJ, de Roeck-Holtzhauer Y. Comparison of cytotoxicity of various surfactants tested on normal human fibroblast cultures using the neutral red test, MTT assay and LDH release. *J Appl Toxicol*. 19(3):163-165. http://www.ncbi.nlm.nih.gov/pubmed/10362266. Accessed January 18, 2018.

185. Nichol JW, Khademhosseini A. Modular Tissue Engineering: Engineering Biological Tissues from the Bottom Up. *Soft Matter*. 2009;5(7):1312-1319. doi:10.1039/b814285h

186. Geckil H, Xu F, Zhang X, Moon S, Demirci U. Engineering hydrogels as extracellular matrix mimics. *Nanomedicine*. 2010;5(3):469-484. doi:10.2217/nnm.10.12

187. Wang Z, Kumar H, Tian Z, et al. Visible light photoinitiation of cell-adhesive gelatin methacryloyl hydrogels for stereolithography 3D bioprinting. *ACS Appl Mater Interfaces*. 2018;10(32):26859-26869.

188. Arakawa T, Timasheff SN. [3]Theory of protein solubility. *Methods Enzymol*. 1985;114:49-77. doi:10.1016/0076-6879(85)14005-X

189. Belch AC, Berkowitz M, McCammon JA. Solvation structure of a sodium chloride ion pair in water. *J Am Chem Soc*. 1986;108(8):1755-1761. doi:10.1021/ja00268a007

190. Kelley M, Donley A, Clark S, Clark A. Structure and Dynamics of NaCl Ion Pairing in Solutions of Water and Methanol. *J Phys Chem B*. 2015;119(51):15652-15661. doi:10.1021/acs.jpcb.5b07492

191. Li W, Zhou R, Mu Y. Salting Effects on Protein Components in Aqueous NaCl and Urea Solutions: Toward Understanding of Urea-Induced Protein Denaturation. *J Phys Chem B*. 2012;116(4):1446-1451. doi:10.1021/jp210769q

192. CRC Handbook of Chemistry and Physics, 2009−2010, 90th ed. CRC Handbook of Chemistry and Physics, 2009−2010, 90th ed . Edited by David R. Lide , Editor-in-Chief, and W. M. “Mickey” Haynes , Associate Editor (National Institute of Standards and Technology, Gaithersburg, MD, USA). CRC Press (an imprint of Taylor & Francis Group): Boca Raton, FL. 2009 . $149.95. ISBN 978-1-4200-9084-0 . *J Am Chem Soc*. 2009;131(35):12862-12862. doi:10.1021/ja906434c

193. Shakhparonov MI, Akhadov YY. Dielectric properties and molecular structure of water-acetone solutions. *J Struct Chem*. 1965;6(1):15-19. doi:10.1007/BF00743862

194. Common Organic Solvents: Table of Properties. https://www.organicdivision.org/orig/organic_solvents.html. Accessed July 13, 2018.

195. Ferguson AL, Malone JG, Case LO. Dielectric Constant Studies. III. Aqueous Gelatin Solutions. *J Chem Phys*. 1934;2(2):94-98. doi:10.1063/1.1749426

196. Ch CS. TECHNICAL BULLETIN REACTION SOLVENT DIMETHYL SULFOXIDE (DMSO). http://chemistry-chemists.com/N3_2011/U/DMSO-technical_bulletin.pdf. Accessed July 13, 2018.

197. DMSO Solubility Data | Gaylord Chemical. http://www.gaylordchemical.com/literature/dmso-solubility-data/. Accessed July 13, 2018.

198. Burgess J. *Metal Ions in Solution*. Ellis Horwood; 1978. https://books.google.ca/books/about/Metal_ions_in_solution.html?id=3gfwAAAAMAAJ&redir_esc=y. Accessed July 13, 2018.

199. Green AA, Hughes WL. [10] Protein fractionation on the basis of solubility in aqueous solutions of salts and organic solvents. *Methods Enzymol*. 1955;1:67-90. doi:10.1016/0076-6879(55)01014-8

200. Scopes RK. *Protein Purification : Principles and Practice*. Springer-Verlag; 1994.

201. CRC Handbook of Chemistry and Physics, 86th Edition Edited by David R. Lide (National Institute of Standards and Technology). CRC Press (an imprint of Taylor and Francis Group): Boca Raton, FL. 2005. 2544 pp. $125.96. ISBN 0-8493-0486-5. 2006. doi:10.1021/JA059868L

202. Gelatin A, Kraft /. *GELATIN MANUFACTURERS INSTITUTE OF AMERICA GELATIN HANDBOOK*. Vol 563. http://www.gelita.comhttp//www.nitta-gelatin.comhttp://www.gelatin.comhttp://www.rousselot.comhttp://www.weishardt.com. Accessed January 30, 2019.

203. *GELATIN MANUFACTURERS INSTITUTE OF AMERICA STANDARD TESTING METHODS FOR EDIBLE GELATIN*.; 2013. http://www.gelatin-gmia.com. Accessed January 30, 2019.

204. Budavari S. *The Merck Index : An Encyclopedia of Chemicals, Drugs, and Biologicals*. 12th ed. Merck; 1996.

205. Lee KY, Mooney DJ. Hydrogels for tissue engineering. *Chem Rev*. 2001;101(7):1869-1879. http://www.ncbi.nlm.nih.gov/pubmed/11710233. Accessed February 12, 2019.

206. Tabata Y. Significance of release technology in tissue engineering. *Drug Discov Today*. 2005;10(23-24):1639-1646. doi:10.1016/S1359-6446(05)03639-1

207. Japan Chemical Industry Ecology-Toxicology & Information Center., Japan. Tsūshō Sangyōshō., Chemicals Inspection & Testing Institute (Japan). *Biodegradation and Bioaccumulation Data of Existing Chemicals Based on the CSCL Japan*. Japan Chemical Industry Ecology-Toxicology & Information Center; 1992.

https://pubchem.ncbi.nlm.nih.gov/compound/glycidyl_methacrylate#section=Flash-Point. Accessed July 13, 2018.

208. Ali Y, Dolan MJ, Fendler EJ LEA. *Disinfection, Sterilization, and Preservation, 5th Ed. SS Block, Ed.; Philadelphia: Lippincott Williams & Wilkins, 2001; 1,504 Pages*. Vol 23. Cambridge University Press; 2001. doi:10.1017/S0195941700084289

209. Wells RG. The role of matrix stiffness in regulating cell behavior. *Hepatology*. 2008;47(4):1394-1400. doi:10.1002/hep.22193

210. Engler AJ, Sweeney HL, Discher DE, Schwarzbauer JE. Extracellular matrix elasticity directs stem cell differentiation. *J Musculoskelet Neuronal Interact*. 7(4):335. http://www.ncbi.nlm.nih.gov/pubmed/18094500. Accessed February 12, 2019.

211. Wang Z, Abdulla R, Parker B, Samanipour R, Ghosh S, Kim K. A simple and high-resolution stereolithography-based 3D bioprinting system using visible light crosslinkable bioinks. *Biofabrication*. 2015;7(4):045009. doi:10.1088/1758-5090/7/4/045009

212. Zhao X, Lang Q, Yildirimer L, et al. Photocrosslinkable Gelatin Hydrogel for Epidermal Tissue Engineering. *Adv Healthc Mater*. 2016;5(1):108-118. doi:10.1002/adhm.201500005

213. Trappmann B, Gautrot JE, Connelly JT, et al. Extracellular-matrix tethering regulates stem-cell fate. *Nat Mater*. 2012;11(7):642-649. doi:10.1038/nmat3339

214. Peppas NA, Hilt JZ, Khademhosseini A, Langer R. Hydrogels in Biology and Medicine: From Molecular Principles to Bionanotechnology. *Adv Mater*. 2006;18(11):1345-1360. doi:10.1002/adma.200501612

215. Nichol JW, Koshy ST, Bae H, Hwang CM, Yamanlar S, Khademhosseini A. Cell-laden microengineered gelatin methacrylate hydrogels. *Biomaterials*. 2010;31(21):5536-5544. doi:10.1016/j.biomaterials.2010.03.064

216. Browning MB, Cereceres SN, Luong PT, Cosgriff-Hernandez EM. Determination of the in vivo degradation mechanism of PEGDA hydrogels. *J Biomed Mater Res A*. 2014;102(12):4244-4251. doi:10.1002/jbm.a.35096

217. Du Y, Lo E, Ali S, Khademhosseini A. Directed assembly of cell-laden microgels for fabrication of 3D tissue constructs. *Proc Natl Acad Sci*. 2008;105(28):9522-9527. doi:10.1073/pnas.0801866105

218. Lam J, Kim K, Lu S, et al. A factorial analysis of the combined effects of hydrogel fabrication parameters on the in vitro swelling and degradation of oligo(poly(ethylene glycol) fumarate) hydrogels. *J Biomed Mater Res A*. 2014;102(10):3477-3487. doi:10.1002/jbm.a.35015

219. Wang Z, Kumar H, Tian Z, et al. Visible Light Photoinitiation of Cell-Adhesive

Gelatin Methacryloyl Hydrogels for Stereolithography 3D Bioprinting. *ACS Appl Mater Interfaces*. 2018. doi:10.1021/acsami.8b06607

220. Tsotsas E, Mujumdar A. Modern Drying Technology Other Volumes Volume 1: Computational Tools at Different Scales Volume 3: Product Quality and Formulation Volume 4: Energy Savings Modern Drying Technology Set (Volumes 1-5). https://onlinelibrary.wiley.com/doi/pdf/10.1002/9783527631704. Accessed July 13, 2018.

221. ICSC 0078 - TOLUENE. http://www.ilo.org/dyn/icsc/showcard.display?p_version=2&p_card_id=0078. Accessed November 6, 2018.

222. Mohamed MGA, Kheiri S, Islam S, Kumar H, Yang A, Kim K. An integrated microfluidic flow-focusing platform for on-chip fabrication and filtration of cell-laden microgels. *Lab Chip*. 2019;19(9):1621-1632. doi:10.1039/C9LC00073A

223. Riddick JA, Bunger WB, Sakano TK. Organic solvents: physical properties and methods of purification. Fourth edition. January 1986. https://www.osti.gov/biblio/6190969. Accessed September 5, 2019.

224. Lide DR, Baysinger G, Berger LI, et al. *CRC Handbook of Chemistry and Physics Editor-in-Chief*.

225. Reichardt C, Welton T. *Solvents and Solvent Effects in Organic Chemistry*. Wiley-VCH; 2011. https://books.google.ca/books?hl=en&lr=&id=6MzGgfWZAIMC&oi=fnd&pg=PA56&dq=effects+of+organic+solvent&ots=0gV9idskoI&sig=qucxmuLQ-aryCkr0aM98POT9U_I&redir_esc=y#v=onepage&q=effects of organic solvent&f=false. Accessed September 5, 2019.

226. CDC - NIOSH Pocket Guide to Chemical Hazards - Toluene. https://www.cdc.gov/niosh/npg/npgd0619.html. Accessed September 3, 2019.

227. Toluene - Study: Market, Analysis, Trends | Ceresana. https://www.ceresana.com/en/market-studies/chemicals/toluene/ceresana-market-study-toluene.html. Accessed November 8, 2018.

228. Britain PS of G. *Pharmaceutical Journal and Transactions.* London : J. & A. Churchill,; 1842. https://www.biodiversitylibrary.org/bibliography/144909. Accessed November 8, 2018.

229. CDC - NIOSH Pocket Guide to Chemical Hazards - Benzene. https://www.cdc.gov/niosh/npg/npgd0049.html. Accessed September 3, 2019.

230. CDC - NIOSH Pocket Guide to Chemical Hazards - Carbon tetrachloride. https://www.cdc.gov/niosh/npg/npgd0107.html. Accessed September 3, 2019.

231. CDC - NIOSH Pocket Guide to Chemical Hazards - Ethylene dichloride. https://www.cdc.gov/niosh/npg/npgd0271.html. Accessed September 3, 2019.

232. Block SS. *Disinfection, Sterilization, and Preservation*. 5th ed. Philadelphia PA: Lippincott Williams & Wilkins; 2001. https://www.worldcat.org/title/disinfection-sterilization-and-preservation/oclc/44110467. Accessed September 5, 2019.

233. Albert J. Gotch *,†, Gary W. Loar ‡, Aaron J. Reeder † and, Glista† EE. Formation of Single-Phase Microemulsions in Toluene/Water/Nonionic Surfactant Systems. 2008. doi:10.1021/LA7024318

234. Vaughan D, Malcolm RE. *Soil Organic Matter and Biological Activity*. Springer Netherlands; 1985. https://books.google.ca/books?id=WvnxCAAAQBAJ&dq=toluene+bacteriostatic+effect&source=gbs_navlinks_s. Accessed October 18, 2018.

235. Jackson RW, DeMoss JA. Effects of toluene on Escherichia coli. *J Bacteriol*. 1965;90(5):1420-1425. http://www.ncbi.nlm.nih.gov/pubmed/5321488. Accessed October 18, 2018.

236. IARC Working Group on the Evaluation of Carcinogenic Risks to Humans., International Agency for Research on Cancer. *Re-Evaluation of Some Organic Chemicals, Hydrazine and Hydrogen Peroxide.* World Health Organization, International Agency for Research on Cancer; 1999. https://publications.iarc.fr/89. Accessed September 3, 2019.

237. *Request for Assistance in Preventing Adverse Health Effects from Exposure to Dimethylformamide (DMF).*; 1990. doi:10.26616/NIOSHPUB90105

238. DMAP Pharmaceuticals and Agrochemicals. https://www.vertellus.com/Documents/ProductLit/DMAP Product Brochure English.pdf. Accessed September 3, 2019.

239. Xu S, Held I, Kempf B, Mayr H, Steglich W, Zipse H. The DMAP-Catalyzed Acetylation of Alcohols—A Mechanistic Study (DMAP=4-(Dimethylamino)pyridine). *Chem - A Eur J*. 2005;11(16):4751-4757. doi:10.1002/chem.200500398

240. *Handbook of Reagents for Organic Synthesis.* Wiley; 1999. https://books.google.ca/books?id=ZklICgAAQBAJ&pg=PA313&lpg=PA313&dq=DMAP+Pharmaceuticals+and+Agrochemicals&source=bl&ots=7eBOywv7jY&sig=ACfU3U22aP0XKGBb3LZc3ZjhrUdeTJmy2w&hl=en&sa=X&redir_esc=y#v=onepage&q=DMAP Pharmaceuticals and Agrochemicals&f=false. Accessed September 3, 2019.

241. Fuchs PL, Charette AB, Rovis T, Bode JW. *Essential Reagents for Organic Synthesis.* Wiley; 2016. https://books.google.ca/books?id=_ch8DAAAQBAJ&pg=PA173&lpg=PA173&dq=DMAP+Pharmaceuticals+and+Agrochemicals&source=bl&ots=Xn5JpHWKrj&sig=ACfU3U0gN720Jn0mdmEkwUauXDHCYGY_iw&hl=en&sa=X&redir_esc=y#v=onepa

ge&q=DMAP Pharmaceuticals and Agrochemicals&f=false. Accessed September 3, 2019.

242. CDC - NIOSH Pocket Guide to Chemical Hazards - Methylene chloride. https://www.cdc.gov/niosh/npg/npgd0414.html. Accessed September 3, 2019.

243. CDC - NIOSH Pocket Guide to Chemical Hazards - n-Butyl alcohol. https://www.cdc.gov/niosh/npg/npgd0076.html. Accessed September 3, 2019.

244. CDC - NIOSH Pocket Guide to Chemical Hazards - 2-Butanone. https://www.cdc.gov/niosh/npg/npgd0069.html. Accessed September 3, 2019.

245. CDC - NIOSH Pocket Guide to Chemical Hazards - Ethyl acetate. https://www.cdc.gov/niosh/npg/npgd0260.html. Accessed September 3, 2019.

246. Lens C, Malet G, Cupferman S. Antimicrobial activity of Butyl acetate, Ethyl acetate and Isopropyl alcohol on undesirable microorganisms in cosmetic products. *Int J Cosmet Sci*. 2016;38(5):476-480. doi:10.1111/ics.12314

247. CDC - NIOSH Pocket Guide to Chemical Hazards - n-Pentane. https://www.cdc.gov/niosh/npg/npgd0486.html. Accessed September 3, 2019.

248. CDC - NIOSH Pocket Guide to Chemical Hazards - n-Hexane. https://www.cdc.gov/niosh/npg/npgd0322.html. Accessed September 3, 2019.

249. CDC - NIOSH Pocket Guide to Chemical Hazards - Cyclohexane. https://www.cdc.gov/niosh/npg/npgd0163.html. Accessed September 3, 2019.

250. CDC - NIOSH Pocket Guide to Chemical Hazards - n-Heptane. https://www.cdc.gov/niosh/npg/npgd0312.html. Accessed September 3, 2019.

251. CDC - NIOSH Pocket Guide to Chemical Hazards - Octane. https://www.cdc.gov/niosh/npg/npgd0470.html. Accessed September 3, 2019.

252. CDC - NIOSH Pocket Guide to Chemical Hazards - Ethyl ether. https://www.cdc.gov/niosh/npg/npgd0277.html. Accessed September 3, 2019.

253. CDC - NIOSH Pocket Guide to Chemical Hazards - Chloroform. https://www.cdc.gov/niosh/npg/npgd0127.html. Accessed September 3, 2019.

254. Femmer T, Jans A, Eswein R, et al. High-Throughput Generation of Emulsions and Microgels in Parallelized Microfluidic Drop-Makers Prepared by Rapid Prototyping. 2015. doi:10.1021/acsami.5b03969

255. Muluneh M, Issadore D. Hybrid soft-lithography/laser machined microchips for the parallel generation of droplets. *Lab Chip*. 2013;13(24):4750-4754. doi:10.1039/c3lc50979f

256. Au AK, Lee W, Folch A. Mail-order microfluidics: evaluation of stereolithography for the production of microfluidic devices. *Lab Chip*. 2014;14(7):1294-1301. doi:10.1039/c3lc51360b